

**Effective Design of Multiplexing  
Networks for Applications  
in Communications Satellites**

by

Shu Qi Li

A thesis Submitted in Partial Fullfillment  
of the Requirements for the Degree of

Master's of Applied Science

in

The Faculty of Engineering and Applied Science

Program

University of Ontario Institute of Technology

July 2011

© Shu Qi Li 2011

# Abstract

Microwave multiplexing networks are widely used in satellite communication systems. Their performances, such as the insertion loss and rejection between channels, are extremely critical. This research aims at effective design of multiplexing networks for applications in communication satellites exploring different design methodologies.

First, the enhanced type of multiplexer has been proven to be able to significantly improve its performances by forming an extra pole in the pass-band of each channel using the existing manifold. For completeness of the design methodology, the design of the enhanced type of multiplexers with H-plane T-junctions is investigated in this thesis. Design equations are given. By changing the distance between the channel filters and the distance between manifold waveguide and channel filter, the resonances and the magnitude of coupling can be readily controlled to satisfy the design requirement. Examples are used to demonstrate the feasibility and effectiveness of the new design using H-plane T-junctions.

Secondly, Artificial Neural Network (ANN) is applied in the spurious mode compensation in the multiplexer design. Channel filter tuning, circuit model simplification, and neural network training processes are detailed in the thesis. Space-Mapping optimization technology has been applied in the tuning of a channel filter. The artificial neural network is applied as the method to compensate disadvantages of both electromagnetic (EM) simulation, which is accurate but extremely time consuming, and circuit model, which is fast but with limited accuracy. The neural network model of a simplified circuit can rapidly and accurately simulate the spurious mode of a channel filter in its out-of-band. Design examples are used to demonstrate the modeling steps. Good agreements are observed between EM simulation and the results from the developed model.

# Acknowledgement

I am greatly thankful to my supervisor, Prof. Ying Wang, whose broad knowledge, enthusiasm, patience, guidance, have been supporting and inspiring me to finish my studies over the past two years. This thesis would never have been possible without her ideas and continuing encouragement.

I would like to express my deepest gratitude to my colleagues and friends from the Faculty of Engineering and Applied Science at UOIT for all the help and support. Appreciation also goes to Mr. Ye Tao for suggestions on my thesis completion.

Lastly, I am grateful to my family: my parents, Huaqing Li and Yankui Zhang, my brother, Shuqin Li, for their love, understanding and patience.

# Table of Contents

<b>Chapter 1</b>	<b>Introduction</b> .....	<b>1</b>
1.1	Literature Review.....	3
1.1.1	Design Methodology Review .....	3
1.1.2	Simulation Model Review .....	5
1.2	Problem Definition and Proposed Approaches.....	10
1.3	Thesis Organization .....	11
<b>Chapter 2</b>	<b>Design of Enhanced Microwave Multiplexing Networks</b> .....	<b>13</b>
2.1	Waveguide T-junction Equivalent Circuit .....	15
2.2	Example of Single Channel Design .....	21
2.3	Enhanced Multiplexer Design Process .....	28
2.4	Example of Non-Contiguous Multiplexer .....	30
2.5	Summary.....	34
<b>Chapter 3</b>	<b>Application of Artificial Neural Network in Spurious Mode Compensation in Multiplexer Design</b> .....	<b>35</b>
3.1	Tune a 4-pole Filter.....	38
3.1.1	Analyze a Classical Dual Mode Filter .....	39
3.1.2	Tune a Filter with Matlab Program.....	41
3.1.3	Tune a Filter with Agilent ADS.....	47
3.2	Simplify a Low Center Frequency Channel.....	51
3.2.1	Equivalent Circuit Model with Different Orders of Inverters .....	53

3.2.2	EM Simulation of Simplified Filter Structure .....	66
3.3	Artificial Neural Network Model.....	74
3.3.1	Data Collection .....	75
3.3.2	Data Organization.....	77
3.3.3	Application of NN Model in ADS.....	85
3.4	Summary.....	89
<b>Chapter 4</b>	<b>Conclusion .....</b>	<b>91</b>
<b>Bibliography</b>	<b>.....</b>	<b>93</b>

# List of Figures

<b>Fig. 2.1</b>	N-channel Manifold –coupled multiplexer.[6]. .....	<b>15</b>
<b>Fig. 2.2</b>	Comparison between conventional design and enhanced design .....	<b>16</b>
<b>Fig. 2.3</b>	Parallel connection of two short-circuited waveguides .....	<b>17</b>
<b>Fig. 2.4</b>	The equivalent circuit of a H-plane T-junction with reference planes .....	<b>20</b>
<b>Fig. 2.5</b>	Group delay responses of the equivalent circuit of the H-Plane T-junction (in Fig 2.3).  (a) the waveguide lengths from table 2.1 a.  (b) the waveguide lengths from table 2.1 b.....	<b>22</b>
<b>Fig. 2.6</b>	Circuit model of H-plane T-junction in ADS .....	<b>24</b>
<b>Fig. 2.7</b>	Group delay responses of co-simulation circuit of an H-plane T-junction  (a) the waveguide lengths from table 2.1 a.  (b) the waveguide lengths from table 2.1 b.....	<b>24</b>
<b>Fig. 2.8</b>	Group delay responses of the equivalent circuit of the H-plane T-junction after optimization. Case 1 to Case 4 in Table 2.2 .....	<b>26</b>
<b>Fig. 2.9</b>	Comparison of responses of four-pole filters connected with waveguide T-junction in different lengths :  (a) insertion loss response; (b) common port return loss. ....	<b>27</b>
<b>Fig. 2.10</b>	Far band insertion losses of four-pole filters with waveguide T-junctions with different cases in Table 2.2 .....	<b>27</b>
<b>Fig. 2.11</b>	Two-channel multiplexer [06] (a) Simplified equivalent circuit.  (b) two channel multiplexer with channel filters .....	<b>30</b>

<b>Fig. 2.12</b>	Group delay at common port with two channel filters replaced by short circuited .....	<b>31</b>
<b>Fig. 2.13</b>	Fig 2.12 Common port return loss $ S_{11} $ , the insertion loss between port 2 and the common port $ S_{12} $ , and the insertion loss between port 3 and the common port $ S_{13} $ of (a) conventional design and (b) the proposed design.....	<b>32</b>
<b>Fig. 2.14</b>	Comparison of conventional and proposed method (a) the insertion loss for Channel 1 (b) the insertion loss for Channel 2.....	<b>33</b>
<b>Fig. 3.1</b>	3-channel output multiplexer .....	<b>36</b>
<b>Fig. 3.2</b>	Classical configuration of a dual mode filter [01] .....	<b>38</b>
<b>Fig. 3.3</b>	The relations between the mode polarization vectors and tuning screws, coupling screws, and coupling irises. [01].....	<b>38</b>
<b>Fig. 3.4</b>	The configuration of A 4-pole dual mode filter in CST .....	<b>40</b>
<b>Fig. 3.5</b>	Comparison between an ideal coupling matrix and an un-tuned EM model of the 4-pole dual mode filter.....	<b>41</b>
<b>Fig. 3.6</b>	Representation of the fine and coarse models [01].....	<b>43</b>
<b>Fig. 3.7</b>	Comparison between the Phases of S11 and S21 w/o loading phase From the simulation of a dual mode filter .....	<b>44</b>
<b>Fig. 3.8</b>	Comparison between response of fine model and response of extracted coupling matrix (a) The return loss and insertion loss in magnitude (b) The return loss and insertion loss in phase. ....	<b>46</b>
<b>Fig. 3.9</b>	Calibration of the coarse model of a 4-pole filter. This schematic extracts pre-assigned coarse parameters $x$ . the coarse and fine model have been pointed in the figure. The goal is to match the coarse and fine model phases and magnitudes of S11 and S21 from 10.95 GHz to 11.2 GHz.	

	The optimization algorithm uses the Gradient method .....	48
<b>Fig. 3.10</b>	Comparison between responses of extracted coupling matrix and measurement. (a) Comparison between Magnitudes of S11 and S21. (b) Comparison between Phases of S11 and S21 .....	50
<b>Fig. 3.11</b>	Three channel output multiplexer with EM Model (a) Simplified equivalent circuit model with EM model at port 4. (b) Equivalent circuit model of EM model in ADS .....	51
<b>Fig. 3.12</b>	Comparison of Return Losses of Ideal and EM model of Channel 3 .....	52
<b>Fig. 3.13</b>	Relationship between reflection coefficient and S11.....	53
<b>Fig. 3.14</b>	Third-degree low-pass prototype ladder networks: the form after addition of the unit inverters [01] .....	55
<b>Fig. 3.15</b>	Simplest low-pass prototype schematic with one inverter and one resonator in Agilent ADS .....	56
<b>Fig. 3.16</b>	Low-pass prototype schematic with two inverters in Agilent ADS .....	57
<b>Fig. 3.17</b>	Low-pass prototype schematic with three inverters in Agilent ADS .....	57
<b>Fig. 3.18</b>	Simplest band-pass prototype schematic with one inverter and one resonator in Agilent ADS .....	60
<b>Fig. 3.19</b>	Band-pass prototype schematic with two inverters in Agilent ADS .....	61
<b>Fig. 3.20</b>	Band-pass prototype schematic with three inverters in Agilent ADS .....	62
<b>Fig. 3.21</b>	Simplified Band-pass filter with two inverters and one spurious mode attached at first resonator. ....	64
<b>Fig. 3.22</b>	Simplified Band-pass filter with two inverters and one spurious mode attached at first inverter. ....	65
<b>Fig. 3.23</b>	Compare CPRL in one cavity and first resonator of 3-channel multiplexer .....	67

<b>Fig. 3.24</b>	An arbitrary microwave network consisting of six-port networks connected together .....	<b>68</b>
<b>Fig. 3.25</b>	Phase comparison in different Modes .....	<b>71</b>
<b>Fig. 3.26</b>	Comparison between the Common Port Return Losses and Insertion Losses from a conventional 3-channel multiplexer, and from simplified 3-channel multiplexers. (a) Compare CPRL in different types of 3-channel multiplexer. (b) Compare CPRL and IL in Channel 1. (c) Compare CPRL and IL in Channel 2 .....	<b>72</b>
<b>Fig. 3.27</b>	Comparison of the multiplexer with EM model, and with Ideal Model. (a) Common Port Return Loss $S_{11}$ . (b) Insertions Loss and Return Loss in Channel 1. (c) Insertion Loss and Return Loss in Channel 2 .....	<b>75</b>
<b>Fig. 3.28</b>	A three layer structure of Artificial Neural Network with two input parameters and two output parameters .....	<b>78</b>
<b>Fig. 3.29</b>	EM simulation of one third cavity with five propagating modes in different slot lengths. (a) The magnitudes of $S_{2(3)2(1)}$ (low linearity). (b) The magnitudes of an $S_{1(1)2(1)}$ (high linearity) .....	<b>79</b>
<b>Fig. 3.30</b>	Simplified Matlab Flowchart .....	<b>80</b>
<b>Fig. 3.31</b>	A three layer structure of Artificial Neural Network with three input parameters and two output parameters .....	<b>81</b>
<b>Fig. 3.32</b>	The phases of reflection coefficient with different slot lengths.....	<b>82</b>
<b>Fig. 3.33</b>	An arbitrary microwave network consisting of multiport networks connected together .....	<b>83</b>
<b>Fig. 3.34</b>	Phases of $S_{21}$ after de-grading matrix .....	<b>85</b>
<b>Fig. 3.35</b>	Three channel output multiplexer with Neural Network Model	

- (a) Simplified equivalent circuit model with NN model at port 4.
- (b) Equivalent circuit model of NN model in ADS .....86

**Fig. 3.36**

Comparison of the multiplexer with EM model, and with NN Model.

- (a) Common Port Return Loss S11.
- (b) Insertion Loss and Return Loss in Channel 1.
- (c) Insertion Loss and Return Loss in Channel 2 .....87

# List of Tables

<b>Table 2.1</b>	Group Delay Responses as Waveguide Lengths Changes .....	<b>23</b>
<b>Table 2.2</b>	Group Delay Responses with Co-simulation Circuit Model .....	<b>25</b>
<b>Table 2.3</b>	Optimized waveguide lengths with corresponding group delay and coupling values for channel filters centered at 12 GHz and with 36 MHz bandwidth.....	<b>26</b>
<b>Table 2.4</b>	Manifold Dimension of Two-channel Multiplexer with Conventional Method and Enhanced Method .....	<b>31</b>
<b>Table 2.5</b>	The width of pass-band in each channel filter. ....	<b>34</b>
<b>Table 3.1</b>	Phases in Low-pass filter Circuit Model with Different Order of Inverters .....	<b>59</b>
<b>Table 3.2</b>	Phases in Band-pass filter Circuit Model with Different Orders of Inverters .....	<b>63</b>
<b>Table 3.3</b>	Values of $p'$ in different mode of a circular waveguide .....	<b>67</b>
<b>Table 3.4</b>	Cavity lengths at Different Resonance Frequencies .....	<b>76</b>
<b>Table 3.5</b>	Error comparison between the ANN model and EM simulations for S-parameters .....	<b>89</b>
<b>Table 3.6</b>	Comparison of Time to obtain S-parameters by NN models and EM models .....	<b>89</b>

# Chapter 1

## Introduction

Satellites not only provide services for military use, but also for the communication broadcasting and mobility aspect. Civil satellites, such as communication, navigational and weather satellites, serve resident and research department.

The microwave frequency is in the range of 3 GHz to 30 GHz. Due to their small wavelength, microwaves are capable of directing in narrow beams by various sizes of antennas. With this advantage, the neighbouring microwave devices are allowed to use the same frequencies without interfering each other, as lower frequency radio waves do. Another advantage is that the bandwidth of high frequency of microwave with same bandwidth ratio has a larger information-carrying capacity than the rest of the radio

spectrum below it. Multiplexers are used in satellite communication systems to combine or separate frequency bands for transmission via a common antenna as part of a satellite [1]. Its performance no doubt strongly affects satellite quality. Different techniques have been developed to enhance the multiplexer design. The design of multiplexer starts from the lump-element circuit theory, and moves to the distributed circuit elements and transmission-line theory, which is more accurate for design and analysis. The discrete resistors, capacitors and inductors are replaced by cavity resonators or resonant lines. Effects of reflection, rejection, polarization and scattering are all studied. In order to save the energy and space, various kinds of light material have been used for multiplexer design, since satellites are very sensitive to the weight and size. In the satellite application, there are four commonly used configurations of multiplexers, namely hybrid-coupled multiplexers, circulator-coupled multiplexers, directional filter multiplexers, and manifold-coupled multiplexers. Base on the advantages of its ability to realize optimum performance for return loss, insertion loss and group delay, and its compact design, manifold-coupled multiplexers are widely used [01], and will also be used as the multiplexer configuration in the following analysis.

For performance enhancement, engineers and scientists have been making great efforts to improve the design of multiplexers. A number of software programs have been exploited to simulate multiplexer performance, and provide optimization process and accurate simulation results.

The objective of this research is to develop a cost-effective methodology for microwave multiplexer design for applications in communications satellites.

## 1.1 Literature Review

Various methods [01][06][07][12] have been developed to enhance the efficiency of multiplexer designs; and various types of software [02][03][04][05] have been provided to rapidly and accurately simulate a multiplexer. Design approaches of a multiplexer are described in section 1.1.1, and simulation software will be reviewed in section 1.1.2.

### 1.1.1 Design Methodology Review

Microwave multiplexing networks are widely used in satellite communication systems [01][17]. The frequency spectrums can be split into a number of smaller frequency bands or Radio Frequency (RF) channels using input multiplexers. Output multiplexers combine several narrowband channels into a single wideband composite signal for transmission. The performances of channel filters, such as the insertion loss and rejection between channels, are extremely critical [21].

A typical multiplexer design involved design and optimization [23]. In the design process, the channel filters will be prepared to meet the specifications [24] [25] with the corresponding coupling matrices synthesized; then set initial value of integral half guided wavelength to the manifold spacing between channel filters, and stub lengths. Optimization process will start from optimizing wideband components, which includes spacing between channel filters, and stub lengths; then optimize first three or four parameters of the first channel filter, then extend the same step onto other channel filters. Optimizations will be repeated for manifold and stub lengths as well as parameters of each channel filter. The network synthesis is applied with frequency-invariant reactance

or frequency-independent reactances elements[26] in asymmetric filter network[27]. This network has been proven with low-pass and band-pass prototype networks.

Increasing the order of filter by adding extra poles to across-coupled filter can improve rejection directly. Nevertheless, adding extra resonators increases the size and the weight of the multiplexer. A method of enhancing the performance of multiplexers has been presented by using the existing manifold structure and introducing extra pole into the pass-band without any extra resonator [06][07]. It has been shown that significant improvement in both in-band and out-of-band performances can be achieved. Since this approach does not introduce any additional resonators, the hardware still retains similar size and weight as conventional design.

In [06], design equations and examples were only given for E-plane waveguide T-junctions. For completeness of the design methodology, we further investigate the design of the enhanced type of multiplexers with H-plane T-junctions in this thesis. In chapter 2, it will be shown how the preliminary dimension of manifold can be obtained from the equivalent circuit of H-plane waveguide T-junction and the required frequency and group delay, which is related to the coupling value. The optimization of a single four-pole filter connected with a T-junction is used as an example. The simulation results exhibit the responses of a five-pole stand-alone filter. The resonances and the magnitude of coupling can be readily controlled to satisfy design requirement. A multi-channel example is then presented using H-plane T-junctions, demonstrating the feasibility and the effectiveness of the new design.

The general multiplexer design can be designed by distributed models [28][29], and various methods are presented [30][31][32]. Flat group delay and pass-band gain and good out-of-band rejection can be achieved through these design and optimization steps. With increasing number of channel filters in multiplexer, a spurious mode occurs in transmission band of multiplexer and damages the responses of the multiplexer. To treat the spurious mode in manifold multiplexer design, [12] has provided a methodology with a hybrid circuit/electromagnetic model to simulate all components of a multiplexer. The method used in [12] is to build a Lumped Element model with one capacitor and one inductor, to simulate input/output cavity. Through the tuning of coupling values, resonance frequencies and manifold waveguide lengths, one can compensate the effect of the spurious mode. An example of a triplexer has been applied in [12] to verify this method.

### **1.1.2 Simulation Model Review**

The main purpose of a simulator is to accurately reflect the performance of both multiplexer and channel filter designs. Simulation models can be classified as circuit-based simulator and three-dimensional (3-D) electromagnetic (EM) simulators, based on their computational method. Both simulators and another novel tool, namely Artificial Neural Network (ANN), are studied in this thesis to design and simulate the performance of multiplexers and channel filters.

#### **A. Circuit-Based Model**

The category of a circuit-based simulator considers theoretical circuit model with lossless connection. For multiplexing networks, the structures can be decomposed into a

set of components, such as filters [18], T-junctions and waveguides. These isolated components are cascaded by ideal transmission lines. Variables in a circuit model include calculated parameterized scattering matrix, or lengths and phases of the transmission waveguides.

The great benefit of a circuit-based simulator, is the speed. The results of a circuit-model can be monitored in real time. Parameters can be set as tuning or optimization variables. After selection of algorithm and optimization, the circuit-based simulator can easily find a result to meet specifications. At the next stage of design, it needs to be proven that the structure and initial values are reasonable for practical use. Most theoretical examples can be proven by circuit-based simulators. Because of this ideal model, it purposely ignores some important information in practice, such as conductor loss, thermal effect, material constant, and dielectric loss. In manufacturing, these parameters intensively influence the performance of multiplexers. Therefore besides circuit-based models, we also need three dimensional electromagnetic simulators.

### **B. Three-dimensional (3-D) Electromagnetic (EM) Simulator**

An EM simulator fully simulates the entire structure to be designed. Even a corner or a small iris should be considered in the EM simulation. The structure in an EM simulation is not a connected circuit-model, but a physical configuration of a multiplexer or a channel filter. An EM simulator usually performs full-wave and parametric analysis. The EM simulator results are close to the measurement results, e.g. by using mesh cells to compute the entire structure. There are time and frequency domain solvers, which

enhances EM simulator functionality. Furthermore, thermal analysis, electric and magnetic field monitor can help to predict whether distortion will occur in manufacturing.

However, EM simulators need significantly more computation time than circuit-based simulator. The computation time is exponentially rising with structure sizes, frequency ranges and the number of parameters. A simulation of a structure with ten parameters in 2 GHz frequency range usually takes half an hour for calculation. If an EM simulator involve with parameter sweeping, it requires more computation time. Direct optimization of the dimensional parameters of the structure using EM simulators is in general not practical.

[2] investigated an approach named co-simulation to utilize the advantages of both EM- and circuit-based simulators. The concept of this method is to use an EM simulator to generate EM-models by analyzing some decomposed components such as waveguide T-junctions, channel filters. Then a circuit-based simulator calls/retrieves EM models during its simulation and optimization process. In a circuit-based model, co-simulation technique imports data from an EM simulator to increase the accuracy. After the optimization of physical dimension, an EM simulator will be reused to check if the structure meets the specifications. In this thesis, this efficient technique is used in simulation and optimization process not only to save time but also to get precise results. Most waveguide T-junctions and some channel filters in this thesis are replaced by EM-models to gain precise results.

As an effective optimization technique, Space Mapping technique has been widely applied in EM optimizations [20]. The technique combines a fast coarse model,

which can be circuit-based, with accurate EM simulations, which is the CPU-intensive fine model. [13] uses examples of a double-terminated five-pole dielectric resonator filter and a ten-channel output multiplexer to illustrate the efficiency of Space Mapping in microwave design.

### C. Artificial Neural Network (ANN)

During the tuning of channel filters, any change in the variable of a filter structure requires full wave EM analysis. Unfortunately, this kind of change may happen numerous times in one filter tuning. Artificial neural network (ANN) can be applied to solve this problem.

As a novel tool, the convenience of ANN has been proven in RF and microwave modeling and design. In this thesis ANN is applied to model the scattering matrix or S-parameters of segments of a filter as a function of dimensional variables, such as iris lengths or cavity lengths, in frequency domain.

The first step in neural model developing is to formulate problems and process data. It includes inputs and outputs identification, data range definition, data generation, data organization and data preprocessing. The output parameters are determined by the purpose of design objectives. In this thesis, a scattering matrix and S-parameters are selected as output parameters in the neural model. The output data must be easily connected into circuit models. The input parameters are dimensional parameters. The data range is usually defined to cover the entire parameter range of interest. Data can be generated from an EM simulator such as Computer Simulation Technique (CST) Studio[19]; they are used in training and testing of a neural network model. After

generation, the data can be classified as training, and testing data, and will be used in different steps of a neural network developing process.

For ANN model, we adopt the commonly used multilayer perceptron. Two external layers are divided to link to input neurons and output neurons. An internal layer, which is the link between an input and output layer, can be more than one layer. Hidden neurons, which are located in internal layers, are trained to matching the relationship between input parameters and output parameters. When enough training data have been fed to the whole system, a data pattern can be created to find proper outputs to a series of inputs. Testing data will be use to evaluate the error of the neural network model after training step. The selection of the quantity of hidden neuron can be decided by comparing the training and testing error. When testing error is much greater than training, the training data cannot be generalized well, which is called over-learning. In this situation, we need to reduce the number of hidden neurons or adding more samples to the training data. Conversely, when training error is much greater than testing error, the system has difficulties in learning training data, which is named under-learning. In this situation, the neural model will need more hidden neurons or perturb the current solution. The neural model is complete only when the training and testing error are both small and close to each other. A successfully developed neural network model takes much less calculation time between input and output parameters. [3], [4] and [5] have treated the theory of Artificial Neural Network with many examples.

## 1.2 Problem Definition and Proposed Approaches

Two problems will be solved in this thesis. One is the design of enhanced microwave multiplexing networks with H-plane T-Junctions. This is a completeness of the design methodology in [6] [7]. In this part, the concept of enhanced multiplexing network is to create another pole into the pass-bands of channel filters by optimizing the dimension of the existing manifold. Instead of increasing the order of a filter, efficient design of waveguide manifold can improve the rejection but retain the weight and size of the multiplexer. With the enhanced type of design, there will be a peak clearly occurs in the group delay which would be flat for conventional design. This group delay or coupling value can be purposely designed with specific values at the resonance frequencies.

The other problem is manifold coupled multiplexer design. The EM simulation of a dual mode cavity filter, which is part of a multiplexer, showing a spurious mode appeared in its out-of-band frequency but still in the full transmission band of the multiplexer. This usually happens when the transmission band of a multiplexer has a wider frequency range than the spurious mode from channel filter. This spurious mode damages the multiplexer transmission. In this thesis a neural network model combined with a circuit-based simulator is used to simulate the spurious mode. The design process is time consuming when using EM simulators. The involvement of Neural Network can rapidly provide a simulation result for the spurious mode. In the filter tuning process, space mapping technique is used for optimization.

A WR75 H-plane is used as T-junction in this thesis and applied in simulations of both problems. The inside dimension is  $0.750 \times 0.375$  inch, the outside dimension is  $0.850 \times 0.475$  inch. The standard frequency range of a WR75 is 10 GHz to 15 GHz, which is proper to the design within frequency range between 10 GHz and 13 GHz. In addition, a classical dual mode cavity filter will be applied in the multiplexer design.

### 1.3 Thesis Organization

The thesis consists of four chapters. The first chapter introduces related models used in the design. They are circuit-based simulator Agilent Advanced Design System (ADS)[02], three-dimensional electromagnetic simulator Computer Simulation Technology (CST) EM Studio [21], and Artificial Neural Network (ANN) [03] [04] [05]. The research problems are also mentioned in this chapter.

The design of enhanced microwave multiplexing networks with H-plane T-junctions is presented in Chapter 2, with basic theory deduction, single channel and multi-channel design examples. The advantages of this method have been fully illustrated through a comparison for different designs, and the obvious improvements of channel filters in simulation results.

Chapter 3 contains detailed steps for, tuning filter with space mapping parameter extraction, simplifying multiplexer circuit models and training a neural network model. In this chapter, CST Studio is used to provide EM data for neural network and T-junction co-simulation; it is also used to verify the optimization results. Additionally, some assumptions and deductions are presented in this chapter to simplify the simulation process. Artificial Neural Network is applied in this chapter to improve the spurious

mode simulation. To improve the accuracy of neural network models, various approaches have been applied in its training process. These approaches are also explained in this Chapter.

In Chapter 4, besides the conclusion of the whole research, some suggestions in the future research are presented.

## Chapter 2

# Design of Enhanced Microwave

## Multiplexing Networks

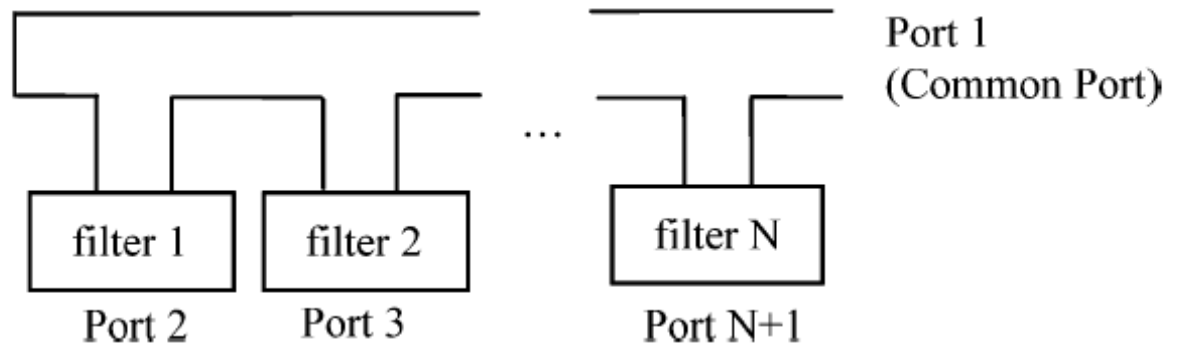
Typical multiplexer structures consist of a number of channel filters coupled to waveguides or transmission line manifolds. Some characteristics are highly critical, such as pass-band gain flatness, group delay flatness and stop-band rejection. They are very important performance measures for a multiplexer.

To improve the rejection, the conventional method is to add extra poles to across-coupled filter by increasing the order of the filter. However, increasing order of a filter will no doubt increase the size and weight of it. In satellite application, introducing extra resonators occupies more space and increases weight of the hardware, which is not favorable because satellite is extremely weight sensitive in space application. Therefore,

this chapter uses a method utilizing the manifold structure to improve rejection of a multiplexer. It is proven that an additional resonator can be generated by re-building the manifold structure that interconnects channel filters. By purposely designing the distance between channel filters and the distance between each channel filter and the manifold, another pole will be produced in the filter.

[06] has given design equations and examples for E-plane waveguide T-junctions. For completeness of the design methodology, the investigation in this chapter is focused on the design of multiplexers with H-plane T-junctions, which has different configuration from E-plane T-junctions. In the first section, the dimensions of T-junction are generated by the analysis of the waveguide T-junction equivalent circuit with required resonance frequency and group delay, which is related to coupling value. Secondly, in the optimization of a single channel multiplexer with a four-pole filter connected to the H-plane T-junction, the results exhibit the near band responses of a five-pole stand-alone filter instead of four-pole; and also show the rejection in out-of-band with great improvement even though some return losses does not achieve five distinct poles. In the third section, the design steps of this enhanced multiplexing network are concluded. Finally, this method is extended to a multi-channel multiplexer design. With the proper group-delay generated by designed transmission line, the responses achieved extra reflection zeros and effectively increase the filter order.

## 2.1 Waveguide T-junction Equivalent Circuit



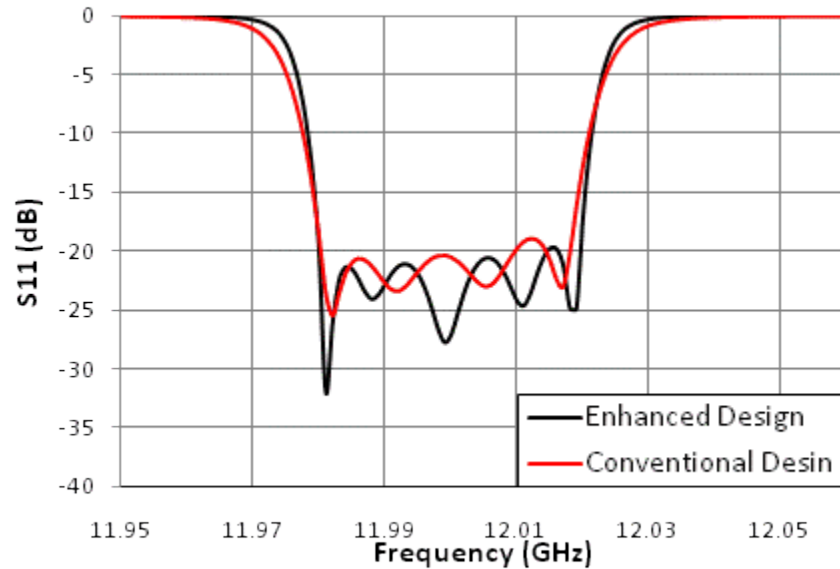
**Fig. 2.1 N-channel manifold –coupled multiplexer. [06]**

Fig. 2.1 shows a conventional multiplexer configuration intended for communication satellites. With the manifold transmission line short-circuited at one end, the other end is used as an output common port. Channel filters are connected to the manifold transmission line through waveguide E- or H-plane T-junctions.

In conventional manifold coupled multiplexer designs [01], the initial manifold distance between E- or H-plane junctions is set to be integral of half guided wavelength, which is given as  $m\lambda_g/2$ ; the initial manifold length of short junction is  $\lambda_g/4$  (H-plane), or  $\lambda_g/2$  (E-plane).  $\lambda_g$  here is the guided wavelength at the center frequency of the nearest channel filter to the common port. The distance between channel filter and manifold junction is presented by  $n\lambda_g/2$ . The group delay is usually flat in the pass-band, and the manifold waveguide serves as matching network to channel filters. Contrast, the group delay in [06] is designed with a peak at resonance frequency instead of being flat.

The paper [06] has analyzed the effect of a waveguide E-plane T-junction. Thus a waveguide H-plane T-junction is treated in this chapter. Taking a four-pole filter as an

example, Fig. 2.2 shows the comparison between the conventional design and enhanced design. Fig. 2.3 is a simplified equivalent circuit of an H-plane T-junction.



**Fig. 2.2 Comparison between conventional design and enhanced design**

In Fig. 2.3,  $l_1$  is the distance between a channel filter to the short circuit;  $l_2$  is the distance between a channel filter to the manifold. Because the T-junction is the farthest one to the manifold common port, the end of  $l_1$  is short-circuited. The channel filter attached to the end of  $l_2$  is replaced with a short circuit in the following analysis. For an H-plane T-junction, the simplified equivalent circuit two short-circuited waveguide connected in parallel, while for E-plane T-junction, the two short-circuited waveguide sections are connected in series. This simplified equivalent circuit is used to obtain the desired resonance frequency and coupling value.

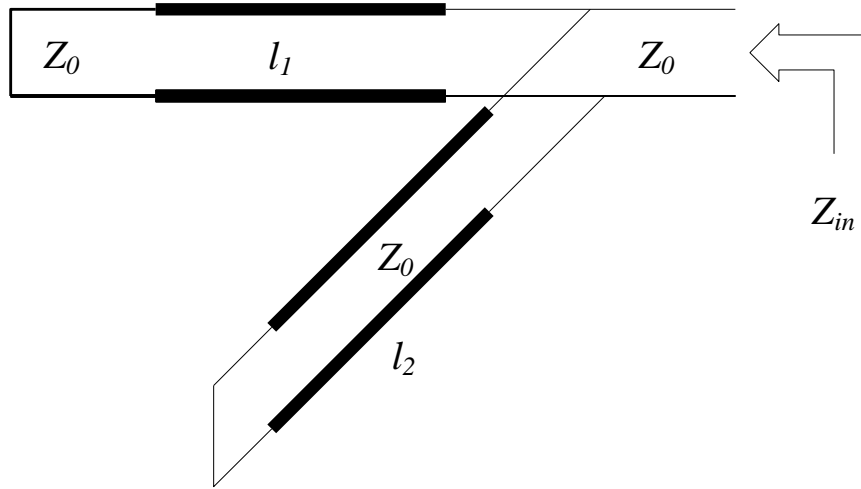


**Fig. 2.3 Parallel connection of two short-circuited waveguides.**

Based on the figure of H-plane T-junction (Fig. 2.3), the impedance at common port can be calculated as :

$$Z_{in} = (jZ_0 \tan \beta l_1) \parallel (jZ_0 \tan \beta l_2) \quad (2.1)$$

where  $Z_0$  is the characteristic impedance;  $\beta$  is the propagation constant, which is equal to  $2\pi/\lambda_g$  ; and  $l_1$   $l_2$  are the lengths of two waveguides, respectively. The loss in the waveguide will not be considered. Resonance should occur when  $Y_{in} = 1/Z_{in} = 0$  or  $l_1 + l_2 = k\lambda_g / 2$  , where  $k = 3,4,5 \dots$  , and  $\lambda_g$  is guided wavelength at resonance frequency. The constant  $k$  must be greater than 3 to ensure the waveguide lengths are physically realizable. The relevant reflection coefficient is computed as:

$$S_{11} = |S_{11}| \angle \phi = \frac{Z_{in} - Z_0}{Z_{in} + Z_0} \quad (2.2)$$

The phase of the reflection coefficient can be expressed as:

$$\begin{aligned}\phi &= -2\cot^{-1} \left[ \frac{\tan\beta l_1 + \tan\beta l_2}{\tan\beta l_1 \tan\beta l_2} \right] \\ &= -2\cot^{-1} [\cot\beta l_1 + \cot\beta l_2]\end{aligned}\quad (2.3)$$

In this design, all channel filters will be operated as narrow-band filters. Thus it is convenient to use group delays of this structure to find out coupling values at resonance frequency. The group delay  $\tau$  will be

$$\tau = -\frac{\partial\phi}{\partial\omega}\quad (2.4)$$

Let  $x = \cot\beta l_1 + \cot\beta l_2$ , and  $\tau(f)$  is written as

$$\tau(f) = -\frac{\partial(-2\cot^{-1}x)}{\partial\omega} = -\frac{1}{\pi} \frac{1}{1+x^2} \frac{\partial x}{\partial f}\quad (2.5)$$

While  $x = 0$ , the group delay at resonance frequency coincides with center frequency [06].

The group delay can be derived as

$$\tau(f_0) = \frac{1}{\pi} \left[ \frac{l_1}{\sin^2\beta l_1} + \frac{l_2}{\sin^2\beta l_2} \right] \frac{\partial\beta}{\partial f}$$

Since  $\lambda_0 = \frac{c}{f}$ , and  $\lambda_g = \frac{\lambda_0}{\sqrt{1 - (\frac{\lambda_0}{2a})^2}}$ , the above equation can be converted to

$$\tau(f_0) = \frac{1}{\pi} \left[ \frac{l_1}{\sin^2\beta l_1} + \frac{l_2}{\sin^2\beta l_2} \right] \frac{2\pi f_0 \lambda_g}{c^2}\quad (2.6)$$

$l_1 + l_2 = k\lambda_g / 2$  at resonance frequency when  $k \geq 3$ , or  $\beta(l_1 + l_2) = k\pi$ . If  $k$  is odd,

$l_1 + l_2 = \lambda_g / 2$ , assuming  $\beta l_1 = \pi + \theta$ , then  $\beta l_2 = k\pi - \beta l_1$ . If  $k$  is even,  $l_1 + l_2 = \lambda_g$ ,

assuming  $\beta l_1 = k\pi/2 + \theta$ , and then  $\beta l_2 = k\pi/2 - \theta$ . The conditions can be concluded as:

$$\begin{cases} \beta l_1 = \pi + \theta, & \beta l_2 = k\pi - \beta l_1 & \text{when } k \text{ is odd;} \\ \beta l_1 = k\pi/2 + \theta, & \beta l_2 = k\pi/2 - \theta & \text{when } k \text{ is even.} \end{cases}$$

These assumptions can reduce the equation to

$$\tau(f_0) = \frac{k f_0 \lambda_g^2}{c^2 \sin^2 \theta} \quad (2.7)$$

The coupling value  $R$  is related to group delay as [06]

$$R = \frac{2}{\pi \cdot BW} \frac{1}{\tau(f_0)} \quad (2.8)$$

where  $BW$  is the bandwidth of the channel filter. Once the required coupling value and resonance frequency are known, we can use (2.7) and (2.8) to get the short-circuited waveguide length of  $l_1$ .

Fig. 2.4 shows an H-plane T-junction with corrected reference planes. The middle figure of Fig. 2.4 shows that the length of short-circuited waveguide in the equivalent circuit model is not a physical length, but the length from the reference plane  $T_1$  or  $T_1'$  to the end of the waveguide. The impedance at common port is not just parallel calculation of two short-circuited waveguides, but has an extra impedance  $jX$  parallel to two waveguides, and the impedance on  $l_2$  has a coefficient. In the general view of Fig. 2.4, the cross section area is defined as  $a \times b$  [11], where  $a$  is the height of a T-junction,  $b$  is the width of each waveguide.

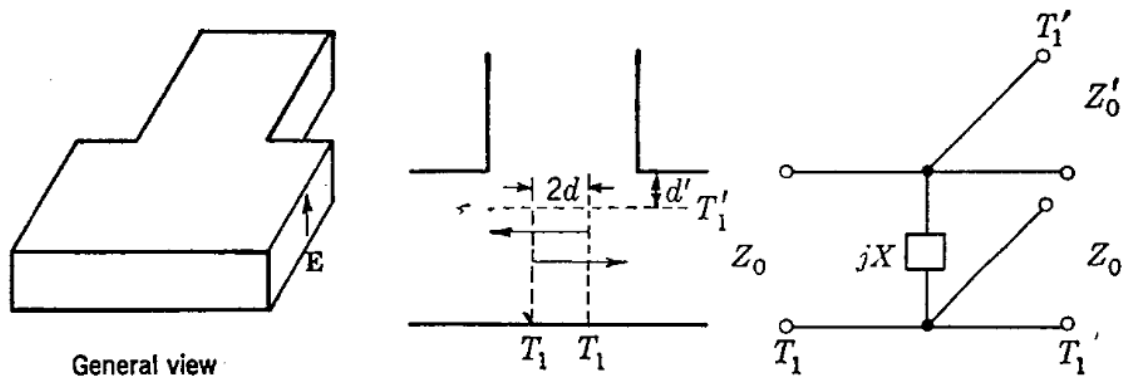


Fig. 2.4 The equivalent circuit of an H-plane T-junction with reference planes [11]

With reference planes, the common port impedance will be correct as

$$Z'_{in} = jX \parallel jZ_0 \tan \beta l_1 \parallel jmZ_0 \tan \beta l_2$$

$$Y'_{in} = \frac{1}{Z'_{in}} = \frac{1}{jX} + \frac{\cot \beta l_1}{jZ_0} + \frac{\cot \beta l_2}{jm \cdot Z_0} \quad (2.9)$$

where,

$$l_1 = L_1 + \left(\frac{a}{2} + d\right)$$

$$l_2 = L_2 + d' \quad (2.10)$$

The constant  $X$ ,  $m$ ,  $d$  and  $d'$  are all given in [11].

With new common port impedance, repeating the previous steps, the reflection coefficient at common port can be re-calculated as

$$S'_{11} = |S'_{11}| \angle \phi' = \frac{Z'_{in} - Z_0}{Z'_{in} + Z_0}$$

$$\phi' = -\cot^{-1} \left( \frac{Z_0}{X} + \cot \beta l_1 + \frac{1}{m} \cot \beta l_2 \right) \quad (2.11)$$

At the resonance frequency  $Y'_{in} = 0$ , and the group delay is modified to

$$\tau'(f_0) \approx \frac{1}{\pi} \left( \frac{l_1}{\sin^2 \beta l_1} + \frac{l_2}{m \cdot \sin^2 \beta l_2} \right) \frac{2\pi f_0 \lambda_g}{c^2} \quad (2.12)$$

Let  $x' = \frac{Z_0}{x} + \cot \beta l_1 + \frac{1}{m} \cot \beta l_2$ . The value of  $l_2$  at resonance frequency can be calculated when  $x' = 0$ . (2.12) provides an accurate group delay. Physical waveguide lengths  $L_1$  and  $L_2$  will be calculated by (2.10).

This waveguide T-junction with particular coupling value at resonance frequency can be used as the first resonator.

## 2.2 Example of Single Channel Design

In the following examples, WR75 will be chosen as waveguide T-junctions, the dimension is 19.05mm  $\times$  9.525mm, which means  $a$  is equal to 19.05mm and  $b$  is equal to 9.525mm. The resonance frequency is 12 GHz. Group delays are set to be 0.5ns, 5ns, 15ns and 20ns, respectively, with 36 MHz bandwidth to compute different waveguide lengths  $l_1$  and  $l_2$ . The center frequency and bandwidth can be changed to other values. 12 GHz center frequency and 36 MHz bandwidth are used as an example for  $K_u$ -band designs of microwave multiplexers. Then  $l_1$  and  $l_2$  are used to find the physical lengths  $L_1$  and  $L_2$ . With the reference planes in the waveguide T-junction shown in Fig. 2.4,  $\tau'(f_0)$  shows different group delay values. The following table shows the lengths of waveguide T-junctions, and a comparison between different group delays. In Table 2.1(a),  $l_1 + l_2 = 3\lambda_g/2$  is used as an example,  $l_1 + l_2 = 2\lambda_g$  is used as another example in

Table 2.1(b). Fig. 2.5 shows simulation results of the equivalent circuit model in circuit-based model.

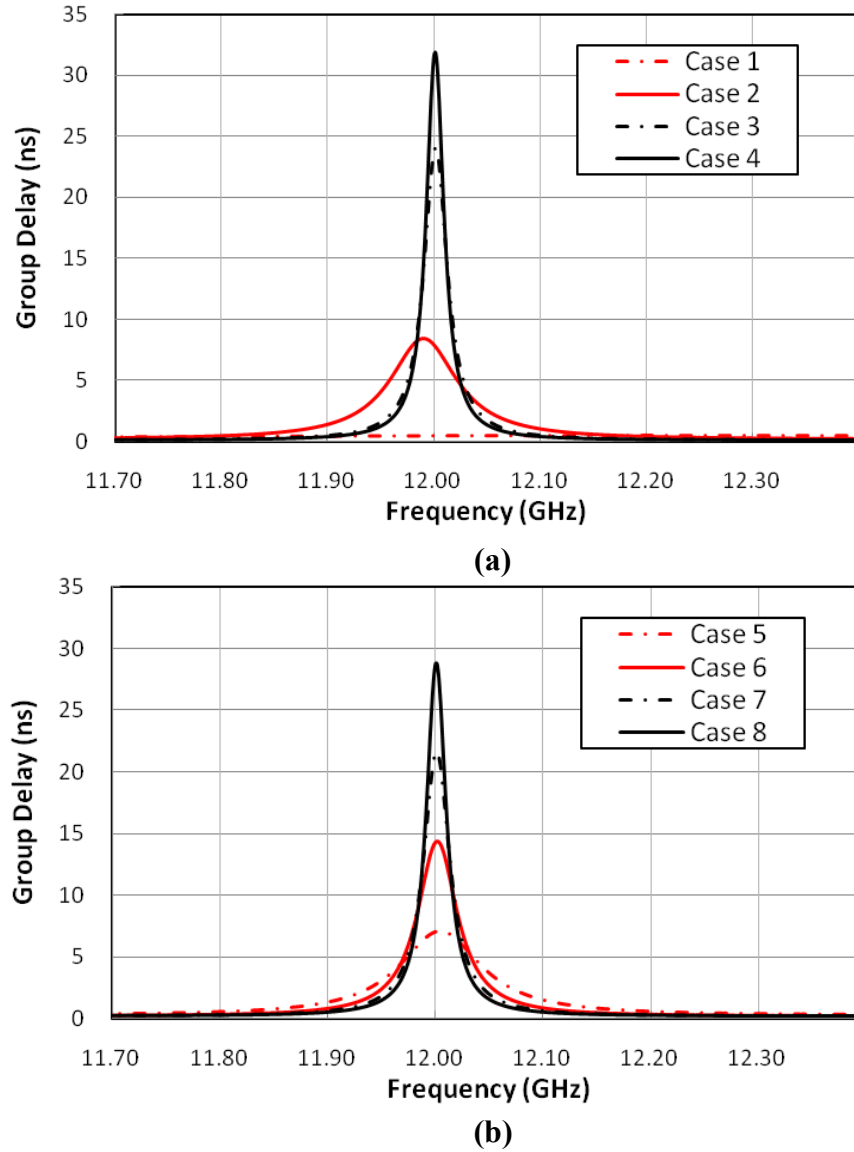


**Fig. 2.5** Group delay responses of the equivalent circuit of an H-plane T-junction (in Fig. 2.4). (a) the waveguide lengths from table 2.1 (a). (b) the waveguide lengths from table 2.1 (b).

**Table 2.1 Group Delay Response as Waveguides Lengths Changes**

Cases	$L_1$ (mm)	$L_2$ (mm)	$l_1$ (mm)	$l_2$ (mm)	$\tau(f_0)$ (ns)	$\tau'(f_0)$ (ns)	Simulation Based on Equivalent Circuit(Fig.2.3)	
							Maximum Group Delay(ns)	$f_0$ (GHz)
(a) $k = 3, i. e. l_1 + l_2 = 3\lambda_g/2$								
1	12.529	22.630	22.966	28.627	0.5	0.471	0.493	12.010
2	7.714	26.284	18.151	32.381	5	7.815	8.764	12.002
3	7.034	26.648	17.471	32.646	15	23.788	25.305	11.996
4	6.912	26.713	17.349	32.711	20	31.739	33.236	11.996
(b) $k = 4, i. e. l_1 + l_2 = 2\lambda_g$								
5	24.534	26.145	34.971	32.142	5	7.053	7.108	12.004
6	23.981	26.444	34.418	32.442	10	14.324	14.384	12.001
7	23.741	26.573	34.178	32.570	15	21.564	21.624	12.001
8	23.599	26.648	34.036	32.646	20	28.788	28.809	12.001

The group delay with different physical lengths of waveguide H-plane T-junctions, has also been co-simulated in circuit-based model. During the simulation process, both EM- and Circuit-based simulators are involved. This co-simulation has been explained in Chapter 1. Fig. 2.6 shows the detailed connection. The T-junction component in the equivalent circuit model is a 3-port S-parameter file, which contains EM data from Computer Simulation Technology (CST) Studio simulation. The H-plane T-junction has been simulated in EM model with wave-port de-embedding. The H-plane T-junction is

connected with a terminal, and the waveguide lengths are expressed as ideal transmission lines in this figure. The co-simulation results are shown in Fig. 2.7.

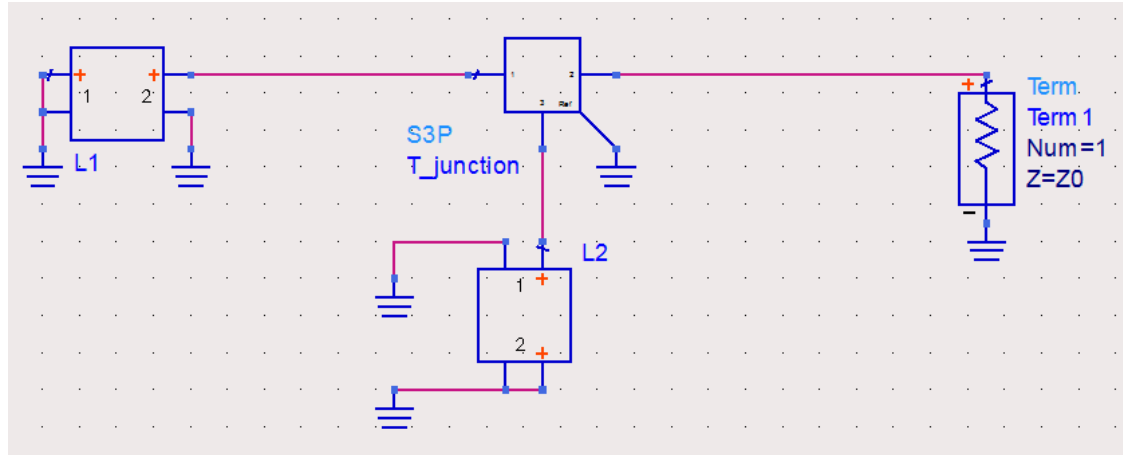


**Fig. 2.6 Circuit model of H-plane T-junction in ADS**

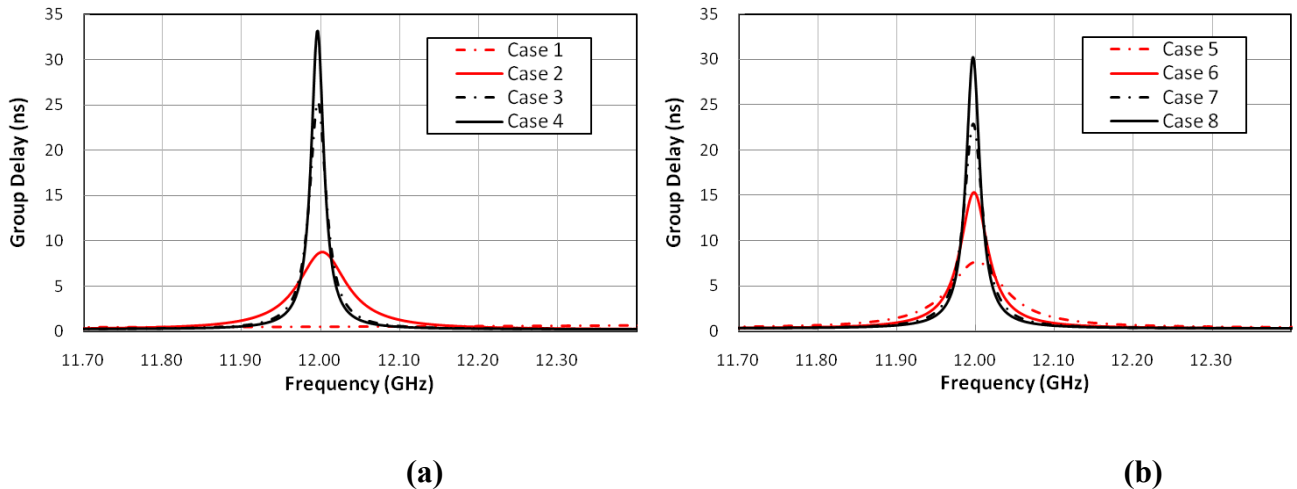


**Fig. 2.7 Group delay responses of co-simulation circuit of an H-plane T-junction. (a) the waveguide lengths from table 2.1 (a). (b) the waveguide lengths from table 2.1 (b).**

It can be easily seen from Table 2.2 that the group delays from co-simulation do not occur right at resonance frequency, but close to it. The group delay values from co-simulation with the physical waveguide lengths are not very close to the initial value  $\tau(f_0)$ , but very close to the corrected group delay  $\tau'(f_0)$ . This difference is due to the

inaccuracy of the circuit model of the waveguide junction. Whereas, the inaccuracy can easily be removed in optimization process. These computed waveguide lengths still serve as good initial values to optimizations.

**Table 2.2 Group Delay Response with Co-simulation Circuit Model**

Cases	$L_1$ (mm)	$L_2$ (mm)	$\tau(f_0)$ (ns)	$\tau'(f_0)$ (ns)	Simulation Based on Co-simulation Circuit(Fig.2.6)	
					Maximum Group Delay(ns)	$f_0$ (GHz)
<b>(a) <math>k = 3, i. e. l_1 + l_2 = 3\lambda_g/2</math></b>						
1	12.529	22.630	0.5	0.471	0.730	12.500
2	7.714	26.284	5	7.815	8.763	12.002
3	7.034	26.648	15	23.788	25.304	11.996
4	6.912	26.713	20	31.739	33.179	11.996
<b>(b) <math>k = 4, i. e. l_1 + l_2 = 2\lambda_g</math></b>						
5	24.534	26.145	5	7.053	7.700	12.001
6	23.981	26.444	10	14.324	15.370	11.997
7	23.741	26.573	15	21.564	22.885	11.996
8	23.599	26.648	20	28.788	32.080	11.999

After tuning the waveguide lengths in Case 1 to Case 4 in Table 2.2, the modified waveguide lengths, group delay at center frequency 12GHz and corresponding coupling value with 36 MHz bandwidth are shown in Table 2.3. The simulation results are plotted in Fig. 2.8. In Fig. 2.8, the group delay of Case 1 to Case 4 occurs right at center frequency 12 GHz, but the group delay of Case 1 is a little worse than predicted.

**Table 2.3 Optimized waveguide lengths with corresponding group delay and coupling values for channel filters centered at 12 GHz and with 36 MHz bandwidth**

Case	$L_1$ (mm)	$L_2$ (mm)	Group Delay/(ns)	$R(\Omega)$
1	13.349	25.856	0.79	22.38
2	8.293	26.051	5.00	3.54
3	7.317	26.481	15.00	1.78
4	7.145	26.563	20.00	0.88

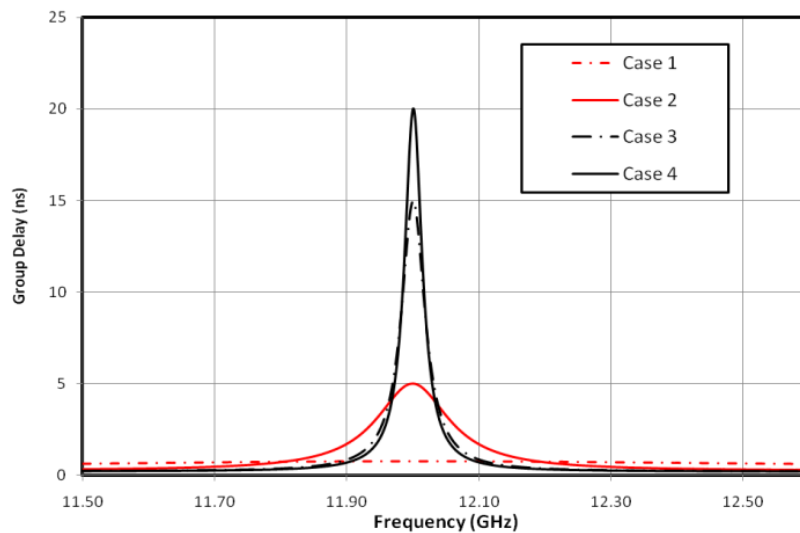


**Fig. 2.8 Group delay response of the equivalent circuit of the H-plane T-junction after optimization. Case 1 to Case 4 in Table 2.2**

In a single channel multiplexer simulation, a 3-port waveguide T-junction is cascaded with one channel filter, expressing as coupling matrix. A four-pole channel filter centered at 12 GHz with 36 MHz bandwidth is attached to the waveguide T-junction. The T-junctions are using dimension from Case 1 to Case 4 in Table 2.3. Parameters in the coupling matrix and the waveguide lengths in channel filters will be all

optimized to obtain required performance in the filter pass-band. After optimization, the return loss and the insertion loss between channel filter and common port are shown in Fig. 2.9.

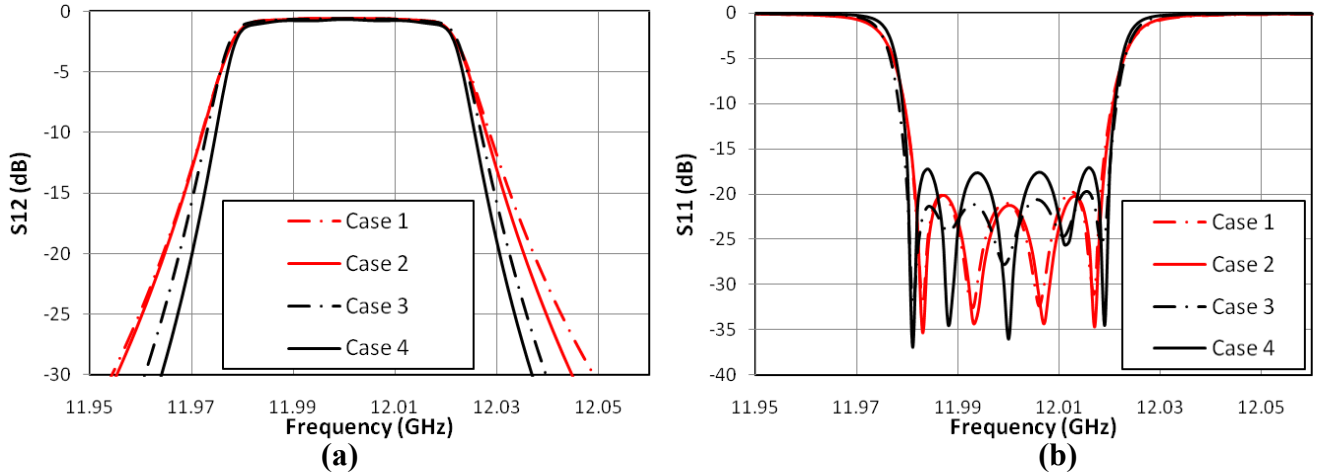


**Fig. 2.9 Comparison of responses of four-pole filters connected with waveguide T-junction in different lengths: (a) insertion loss response; (b) common port return loss.**

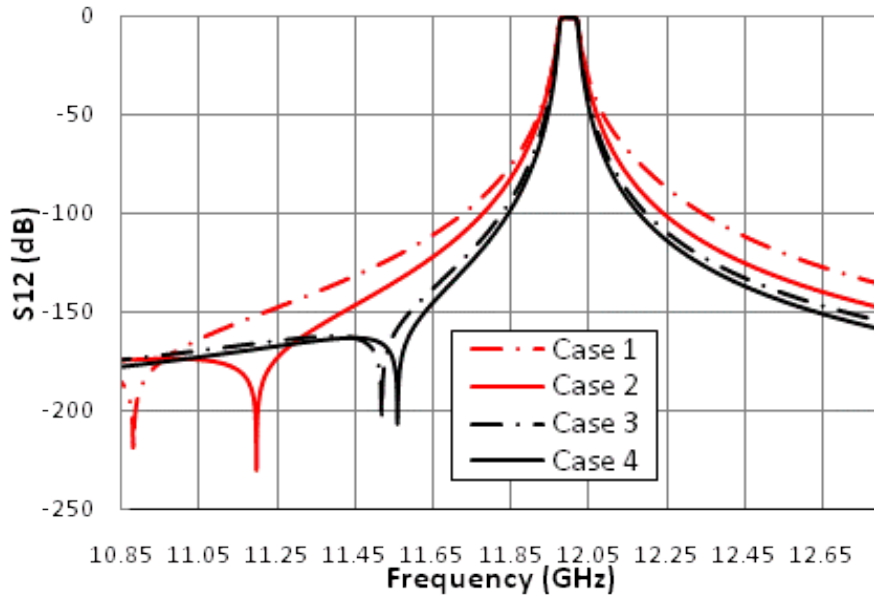


**Fig. 2.10 Far band insertion losses of four-pole filters connected with waveguide T-junctions with different cases in Table 2.2**

Fig. 2.9 (a) shows the near-band response of insertion loss with different T-junction dimensions. Obviously, when a group delay increases or a coupling value

decreases, the improvement of the insertion loss in out-of-band is increased. This implies that the good performance of out-of-band rejection requires small coupling values or large group delays. However, a large group delay causes difficulty to achieve good return loss. Fig. 2.9(b) shows a larger group delay with worse return loss. For example, the return loss  $|S_{11}|$  of the single channel multiplexer of Case 3 with 15 ns group delay, is worse than  $|S_{11}|$  of Case 2 with 10 ns group delay. It can also be seen that, out-of-band rejections still show improvements even though the return losses do not show five stand-alone poles, such as the plot of  $|S_{11}|$  in Case 2. The responses of out-of-band rejection with an extra pole are shown in Fig. 2.10, which shows far-band responses of insertion loss. The extra pole in insertion losses is caused by the length of  $L_1$ . It pulls the out-of-band rejection down when it is close to filter center frequency. For example, the insertion loss  $|S_{21}|$  of the single channel multiplexer in Case 4 with 20 ns group delay, has a closer extra pole and better rejection than  $|S_{21}|$  in Case 3 with 15 ns group delay. A larger group delay definitely has much benefit on the rejection performance, but it brings other problems in multi-channel designs.

## 2.3 Enhanced Multiplexer Design Process

This method can be extended to multi-channel designs. The connecting waveguide T-junctions are designed to bring an extra reflection zero into the pass-band of each channel filter. It creates additional resonator without increasing the order of a channel filter. Taking advantages of a manifold structure, it not only improves the performance of multiplexers, but also maintains its size and weight. The detailed design steps have been concluded as follows[06]:

- (1) Take the manifold with all channel filters replaced by short circuits as a design object, since the channel filters all perform as a short circuit in their out-of-band. Then calculate and optimize the distances between channel filters and manifold waveguide, and the distances between channel filters to obtain required coupling values. After this step, the waveguide T-junction have gained the desired group delay or coupling value at resonance frequency with specific bandwidth.
- (2) Check all the dimensions if they are physically reasonable. A physical dimension must be available to accommodate every channel filter. If not, repeat step 1.
- (3) Attach all single-ended channel filters to the optimal manifold waveguide.
- (4) Optimize all variables to meet performance requirement, including the distances between channel filters, distances between channel filter and manifold, and also internal dimensions of the channel filters.

As demonstrated in Fig. 2.9, the rejection shows better performance with small coupling value or large group delay, whereas it is difficult to obtain large group delay in general. The return loss with large group delay is also hard to achieve high level performance. Besides, the response with large group delay is very sensitive. In Table 2.3, the manifold lengths of 20 ns group delay are close to the ones of 15 ns group delay. Therefore, large group delay should be carefully selected to balance the improvement of out-of-band rejection and pass-band return loss; it cannot be used in all situations of multiplexer designs. Furthermore, in the design of multi-channel multiplexers, the group delay should be relatively low when the number of channel filters increases. A suitable group delay in multi-channel multiplexers design is constraint by the overall size of the

multiplexer, the number of channels and the center frequency and bandwidth of each channel filter.[6]

## 2.4 Example of Non-Contiguous Multiplexer

To extend the design steps from single channel to multi-channel design, a non-contiguous two-channel multiplexer with H-plane T-junction is designed as an example. The first channel of the multiplexer is centered at 12.2 GHz, while the second channel is centered at 12.05 GHz; the bandwidths are both 36MHz.

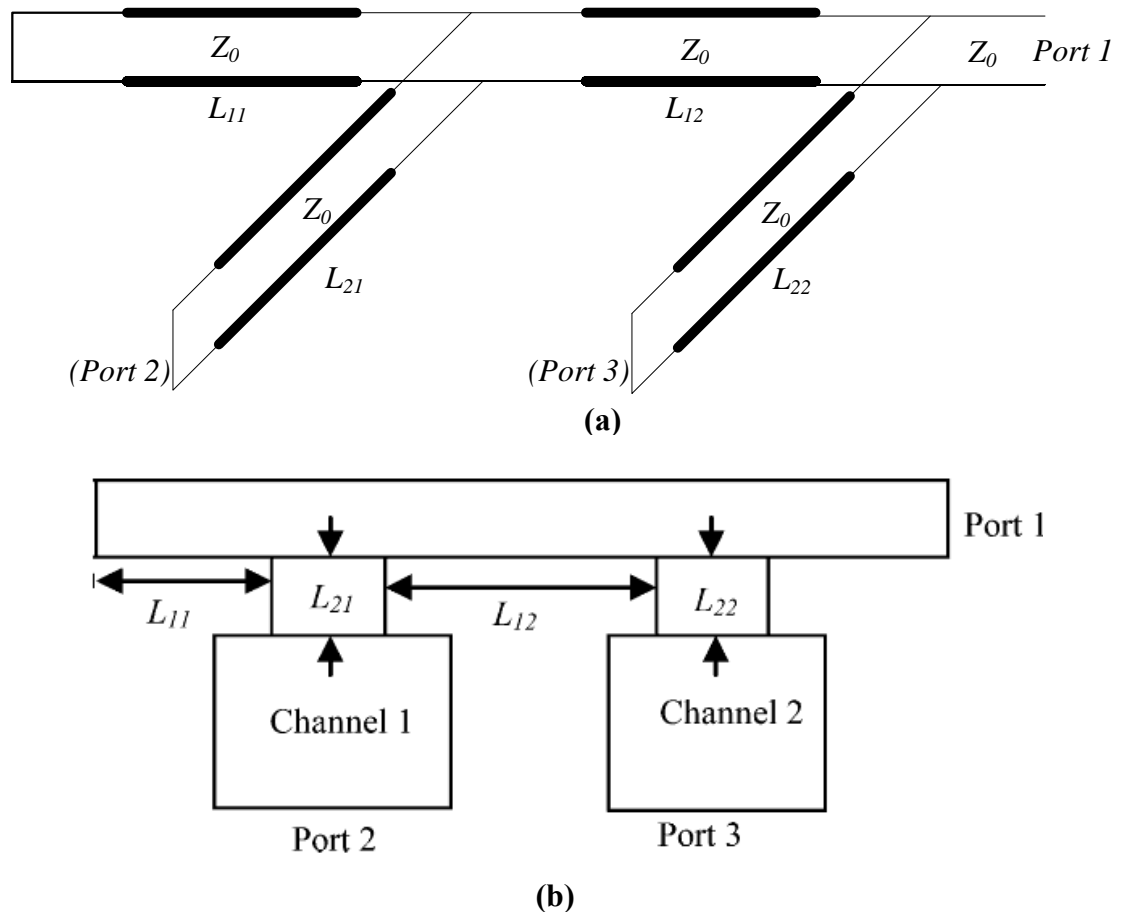
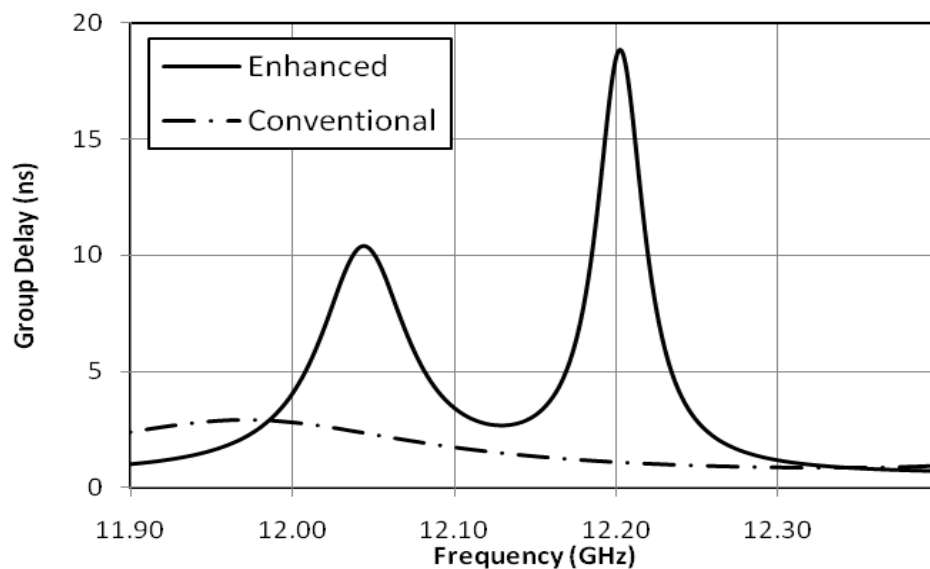


Fig. 2.11 Two-channel multiplexer [06] (a) Simplified equivalent circuit. (b) two channel multiplexer with channel filters.

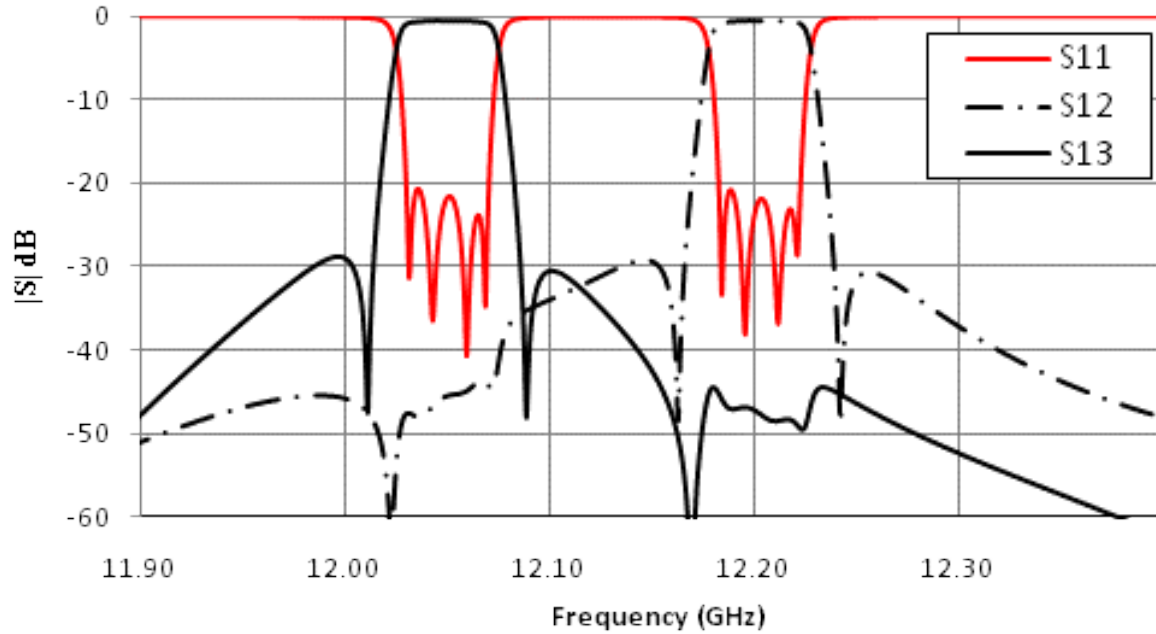
Fig. 2.11(a) shows the simplified equivalent circuit for the manifold waveguide with channel 1 filter (with port 2 as the input port) and channel 2 (with port 3 as the input port) replaced by short circuits. The parameters in the waveguide T-junction are  $L_{11}$ ,  $L_{21}$ ,  $L_{12}$  and  $L_{22}$ . For comparison, the dimension of the manifold designed by conventional technique and the enhanced type of multiplexer design are both listed in Table 2.4. The group delay at common port with proposed method is shown in Fig. 2.12. The proposed curve shows two identical peaks at 12.05 GHz and 12.2 GHz, which are the resonance frequencies of channel filters. Compared to the enhanced method, a relative flat curve of group delay in conventional method is also shown in Fig. 2.12.

**Table 2.4 Manifold Dimension of Two-channel Multiplexer with Conventional Method and Enhanced Method**

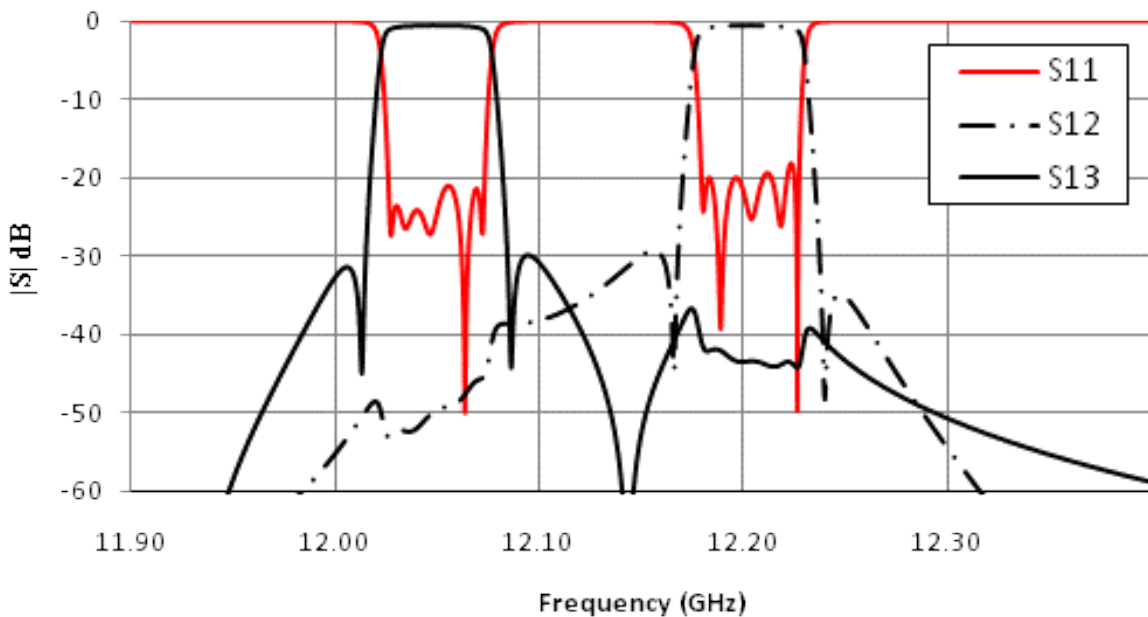
Lengths	Conventional Method	Proposed Method
$L_{11}$ (mm)	28.06	23.66
$L_{21}$ (mm)	24.45	25.73
$L_{12}$ (mm)	56.92	61.71
$L_{22}$ (mm)	23.30	24.96



**Fig. 2.12 Group delay at common port with two channel filters replaced by short circuits.**



(a)



(b)

**Fig. 2.13** Common port return loss  $|S_{11}|$ , the insertion loss between port 2 and the common port  $|S_{12}|$ , and the insertion loss between port 3 and the common port  $|S_{13}|$  of (a) conventional design and (b) the proposed design.

The responses of the two-channel multiplexer (with channel filters attached as shown in Fig. 2.11(b)) are shown in Fig. 2.13. The responses include common port return loss  $|S_{11}|$ , two transmission coefficients  $|S_{21}|$  and  $|S_{31}|$ , one is between port 1 and

port 2, the other one is between port 1 and port 3. The plots in Fig. 2.13 (a) can be seen as a combination of two four-pole channel filters, while using a conventional design in multiplexer. By contrast with Fig. 2.13 (a), the plots in Fig. 2.13 (b) show a combination of two five-pole channel filters, while using the enhanced multiplexing network. The fifth pole is produced by the manifold.

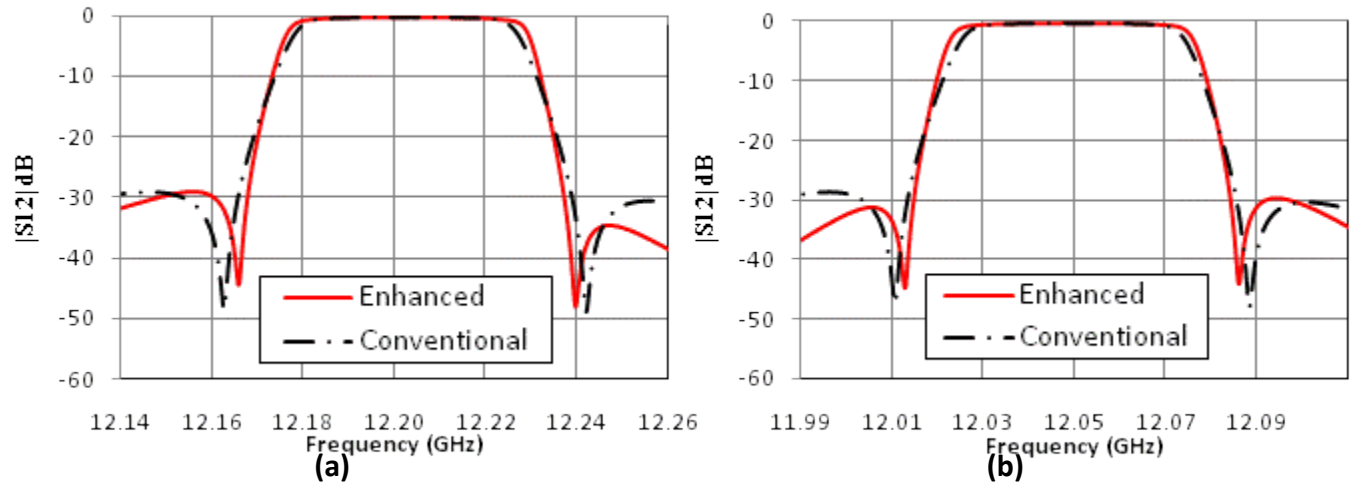


**Fig. 2.14 Comparison of conventional and proposed method (a) the insertion loss for Channel 1 (b) the insertion loss for Channel 2.**

Fig. 2.14 shows more visible improvement in the performance of each channel filter. Individual channel filter is isolated from Fig. 2.13, and the comparison of channel 1 between conventional method and proposed method is shown in Fig. 2.14(a); the comparison of channel 2 between those two methods is shown in Fig. 2.14(b). Obviously, the curve of proposed method in channel 1 achieved wider bandwidth than the conventional method. Without sacrificing the rejection in out-of-band for wider in-band bandwidth, the rejection coefficient is still improved. This is a significant progress, as in conventional design the in-band bandwidth is increased by lower down the quality of rejection, while this method improves both crucial factors at the same time. The insertion loss in channel 2 shows similar improvement. Table 2.5 compares the bandwidth in

different normalized value between the proposed method and the conventional method. The range of usable bandwidth increases from 4.1 MHz to 5.1 MHz.

**Table 2.5 The width of pass-band in each channel filter.**

	Conventional Method	Proposed Method	Difference
Bandwidth over which the normalized $ S_{j1}  > -1.0 \text{ dB}$			
Channel 1	41.8 MHz	45.9 MHz	4.1 MHz
Channel 2	41.9 MHz	46.8 MHz	4.9 MHz
Bandwidth over which the normalized $ S_{j1}  > -1.1 \text{ dB}$			
Channel 1	42.6 MHz	47.1 MHz	4.5 MHz
Channel 2	42.7 MHz	47.7 MHz	5.0 MHz
Bandwidth over which the normalized $ S_{j1}  > -1.6 \text{ dB}$			
Channel 1	45.0 MHz	49.8 MHz	4.8 MHz
Channel 2	45.1 MHz	50.2 MHz	5.1 MHz

## 2.5 Summary

This method enhances the rejection of multiplexer without introducing extra resonator. According to the requirement, changing the distance between the channel filters and the distance between manifold waveguide and channel filter, one can control the pole appear in different resonance frequency with different value. The simulations show the feasibility of this method. Additional pole created in pass-band significantly enhances the performances of rejection, while maintaining the order of the channel filter in the meantime.

This method can not only be used in manifold configuration multiplexer, but also in the other transmission line configurations.

## Chapter 3

# Application of Artificial Neural Network in Spurious Mode Compensation in Multiplexer Design

Spurious modes are important in the design of multiplexer. The responses of spurious modes are unique for different resonators and unrelated to the fundamental. The spurious mode from a channel filter can dramatically damage the multiplexer as the number of channels and the transmission band of a multiplexer increase. Therefore, the simulation of a spurious mode of a channel filter is necessary in the multiplexer designs.

There are three types of models involved in the following discussion: EM model, which is the most accurate but computational intensive; circuit models, e.g. transmission

line model and coupling matrix model for channel filters, which are fast yet with limited accuracy; and Artificial Neural Network (ANN) models, which are developed based on EM data, fast and accurate, when properly trained.

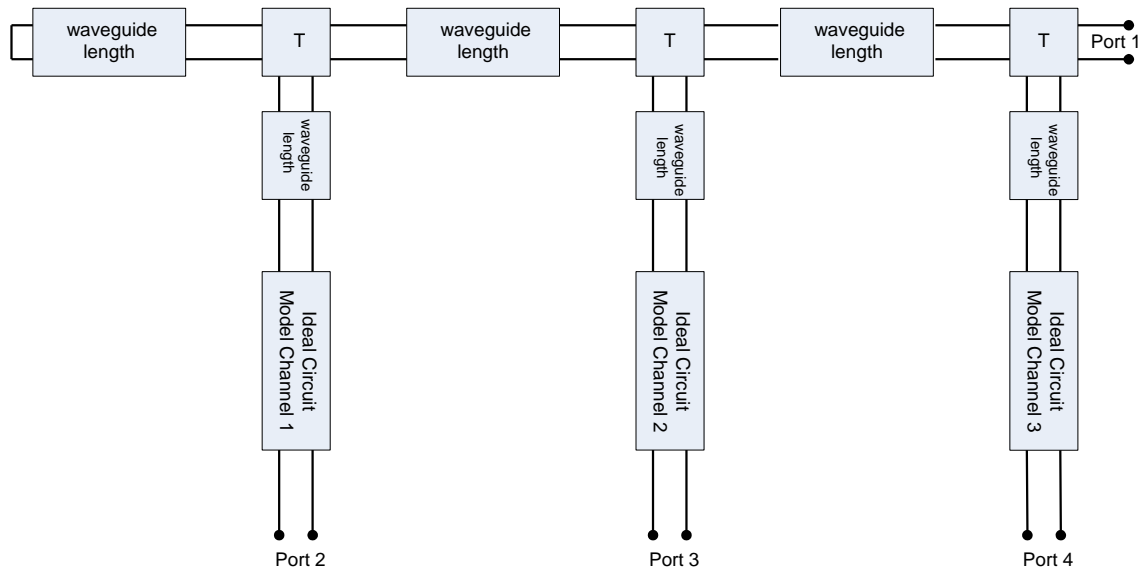


**Fig. 3.1 3-channel output multiplexer**

The spurious mode is considered in [12], since the multiplexer is severely affected by it. In the three-channel multiplexer discussed in [12], a spurious mode from channel filter 1 with low center frequency, disturbs the response of filter 3 with high center frequency. The spurious mode from filter 1 occurs around 12.4 GHz, which is right in the pass band of filter 3. In the method presented in [12] to compensate the effect of the spurious mode, lumped element model is used to model the response of channel 1. The resonance frequencies, the coupling values in the channel filter 2 and filter 3, and the manifold waveguide lengths, are then optimized to compensate the spurious mode. However the method cannot be easily generalized for filters with any center frequency or bandwidth. A new lumped-element model would need to be re-generated.

In this chapter, we present a new method to model the spurious mode with application of Artificial Neural Network (ANN). The neural models are developed based on EM data. Due to the fact that generation of EM data is very time consuming, we simplify the filter model to have the minimum structural features, yet still capable of modeling the effect accurately. In doing so, the number of variables is reduced to minimum, which significantly reduces the cost of EM data generation for neural model training and testing. It enables the modeling of filter structures covering a wide frequency range, which also increases flexibility of the model.

The three-channel multiplexer shown in Fig. 3.1 is used as an example to demonstrate this method. The multiplexer consists of three manifold waveguide T-junctions and three channel filters. In Fig. 3.1, the letter ‘T’ in the figure represents an EM model of the waveguide T-junction. In the triplexer, a classical circular waveguide dual mode filter, which is shown in Fig. 3.2, is applied in each channel. This type of filter has a interconnecting iris between cavities and three tuning screws in the middle of each cavity. Fig. 3.3 shows the relations between the mode polarization vectors and tuning screws, coupling screws, and coupling irises. The screw at  $45^\circ$  angle from the polarization axes is used to couple the dual modes in the same cavity, while the other two tuning screws are used for adjusting resonant frequencies. The interconnecting iris couples the modes between different cavities. A rectangular waveguide, used as an input/output, is placed at the end of the cavities. The three 4-pole filters are listed as follow:

- Filter 1 (Channel 1) :  $f_{01} = 12700 \text{ MHz}$ ,  $BW_{01} = 29.8 \text{ MHz}$
- Filter 2 (Channel 2) :  $f_{02} = 11656 \text{ MHz}$ ,  $BW_{02} = 26.0 \text{ MHz}$
- Filter 3 (Channel 3) :  $f_{03} = 11037 \text{ MHz}$ ,  $BW_{03} = 26.0 \text{ MHz}$

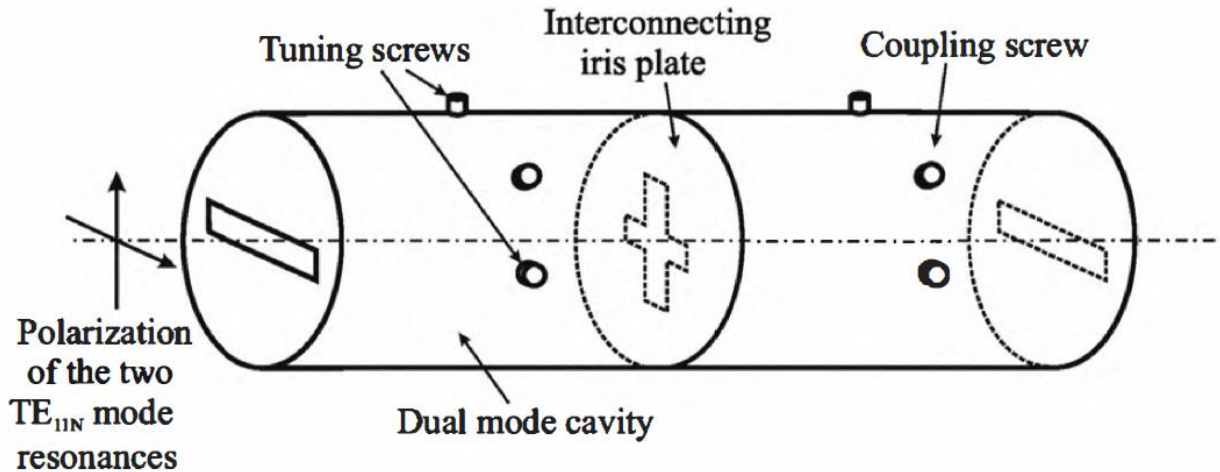


Fig. 3.2 Classical configuration of a dual mode filter [01]

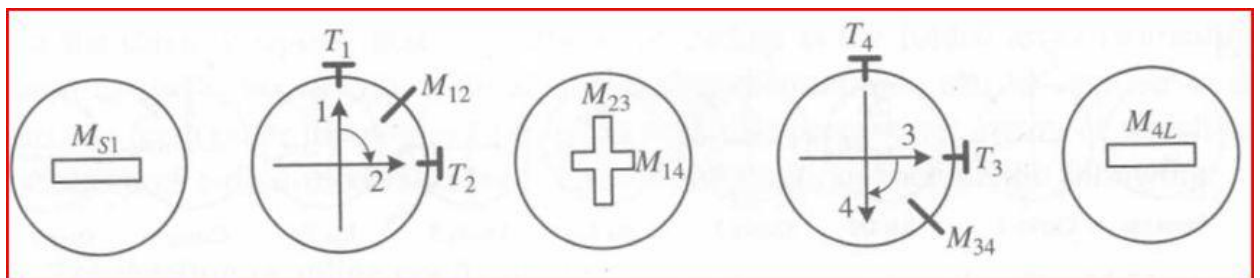


Fig. 3.3 The relations between the mode polarization vectors and tuning screws, coupling screws, and coupling irises. [01]

### 3.1 Tuning a 4-pole Filter

The purpose of this chapter is to simulate the response of filter 3, which has the lowest center frequency, in out-of-band frequencies. Thus, manifold transmission lines (not waveguide T-junctions), filter 1 and filter 2 are all using the ideal circuit based models. Filter 3 and waveguide E-plane T-junctions adopt the EM data in the following analysis. Before starting the investigation, a well tuned filter should be prepared for filter 3. Accordingly, the process of tuning a classical dual mode filter model is presented in

this section to meet the specifications of filter 3 using Computer Simulation Technique (CST) Microwave Studio [19] as an EM simulator.

### 3.1.1 Analyze a Classical Dual Mode filter

The EM model used for channel 3 is a 4-pole dual mode filter. There are two input/output irises, two cavities with six tuning screws, and an interconnecting iris between two cavities. The width of each iris and the lengths of cavities are fixed. The lengths of iris and the depth of tuning screws are optimized. There are ten variables in this filter can be optimized to meet requirements. As previously introduced, channel 3 is a 4-pole filter with 26 MHz bandwidth at the center frequency of 11037 MHz.

Fig. 3.4 shows the EM model of the 4-pole dual mode filter with physical dimensions related to a  $[N+2]$  ( $N$  is the order of the filter) coupling matrix, which is shown in the following equation [01]:

$$M = \begin{bmatrix} 0 & M_{S1} & 0 & 0 & 0 & 0 \\ M_{S1} & M_{11} & M_{12} & 0 & M_{14} & 0 \\ 0 & M_{12} & M_{22} & M_{23} & 0 & 0 \\ 0 & 0 & M_{23} & M_{33} & M_{34} & 0 \\ 0 & M_{14} & 0 & M_{34} & M_{44} & M_{4L} \\ 0 & 0 & 0 & 0 & M_{4L} & 0 \end{bmatrix} \quad (3.1)$$

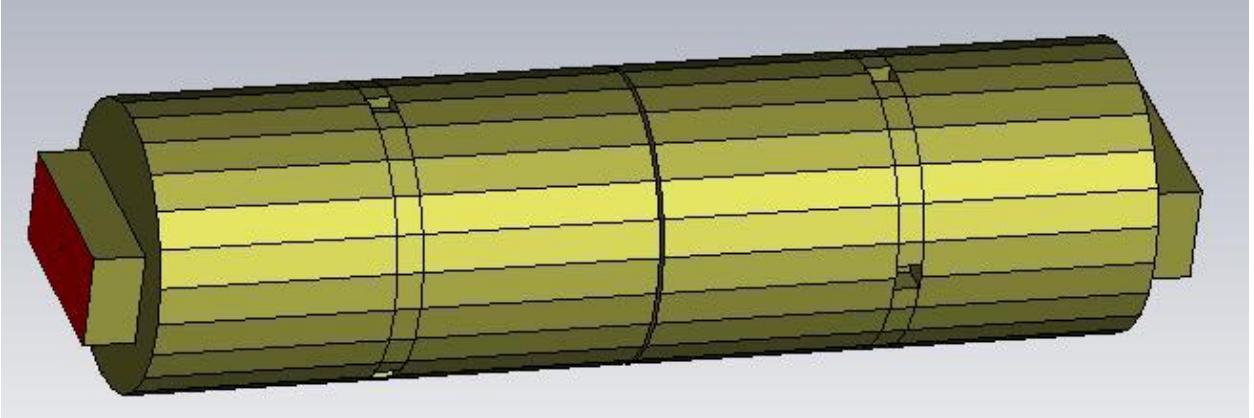


**Fig. 3.4 The configuration of a 4-pole dual mode filter in CST.**

The entries on the main diagonal line of M-matrix are self-coupling  $M_{i,i}$  ( $i = 1, \dots, 4$ ). The mainline coupling are referred to  $M_{i,i+1}$  ( $i = 1, \dots, 3$ ), which is the coupling between sequentially numbered nodes, and  $M_{1,4}$ , which is cross-coupling between the non-sequentially numbered nodes.  $M_{S,1}$  and  $M_{4,L}$  are related to the mainline coupling from the source to the first resonator node and the mainline coupling from the last resonator node to the load termination. Because the network is reciprocity, the matrix has  $M_{i,j} = M_{j,i}$ . Other coupling values are zeros. The terminating impedances are expressed as

$$R_S = M_{S1}^2 \quad \text{and} \quad R_L = M_{4L}^2 \quad (3.2)$$

The values of N+2 coupling matrix are shown in (3.3). It is an ideal 4-pole coupling matrix used in the 3-channel multiplexer. After optimization of the EM model, the responses generated from the EM model, i.e. S-parameters, should match the responses from the ideal coupling matrix.

$$M = \begin{bmatrix} 0.0000 & 0.9271 & 0.0000 & 0.0000 & 0.0000 & 0.0000 \\ 0.9271 & 0.2519 & 0.9116 & 0.0000 & -0.1289 & 0.0000 \\ 0.0000 & 0.9116 & -0.0002 & 0.7666 & 0.0000 & 0.0000 \\ 0.0000 & 0.0000 & 0.7666 & -0.0104 & 0.9288 & 0.0000 \\ 0.0000 & -0.1289 & 0.0000 & 0.9288 & -0.0237 & 1.0884 \\ 0.0000 & 0.0000 & 0.0000 & 0.0000 & 1.0884 & 0.0000 \end{bmatrix} \quad (3.3)$$

In the next, we tune the filter according to the ideal coupling matrix.

### 3.1.2 Tune a Filter with Matlab Program

Comparing the EM results of the filter model and Matlab plots of the ideal coupling matrix, it is obviously shown in Fig. 3.5 that the EM model is only a rough design which still needs tuning on each variable to match the response of the ideal coupling matrix. A Matlab program is used to extract a coupling matrix of the EM model in this section. The parameter extraction is part of Space mapping technology [13].

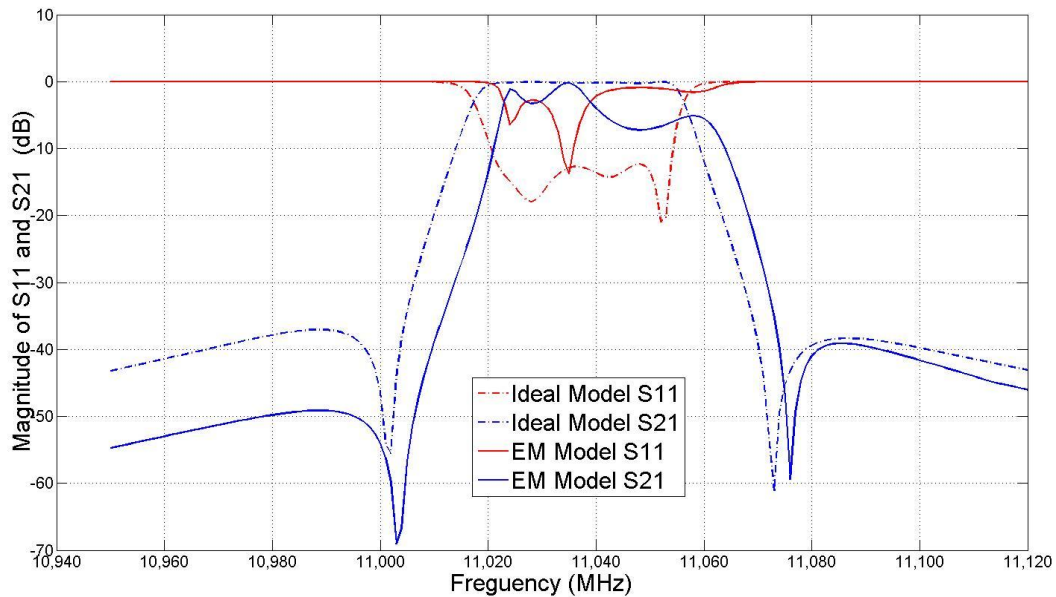


**Fig. 3.5 Comparison between an ideal coupling matrix and an un-tuned EM model of the 4-pole dual mode filter.**

Space Mapping is an optimization technique which needs two models: one is coarse model, the other one is fine model. The theory of Space Mapping is to use a coarse model to find optimization results, and then use a fine model to test the results. During this process, if the error after the testing in the fine model was over a certain tolerance, the error returns to the coarse model for another re-optimization is performed to gain a new result. The new result would be re-send to fine model for testing. Space Mapping repeats these steps until the error is lower than a user define.

In Space Mapping, a coarse model needs to be simple and fast. The accuracy of a coarse model is not critical. Here we use the coupling matrix as the coarse model in a filter tuning process, which will be applied in a Matlab program. On the other hand, a fine model must be accurate and thus usually very time-consuming. The fine model used in the filter tuning step, is an EM simulator. The Space Mapping technology establishes a mathematical link (mapping) between the spaces of the design parameters of two models: the accurate and time-intensive fine model and the less accurate but fast coarse model.

Fig. 3.6 presents a fine and coarse model. In the figure,  $x_f$  is a vector of parameters in fine model, which represent the dimensions of the filter; and  $x_c$  is a vector of parameters in coarse model, which represent the value of coupling matrix. The responses of a coarse model and fine model denoted by  $R_c(x_c)$  and  $R_f(x_f)$ , respectively, are also shown in Fig. 3.6. The space mapping between two models is denoted as  $x_c = P(x_f)$ , when  $|R_f(x_f) - R_c(x_c)|$  is minimized. This step is so-called parameter extraction.

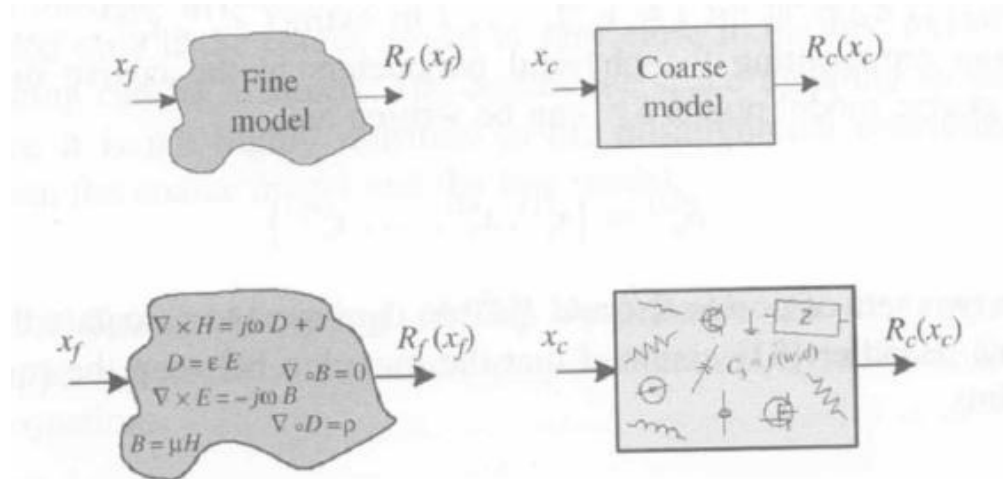


**Fig. 3.6 Representation of the fine and coarse models [01]**

In this section, we use the concept of Space Mapping, instead of a strict implementation of the algorithm. Therefore, we do not try and build the exactly space mapping  $x_c = P(x_f)$  between two models, but to optimize the coarse model parameters  $x_c$  to minimize the difference  $|R_f(x_f) - R_c(x_c)|$  between responses of two models, i.e. the parameter extraction step in space mapping. Then the extracted coarse model parameter  $x_c^*$ , which is a coupling matrix, is compared with the ideal coupling matrix, which is shown in (3.3), in order to find the next tuning step on the fine model parameters  $x_f$ , which are dimension of a dual mode filter. With new fine model parameters, repeat the previous steps to see how the extracted coarse parameters change. It takes several iterations to make the coarse parameters close to the values of ideal coupling matrix.

Before using a Matlab program to extract the related coupling matrix, a phase loading should be considered in the parameter extraction, which is caused by the input/output iris. It has been proven by [15] that a constant phase can be found by comparing S-parameters of the measurement and the corresponding circuit model. The

phases of  $S_{11}$  and  $S_{22}$  in far band should be symmetric about zero degree in circuit model. It is easy to remove the loading phases by comparing the phases of  $S_{11}$  and  $S_{22}$  at their symmetric positions. The loading phases will be subtracted from S-parameters before they are used in the parameter extraction. To ensure the accuracy, a phase is expressed as

$$\theta = \frac{2\pi}{\lambda_g} \cdot l$$

where ' $l$ ' represents the length of waveguide, and the guided wavelength  $\lambda_g$  varies by the frequency. Calculated results show that the lengths of  $S_{11}$  and  $S_{22}$  are 0.0516 inch and 0.0658 inch, respectively.

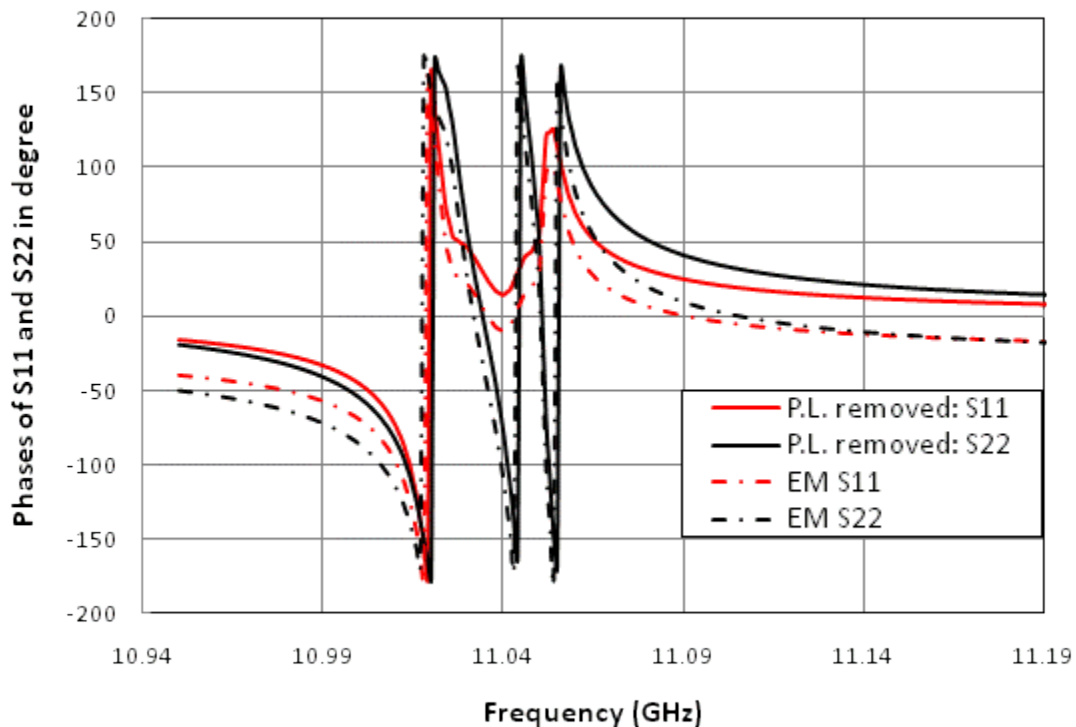
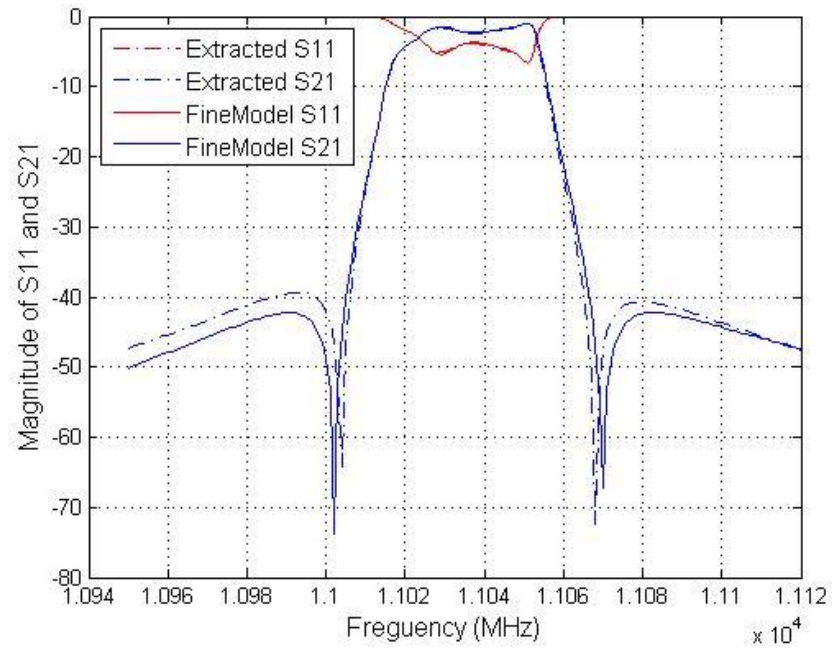


**Fig. 3.7 Comparison between the Phases of  $S_{11}$  and  $S_{21}$  w/o loading phase from the simulation of a dual mode filter.**

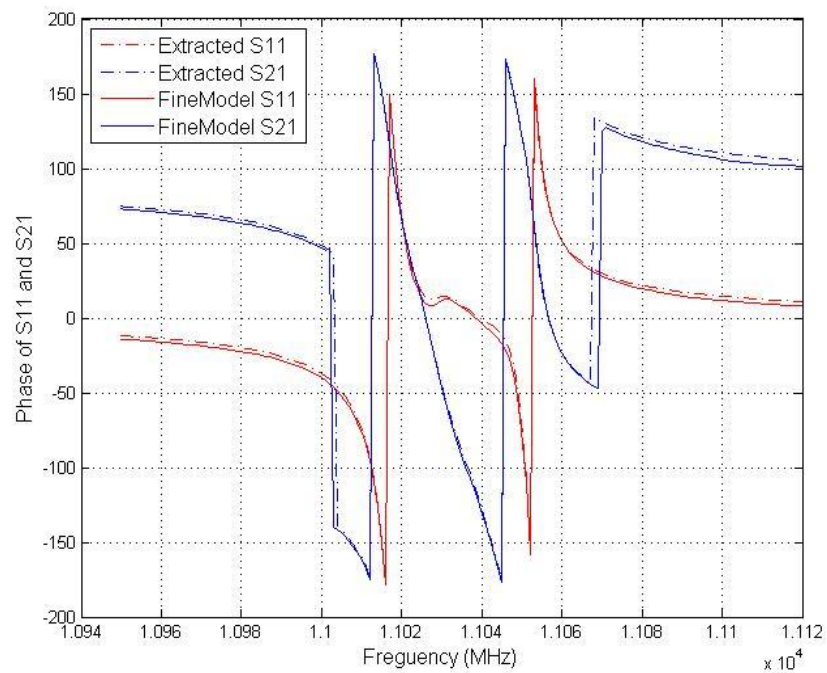
Fig. 3.7 shows the simulation results of an EM model with and without the loading phase and without it. After deleting the extra lengths, the plots of phases from  $S_{11}$  and  $S_{22}$ , are symmetrical to zero degree line. Within these steps, the S-parameters are ready to be used in the parameter extraction.

A Matlab program is used to extract the coarse model parameters, or a coupling matrix, from the response of a fine model. The algorithm in the program is *fmincon*, which is a function to find the minimum of the constrained nonlinear multivariable. The initial values of this optimization are set to be the ideal coupling matrix, which is shown in (3.3), for the first iteration. Then the following iterations use the previous extracted coupling matrix as the initial values. Ten coarse model parameters shown in (3.1) are constrained in a reasonable range, i.e.  $-1 \leq M_{14} \leq 0$  ,  $-1 \leq M_{23} \leq 1.5$  . The error function in the optimization is expressed as the differences between phases, and between magnitudes of S-parameters in the pass-band.

From the first iteration, the plots of an extracted coupling matrix after optimization cannot match the response of the fine model as well as expected, which means the extracted coupling matrix is not very accurate. Manual adjustment of the coupling matrix has been tried, which helps to bring coarse model response get closer to the response of the fine model. After repeatedly tuning the filter in EM model and exacting coupling matrix several iterations, the plots in Fig. 3.8 still shows differences between the responses of the extracted coupling matrix, and the ones of fine model. In addition, the extracted coupling matrix still shows unreasonable change when tuning the related dimension of the filter. This in-accuracy is due to the algorithm, which is not adequate. Another better method of parameter extraction is needed.



(a)



(b)

**Fig. 3.8 Comparison between response of fine model and response of extracted coupling matrix (a) The return loss and insertion loss in magnitude (b) The return loss and insertion loss in phase.**

### 3.1.3 Tune a Filter with Agilent ADS

[14] has implemented the Space Mapping technique into the Agilent Advanced Design System (ADS) design, as the Agilent ADS provides visible designs and multiple optimizations. This section will follow the steps in [14] on parameter extraction and illustrate an Agilent ADS design schematic in tuning process.

Step 1) Set up a coarse model in the Agilent ADS. The coarse model is cascading with J-inverters, which represents each coupling value.

Step 2) Import the fine model data into Agilent ADS. The data file in the S2P component is the responses of the filter generated from EM simulator. In Fig. 3.9, the fine model data has already removed the loading phase to guarantee the accuracy.

Step 3) Set initial values of the coarse model parameters and optimize them. The coarse parameters are variables of the coupling matrix. In Fig. 3.9, the coupling values all work as inverters. In the first optimization iteration, the initial values will be set with the ideal coupling matrix. In the subsequent iterations, the initial values can be set as the previous optimization results. The goals are to match the phases and magnitudes of a coarse model, to the fine model. Quasi-Newton and gradient algorithms are selected to optimize all the parameters. The goals and optimum setting are shown in Fig. 3.9.

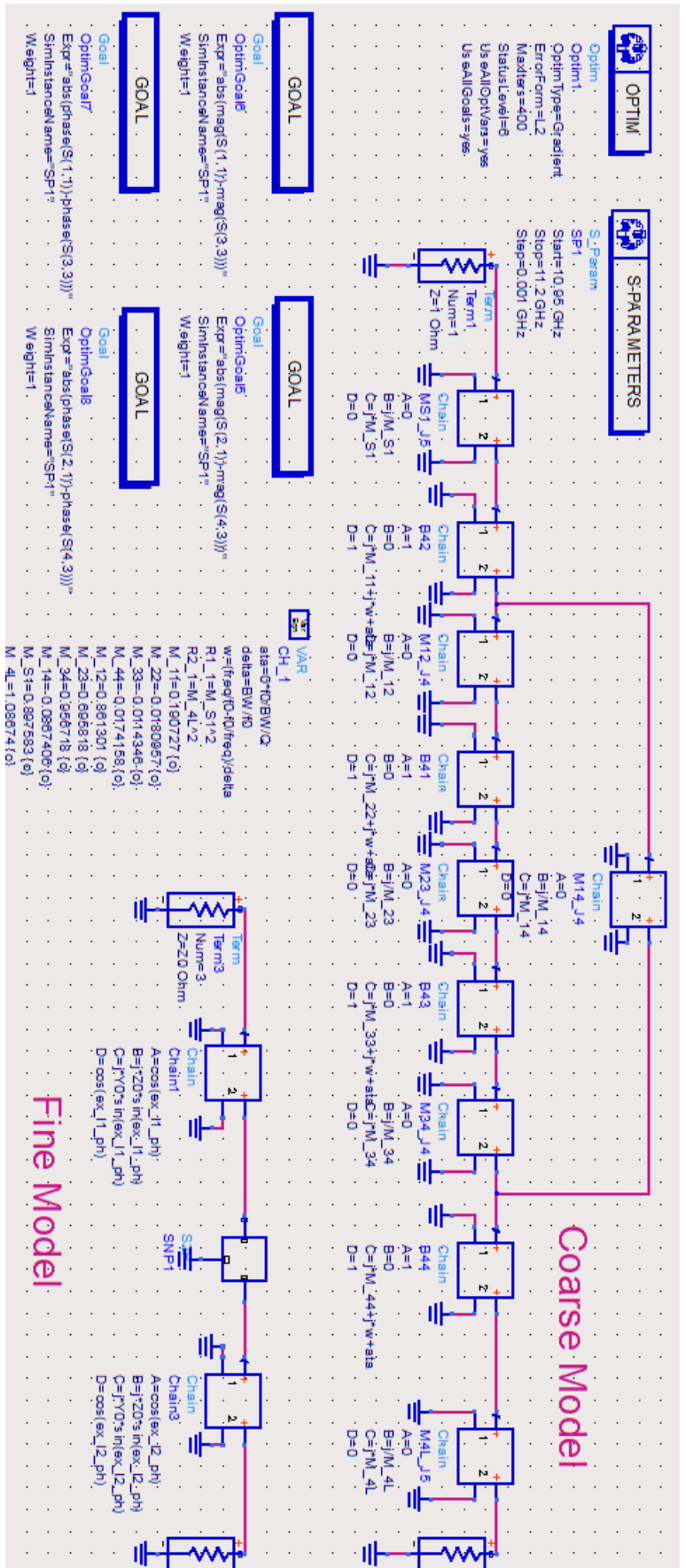


Fig 3.9 Calibration of the coarse model of a 4-pole filter. This schematic extracts pre-assigned coarse parameters  $x$ . the coarse and fine model have been pointed in the figure. The goal is to match the coarse and fine model phases and magnitudes of S11 and S21 from 10.95 GHz to 11.2 GHz. The optimization algorithm uses the Gradient method.

Step 4) Predict the next solution of the fine model by comparing the extracted coupling matrix and the ideal coupling matrix. Tune the related screws or irises to improve the responses of the filter closer to the ideal response.

Step 5) Update the fine model data file in the fine model of ADS schematic; repeat step 3 and step 4 until the responses of the filter are satisfactory.

After several iterations, the extracted coupling matrix is getting close to the ideal matrix, while the responses of the 4-pole filter are getting better. Fig. 3.10 shows the responses of the extracted coupling matrix and the ones of the EM simulation. Those two curves overlap perfectly to each other. Besides, the extracted coupling matrix is expressed as:

$$M = \begin{bmatrix} 0.0000 & 0.9140 & 0.0000 & 0.0000 & 0.0000 & 0.0000 \\ 0.9140 & 0.2773 & 0.8787 & 0.0000 & -0.1289 & 0.0000 \\ 0.0000 & 0.8787 & -0.0274 & 0.6952 & 0.0000 & 0.0000 \\ 0.0000 & 0.0000 & 0.6952 & -0.0031 & 0.9230 & 0.0000 \\ 0.0000 & -0.1289 & 0.0000 & 0.9230 & -0.0260 & 1.0562 \\ 0.0000 & 0.0000 & 0.0000 & 0.0000 & 1.0562 & 0.0000 \end{bmatrix} \quad (3.4)$$

Obviously, the extracted result is very close to the ideal coupling matrix. Therefore this parameter extraction model is reliable, and the tuned 4-pole filter will be used in the following sections.

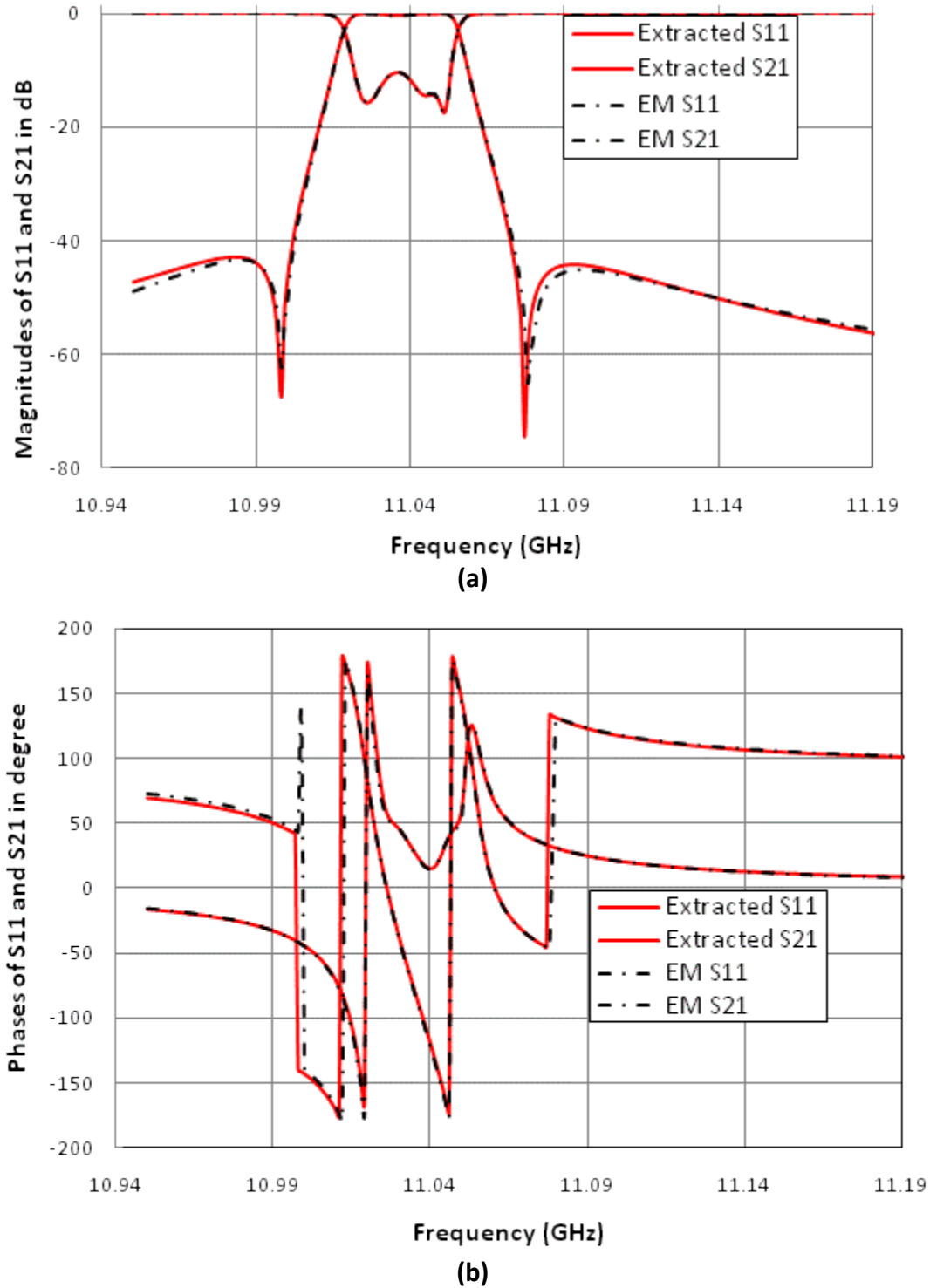
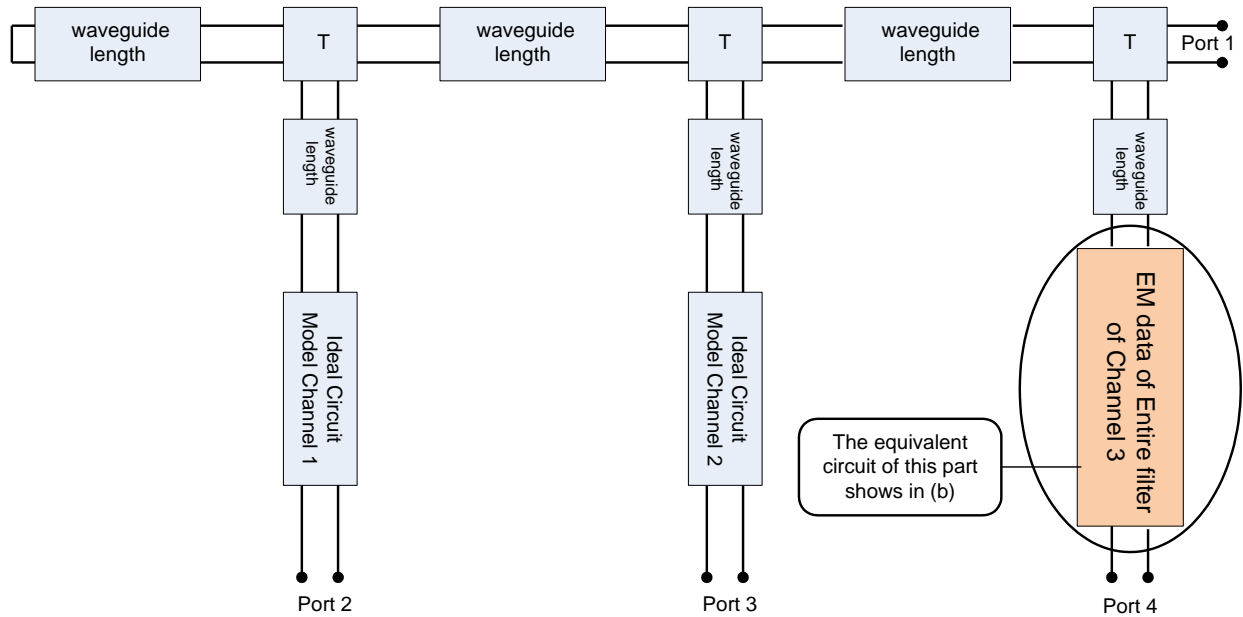
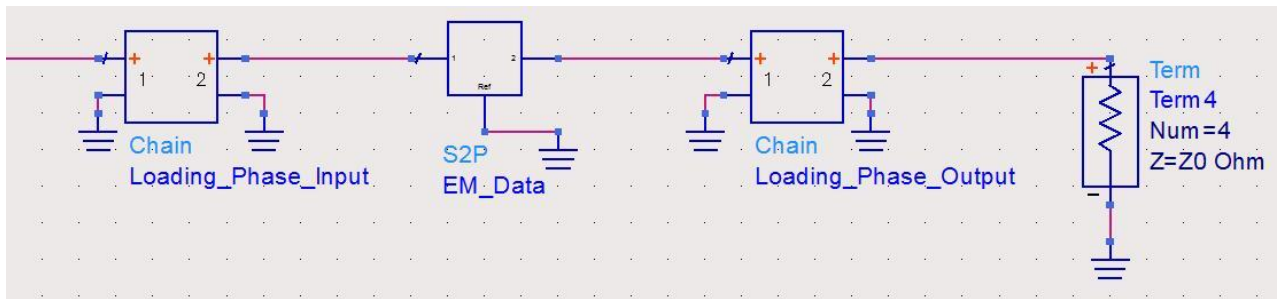


**Fig. 3.10 Comparison between responses of extracted coupling matrix and EM results. (a) Comparison between Magnitudes of S11 and S21. (b) Comparison between Phases of S11 and S21.**

## 3.2 Simplify a Low Center Frequency Channel



(a)



(b)

**Fig. 3.11 Three channel output multiplexer with EM Model (a) Simplified equivalent circuit model with EM model at port 4. (b) Equivalent circuit model of EM model in ADS.**

As explained at the beginning of this chapter, a channel with low center frequency usually brings a spurious mode into the high transmission bands. Fig. 3.11 shows a three-channel multiplexer with EM data in channel 3, which is at low center

frequency. In Fig. 3.12, the insertion loss of an ideal channel 3 shows high rejection in out-of-band, but the responses of EM simulated channel 3 obviously affect channel 1 in high frequency, and slightly affect channel 2.

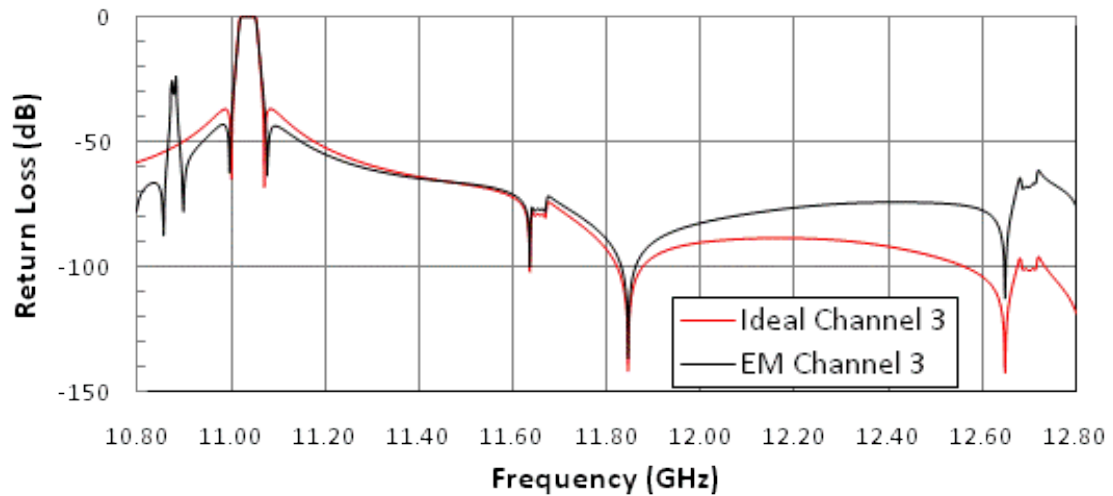


**Fig. 3.12 Comparison of Insertion Losses of Ideal and EM model of Channel 3.**

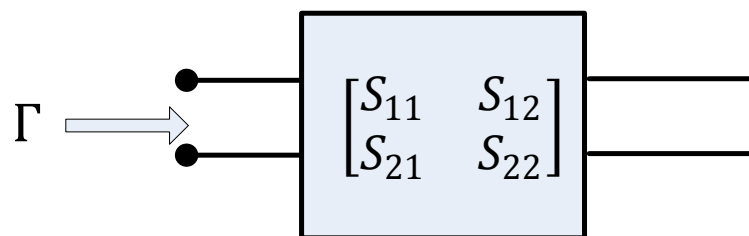
If the full wave EM response of the whole filter was used to provide the effect in out-of-band frequency, the simulation was no doubt the most accurate result. However the full EM simulation on entire filter, include meshing and wide band sweep, will take more than half an hour to get precise responses. Optimization using the EM simulator is not practical. We propose the use of the article neural network in design simulation and optimization. The collection of training and testing data for ANN is the main issue. It could take incredibly long time, because the training and testing data are generated by EM simulators, especially when the number of variables is large. However, it is not necessary to use the entire filter to simulate the responses in high frequency, as only part of the filter mainly effects the out-of-band rejection. Simulating the crucial part of the filter can accurately predict the responses in out-of-band frequency. The spurious mode occurs in out-of-band frequency mostly depends

on the phase of the reflection coefficient of the channel filter. In the following, we prove that using the first inverter and resonator of the filter, the spurious mode effect can be captured. The effort of data collecting is thus significantly reduced, which enables the development of ANN models for this application.

### 3.2.1 Equivalent Circuit Model with Different Orders of Inverters

The purpose in the deduction is to demonstrate that the phases in short-circuited network with different order of inverters have the same responses in out-of-band frequency. The characteristic of the first inverter can fully represent the phase of the whole circuit network. There are two parts in this section to prove the assumption. The first part proved the phase of a short-circuited network is equal to the phase of  $S_{11}$  in a match-load-circuited network, when both models have the same components; the second part proved the phase of  $S_{11}$  in a two-port network is only related to the value of the first inverter in a circuit model.

#### I. Phase in short-circuited model and match-load-circuited model



$$\Gamma = S_{11}$$

**Fig. 3.13** A two-port network with port 2 short-circuited.

As shown in Fig. 3.13, assuming the S-parameters in a two-port network is

$\begin{bmatrix} S_{11} & S_{12} \\ S_{21} & S_{22} \end{bmatrix}$ , the reflection coefficient  $\Gamma$  can be expressed as:

$$\begin{aligned} \Gamma &= S_{11} - \frac{S_{12} \times S_{21}}{1 + S_{22}} \\ &= \frac{S_{11} + S_{11} \times S_{22} - S_{12} \times S_{21}}{1 + S_{22}} \end{aligned} \quad (3.6)$$

In general,  $\Gamma$  is different from  $S_{11}$ . However for band-pass or low-pass filter,  $|S_{12}| = |S_{21}| \approx 0$  in out-of-band, then we have

$$\Gamma \approx S_{11} \quad (3.7)$$

Therefore, the phase of  $S_{11}$  can represent the phase of reflection coefficient in out-of-band frequencies, when port 2 of the channel filter is short-circuited. This conclusion will be used in the following filter model simplification.

## II. Reduction of Filter Order

This part compares the phases from the networks with both two inverters (one pole filter) and three inverters (two pole filter). A low-pass filter prototype will be treated before the discussion of a band-pass filter.

### A. Low-pass Prototype

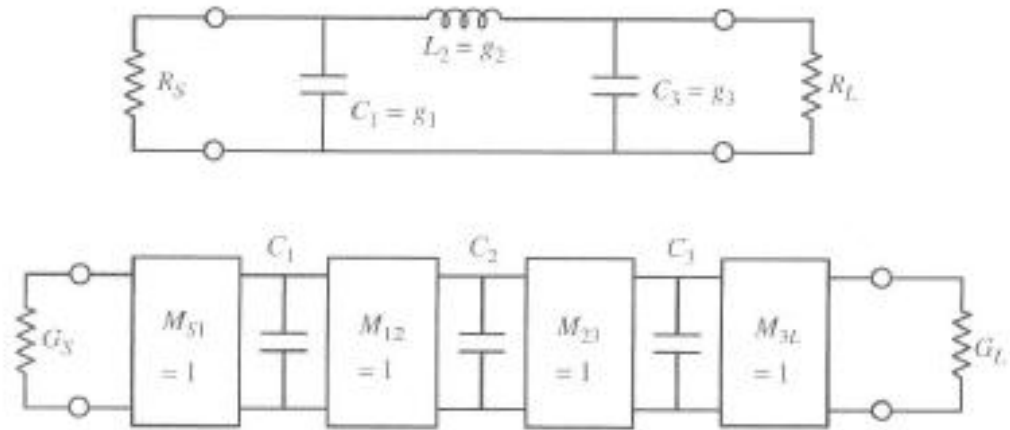


**Fig. 3.14 Third-degree low-pass prototype ladder networks: the form after addition of the unit inverters [01]**

Fig. 3.14 from [01] shows on the process of modifying low-pass prototype filters to immittance inverters model. The low-pass filter consists with inverters and capacitors. All inverters used in this part are unit inverters before normalizing capacitors and inductors; the cutoff frequency  $\omega_c$  is 1 for prototype low-pass filter. The inverters and capacitors are expressed in [ABCD] matrix as:

$$J_N = \begin{bmatrix} 0 & j/J_N \\ j * J_N & 0 \end{bmatrix} \quad , \quad C_N = \begin{bmatrix} 1 & 0 \\ \frac{j\omega g_n}{\omega_c} & 1 \end{bmatrix} \quad (3.8)$$

where  $J_N = 1$  .

Fig. 3.15 is a simplified schematic from a low-pass filter prototype keeping only one inverter and one resonator in the circuit-based model. The cascaded result is:

$$\begin{bmatrix} A & B \\ C & D \end{bmatrix} = \begin{bmatrix} 0 & \frac{j}{J_1} \\ j * J_1 & 0 \end{bmatrix} \times \begin{bmatrix} 1 & 0 \\ \frac{j\omega g_1}{\omega_c} & 1 \end{bmatrix}$$

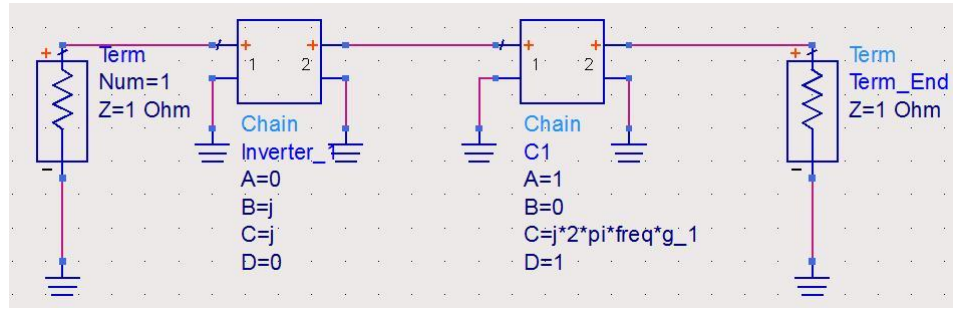


**Fig. 3.15 Simplest low-pass prototype schematic with one inverter and one resonator in Agilent ADS**

$S_{11}$  is calculated in the following equation,

$$S_{11} = \frac{A + \frac{B}{Z_0} - CZ_0 - D}{A + \frac{B}{Z_0} + CZ_0 + D} \quad (3.9)$$

Simplifying (3.9) with  $\left(\frac{\omega_c}{\omega}\right)^2 = 0$ , when  $\frac{\omega_c}{\omega} \leq 0.015$ , the result can be written as

$$\tan_{\text{inverers}}(\phi) = \frac{\text{img}}{\text{real}} \approx \frac{2J_1^2}{g_1} \left(\frac{\omega_c}{\omega}\right) \quad (3.10)$$

Fig. 3.16 is the schematic of a low-pass filter prototype with two inverters and one resonator in Agilent ADS. The cascaded result is:

$$\begin{bmatrix} A & B \\ C & D \end{bmatrix} = \begin{bmatrix} 0 & j \\ j * J_1 & 0 \end{bmatrix} \times \begin{bmatrix} 1 & 0 \\ \frac{j\omega g_1}{\omega_c} & 1 \end{bmatrix} \times \begin{bmatrix} 0 & j \\ j * J_2 & 0 \end{bmatrix}$$

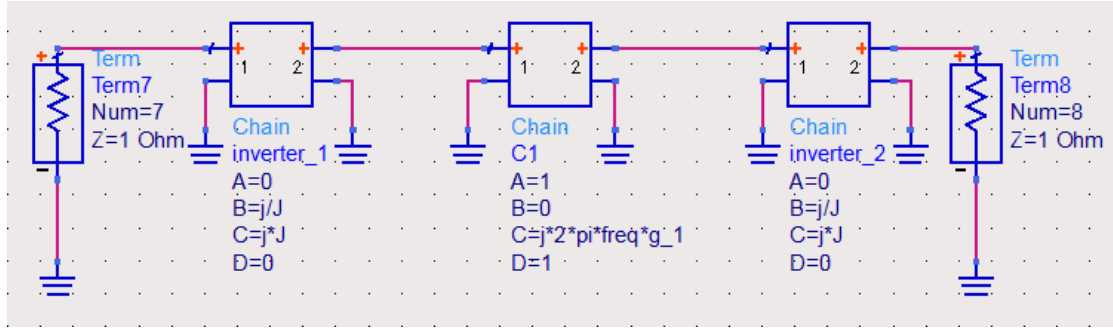


Fig. 3.16 Low-pass prototype schematic with two inverters in Agilent ADS

Reuse (3.9) with  $(\frac{\omega_c}{\omega})^2 = 0$ , when  $\frac{\omega_c}{\omega} \leq 0.015$ , and the result can be approximated as

$$\tan_{2inverers}(\phi) = \frac{img}{real} \approx \frac{2J_1^2}{g_1} \left( \frac{\omega_c}{\omega} \right) \quad (3.11)$$

After getting the phase of reflection coefficient of the 2-inverter circuit network, the 3-inverter circuit model is calculated for comparison. Fig. 3.17 is the schematic of a low-pass filter prototype with three inverters. The cascaded result is:

$$\begin{bmatrix} A & B \\ C & D \end{bmatrix} = \begin{bmatrix} 0 & j/J_1 \\ j*J_1 & 0 \end{bmatrix} \times \begin{bmatrix} 1 & 0 \\ j\omega g_1 & 1 \end{bmatrix} \times \begin{bmatrix} 0 & j/J_2 \\ j*J_2 & 0 \end{bmatrix} \times \begin{bmatrix} 1 & 0 \\ j\omega g_2 & 1 \end{bmatrix} \times \begin{bmatrix} 0 & j/J_3 \\ j*J_3 & 0 \end{bmatrix}$$

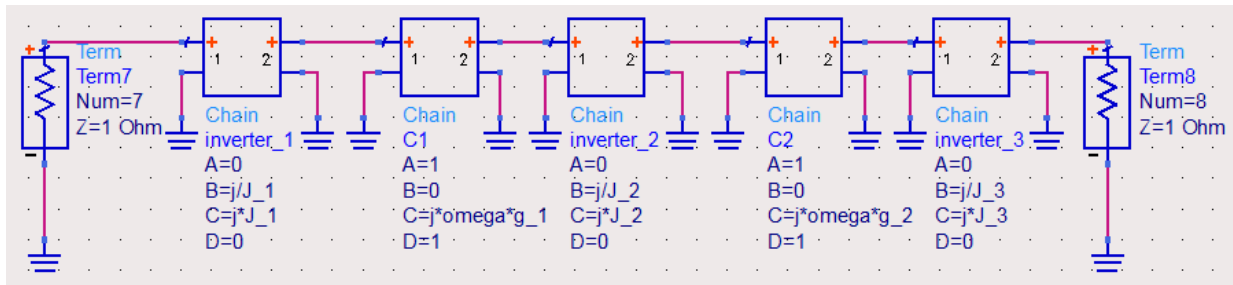


Fig. 3.17 Low-pass prototype schematic with three inverters in Agilent ADS

Reuse (3.9) to find  $S_{11}$ , and simplify it with the same condition:  $(\frac{\omega_c}{\omega})^2 = 0$ , when  $\frac{\omega_c}{\omega} \leq 0.015$ . The result is:

$$\tan_{3inverters}(\phi) = \frac{img}{real} = \frac{2J_1^2}{g_1} \left( \frac{\omega_c}{\omega} \right) \quad (3.12)$$

Obviously, the phase of  $S_{11}$  mainly depends on the first inverter and resonator.

In the circuit-based simulation, the variables are set as:

$$J_1 = J_2 = J_3 = 1 \quad \omega_c = 1 \text{ GHz}$$

$$g_1 = g_2 = 1.4142/\omega_c$$

Based on the schematics above, data are collected to validate this conclusion and show errors caused by our assumptions. The phase of simplest structure, which only has one inverter, has exactly the same value as the filter with two inverters. The phase difference of the filter with two inverters and the filter with three inverters, are considered acceptable when the difference is smaller than  $1^\circ$ . This condition is more loose than  $\frac{\omega_c}{\omega} \leq 0.015$  or  $\omega \geq 66.7 \cdot \omega_c$ . Table 3.1 shows the relationship between the phase differences and  $\frac{\omega_c}{\omega}$ . As shown in Table 3.1, the phases from different orders of inverters are close to each other when frequency increases, when  $\omega \geq 4.2 \cdot \omega_c$ . The value of the phase is mainly decided by  $J_1$  and  $g_1$  of a low-pass circuit model.

**Table 3.1 Phases in Low-pass filter Circuit Model with Different Order of Inverters  
(Scale to Low-pass filter with  $\omega_c = 1 \text{ GHz}$ )**

Frequency /GHz	* $\phi$ /degree	$\phi_{2\text{-inverter}}$ /degree	$\phi_{3\text{-inverter}}$ /degree	$\Delta\phi = \phi_3 - \phi_2$ /degree	$\frac{\omega_c}{\omega}$
...	...	...	...	...	...
3.60	21.447	21.447	23.059	1.582	$3.597\omega_c = \omega$
3.70	20.918	20.918	22.409	1.491	$3.770\omega_c = \omega$
3.80	20.414	20.414	21.794	1.380	$3.802\omega_c = \omega$
3.90	19.932	19.932	21.213	1.281	$3.906\omega_c = \omega$
4.00	19.471	19.471	20.663	1.192	$4.000\omega_c = \omega$
4.10	19.031	19.031	20.141	1.110	$4.098\omega_c = \omega$
4.20	18.609	18.609	19.644	1.035	$4.202\omega_c = \omega$
4.30	18.206	18.206	19.172	0.966	$4.292\omega_c = \omega$
4.40	17.818	17.818	18.723	0.905	$4.405\omega_c = \omega$
4.50	17.447	17.447	18.294	0.847	$4.505\omega_c = \omega$
4.60	17.090	17.090	17.884	0.794	$4.608\omega_c = \omega$
4.70	16.747	16.747	17.493	0.746	$4.695\omega_c = \omega$
4.80	16.417	16.417	17.119	0.702	$4.808\omega_c = \omega$
4.90	16.099	16.099	16.760	0.661	$4.902\omega_c = \omega$
5.00	15.793	15.793	16.417	0.624	$5.000\omega_c = \omega$
...	...	...	...	...	...

$$*\phi = \tan^{-1}\left[\frac{2J_1^2}{g_1}\left(\frac{\omega_c}{\omega}\right)\right]$$

### B. Band-pass prototype

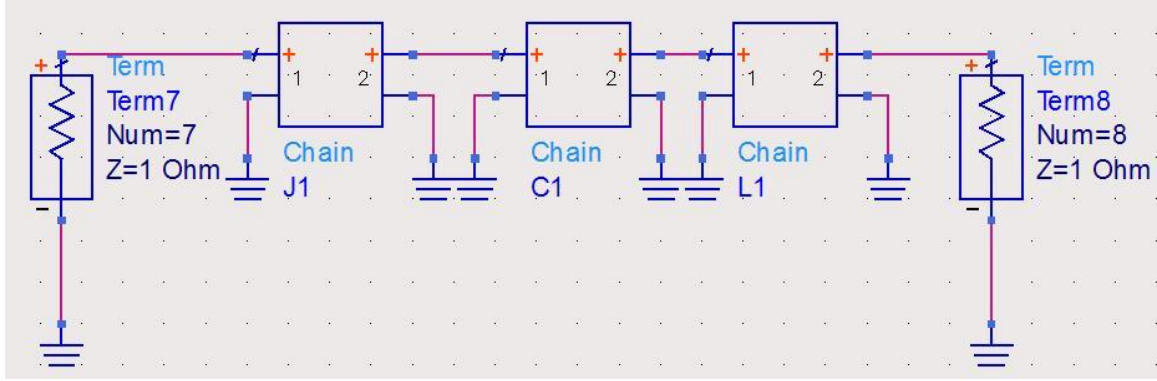
For band-pass filter, the unit inverters and LC components are expressed in [ABCD]

matrix as:

$$J_N = \begin{bmatrix} 0 & j/J_N \\ j * J_N & 0 \end{bmatrix}$$

$$C_N = \begin{bmatrix} 1 & 0 \\ \frac{j\omega g_N}{\Delta\omega} & 1 \end{bmatrix}, \quad L_N = \begin{bmatrix} 1 & 0 \\ \frac{\omega_0^2 g_N}{j\omega * \Delta\omega} & 1 \end{bmatrix}$$

where  $\Delta\omega$  is the bandwidth of a band-pass filter. Other variables have been explained in the low-pass prototype deduction.



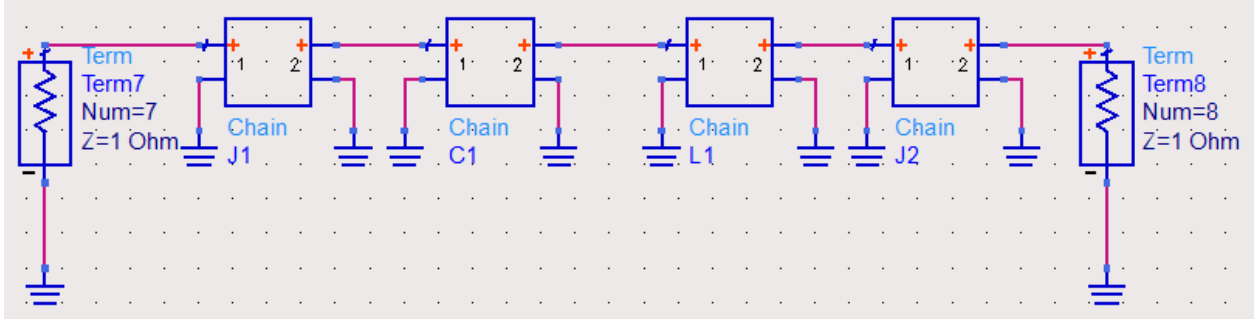
**Fig. 3.18 Simplest band-pass prototype schematic with one inverter and one resonator in Agilent ADS**

Fig. 3.18 shows a schematic of a simplified band-pass filter with only one inverter, capacitor and inductor. The cascaded result is:

$$\begin{bmatrix} A & B \\ C & D \end{bmatrix} = \begin{bmatrix} 0 & j/J_1 \\ j * J_1 & 0 \end{bmatrix} \times \begin{bmatrix} 1 & 0 \\ \frac{j\omega g_1}{\Delta\omega} & 1 \end{bmatrix} \times \begin{bmatrix} 1 & 0 \\ \frac{\omega_0^2 g_1}{j\omega * \Delta\omega} & 1 \end{bmatrix}$$

Reuse (3.9), and simplify  $S_{11}$  with  $(\frac{\Delta\omega}{\omega})^2 = 0$ , when  $\frac{\Delta\omega}{2|\omega - \omega_0|} \leq 0.015$ . The result is,

$$\begin{aligned} \tan_{2inverers}(\phi) &= \frac{img}{real} = \frac{2J_1^2 \frac{\Delta\omega}{\omega} [\omega^2 - \omega_0^2]}{\frac{g_1}{\omega^2} [\omega^4 - 2\omega^2\omega_0^2 + \omega_0^4]} \\ &= \frac{2J_1^2 \frac{\Delta\omega}{\omega} [\omega^2 - \omega_0^2]}{\frac{g_1}{\omega^2} [\omega^2 - \omega_0^2]^2} \\ &= \frac{2J_1^2 \frac{\Delta\omega}{\omega}}{g_1 [1 - (\frac{\omega_0}{\omega})^2]} \end{aligned} \quad (3.13)$$



**Fig. 3.19 Band-pass prototype schematic with two inverters in Agilent ADS**

Fig. 3.19 shows a schematic of a band-pass filter with two inverters (one pole). The cascaded result is:

$$\begin{bmatrix} A & B \\ C & D \end{bmatrix} = \begin{bmatrix} 0 & j/J_1 \\ j * J_1 & 0 \end{bmatrix} \times \begin{bmatrix} 1 & 0 \\ j\omega g_1 & 1 \end{bmatrix} \times \begin{bmatrix} 1 & 0 \\ \frac{\omega_0^2 g_1}{j\omega * \Delta\omega} & 1 \end{bmatrix} \times \begin{bmatrix} 0 & j/J_2 \\ j * J_2 & 0 \end{bmatrix}$$

Reuse (3.9), and simplify  $S_{11}$  with  $(\frac{\Delta\omega}{\omega})^2 = 0$ , when  $\frac{\Delta\omega}{2|\omega - \omega_0|} \leq 0.015$ . The result is,

$$\tan_{2inverers}(\phi) = \frac{img}{real} = \frac{2J_1^2 \frac{\Delta\omega}{\omega} [1 - (\frac{\omega_0}{\omega})^2]}{g_1 [1 - 2(\frac{\omega_0}{\omega})^2 + (\frac{\omega_0}{\omega})^4]}$$

$$= \frac{2J_1^2 \frac{\Delta\omega}{\omega} [1 - (\frac{\omega_0}{\omega})^2]}{g_1 [1 - (\frac{\omega_0}{\omega})^2]^2}$$

$$\approx \frac{2J_1^2 \frac{\Delta\omega}{\omega}}{g_1 [1 - (\frac{\omega_0}{\omega})^2]} \quad (3.14)$$

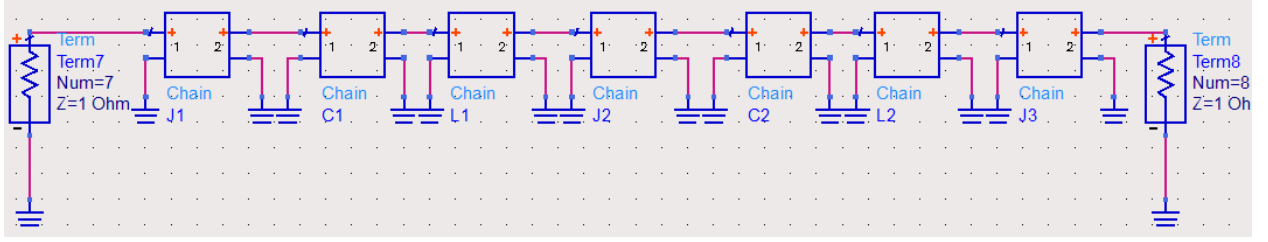


**Fig. 3.20 Band-pass prototype schematic with three inverters in Agilent ADS**

A schematic of a band-pass filter with three inverters (two pole) is shown in Fig.

3.20, the cascaded results are

$$\begin{aligned} \begin{bmatrix} A & B \\ C & D \end{bmatrix} &= \begin{bmatrix} 0 & j/J_1 \\ j * J_1 & 0 \end{bmatrix} \times \begin{bmatrix} 1 & 0 \\ j\omega g_1 & 1 \end{bmatrix} \times \begin{bmatrix} 1 & 0 \\ \frac{\omega_0^2 g_1}{j\omega * \Delta\omega} & 1 \end{bmatrix} \times \begin{bmatrix} 0 & j/J_2 \\ j * J_2 & 0 \end{bmatrix} \times \begin{bmatrix} 1 & 0 \\ j\omega g_2 & 1 \end{bmatrix} \\ &\times \begin{bmatrix} 1 & 0 \\ \frac{\omega_0^2 g_2}{j\omega * \Delta\omega} & 1 \end{bmatrix} \times \begin{bmatrix} 0 & j/J_3 \\ j * J_3 & 0 \end{bmatrix} \end{aligned}$$

Repeat the previous steps, the simplified result of  $S_{11}$  is

$$\begin{aligned} \tan_{3inverers}(\phi) &= \frac{img}{real} \\ &\approx \frac{2J_1^2 \frac{\Delta\omega}{\omega} [-\left(\frac{\omega_0}{\omega}\right)^6 + 3\left(\frac{\omega_0}{\omega}\right)^4 - 3\left(\frac{\omega_0}{\omega}\right)^2 + 1]}{g_1 [1 - 4\left(\frac{\omega_0}{\omega}\right)^2 + 6\left(\frac{\omega_0}{\omega}\right)^4 - 4\left(\frac{\omega_0}{\omega}\right)^6 + \left(\frac{\omega_0}{\omega}\right)^8]} \\ &= \frac{2J_1^2 \frac{\Delta\omega}{\omega} [1 - \left(\frac{\omega_0}{\omega}\right)^2]^3}{g_1 [1 - \left(\frac{\omega_0}{\omega}\right)^2]^4} = \frac{2J_1^2 \frac{\Delta\omega}{\omega}}{g_1 [1 - \left(\frac{\omega_0}{\omega}\right)^2]} \end{aligned} \quad (3.15)$$

(3.15) is the same as (3.14). Therefore, in out-of-band frequency, the phase of  $S_{11}$  mostly depends on the first resonator of the band-pass filter.

In the circuit-based simulation, all variables are set as:

$$J_1 = J_2 = J_3 = 1 \quad g_1 = g_2 = 1.4142$$

$$\omega_0 = 12 \text{ GHz} \quad \Delta\omega = 30 \text{ MHz}$$

The phase of the simplest structure is one with two inverters. Table 3.2 shows the simulation results of Fig. 3.19 and Fig. 3.20. The filter in Table 3.2 is a band-pass filter with 30 MHz bandwidth at center frequency of 12 GHz. In this table, the difference between those two phases is less than  $1^\circ$  when  $\omega \geq \omega_0 + 10\Delta\omega$  or  $\omega \leq \omega_0 - 10\Delta\omega$ , which is in a looser condition than the one in the deduction process.

**Table 3.2 Phases in Band-pass filter Circuit Model with Different Orders of Inverters**

Frequency /GHz	* $\phi$ /degree	$\phi_{2\text{-inverter}}$ /degree	$\phi_{3\text{-inverter}}$ /degree	$\Delta\phi =  \phi_3 - \phi_2 $ /degree	$\frac{\Delta\omega}{2 \omega - \omega_0 }$
...	...	...	...	...	...
11.92	-14.804	-14.804	-15.315	0.511	$\omega = \omega_0 - 2.22\Delta\omega$
11.93	-16.813	-16.813	-17.569	0.756	$\omega = \omega_0 - 1.94\Delta\omega$
11.94	-19.426	-19.426	-20.609	1.183	$\omega = \omega_0 - 1.67\Delta\omega$
11.95	-22.947	-22.947	-24.941	1.994	$\omega = \omega_0 - 1.39\Delta\omega$
11.96	-27.899	-27.899	-31.623	3.724	$\omega = \omega_0 - 1.11\Delta\omega$
11.97	-35.231	-35.231	-43.255	8.024	$\omega = \omega_0 - 0.83\Delta\omega$
11.98	-46.663	-46.663	-67.525	20.862	$\omega = \omega_0 - 0.56\Delta\omega$
11.99	-64.752	-64.752	-120.482	55.73	$\omega = \omega_0 - 0.28\Delta\omega$
12.00	0.000	0.000	0.000	0	$\omega = \omega_0$
12.01	64.770	64.770	120.537	55.767	$\omega = \omega_0 + 0.28\Delta\omega$
12.02	46.710	46.710	67.646	20.936	$\omega = \omega_0 + 0.56\Delta\omega$
12.03	35.298	35.298	43.374	8.076	$\omega = \omega_0 + 0.83\Delta\omega$
12.04	27.978	27.978	31.736	3.758	$\omega = \omega_0 + 1.11\Delta\omega$
12.05	23.033	23.033	25.051	2.018	$\omega = \omega_0 + 1.39\Delta\omega$
12.06	19.516	19.516	20.716	1.2	$\omega = \omega_0 + 1.67\Delta\omega$
12.07	16.906	16.906	17.674	0.768	$\omega = \omega_0 + 1.94\Delta\omega$
...	...	...	...	...	...

$$*\phi = \tan^{-1} \left\{ \frac{2J_1^2 \frac{\Delta\omega}{\omega}}{g_1 \left[ 1 - \left( \frac{\omega_0}{\omega} \right)^2 \right]} \right\}$$

### C. Simplified Circuit Model with Spurious Mode

There are assumptions about the locations of the spurious mode. First, the spurious is assumed to be cascaded with the first resonator, Fig. 3.21 shows the configuration.

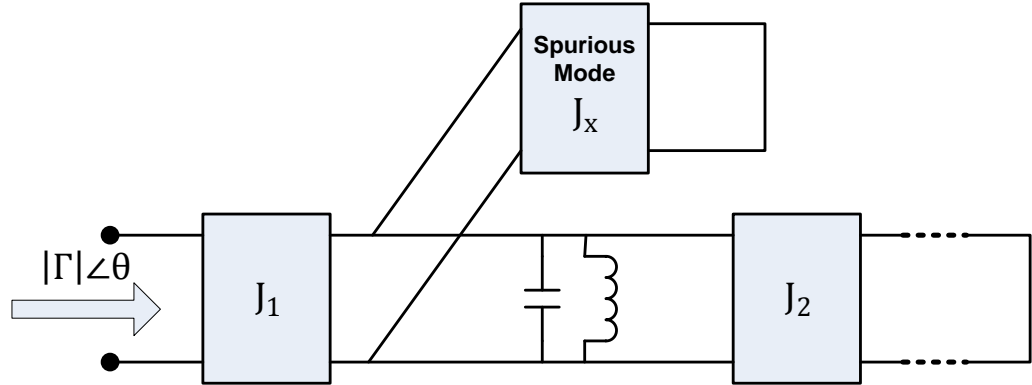


**Fig. 3.21 Simplified Band-pass filter with two inverters and one spurious mode attached at first resonator.**

Repeat the previous steps in Section A and Section B, the simplified phase of the related reflection coefficient in out-of-band is expressed as:

$$\tan\theta \approx \frac{2J_1^2 \frac{\Delta\omega}{\omega}}{g_1 \left[ 1 - \left( \frac{\omega_0}{\omega} \right)^2 \right]}$$

where  $\left( \frac{\Delta\omega}{\omega} \right)^2 = 0$ , when  $\frac{\Delta\omega}{2|\omega - \omega_0|} \leq 0.015$ . The item of  $J_x$  is disappear after simplification in out-of-band, and it is not consistent with the EM simulation results. Thus the assumption is incorrect. Another assumption is shown in Fig. 3.22.

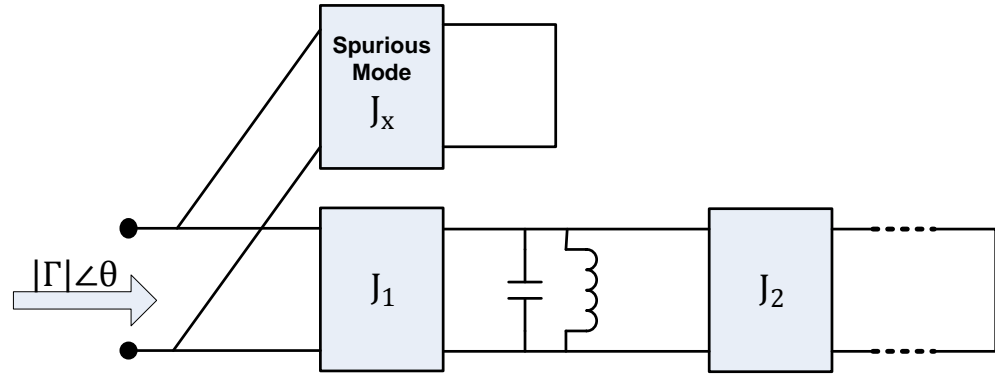


**Fig. 3.22 Simplified Band-pass filter with two inverters and one spurious mode attached at first inverter.**

Repeat the same steps as the previous deduction, the simplified equation of the phase of related reflection coefficient in out-of-band is:

$$\tan\theta \approx \frac{2J_1^2 \frac{\Delta\omega}{\omega} \left[1 - \left(\frac{\omega_0}{\omega}\right)^2\right]}{g_1 \left[1 - \left(\frac{\omega_0}{\omega}\right)^2\right]^2 - J_x^2 g_1 \left[1 - 2\left(\frac{\omega_0}{\omega}\right)^2\right]}$$

The simplified equation still have the item of first inverter  $J_1$ , the first resonator  $g_1$ , and the spurious mode  $J_x$ . This assumption is consistent with the EM simulation results.

The comparison of these two assumptions obviously illustrate that the spurious mode of a filter is only related to the first inverter or the first iris of the filter. Through the results of the band-pass and low-pass prototypes, all of the inverters will not significantly affect the responses of the reflection coefficient except for the first inverter.

### III. Conclusion

We have proved that the phase of  $S_{11}$  in out-of-band frequencies is related to the first resonator in an equivalent network. Furthermore, port 2 can be short-circuited and the phase of reflection coefficient is not affected in the out-of-band. In the following, we simplify the filter structure by keeping only the first resonator and show that a full EM simulation of the first iris slot, which serves as the first inverter is sufficient.

#### 3.2.2 EM Simulation of Simplified Filter Structure

Simulation of the first cavity can be done by EM simulation of the first iris only. Compared to simulating the entire first cavity, the advantage is that the number of variables is reduced, since the cavity length is not a variable, which is very important for data collection for ANN models. The EM simulation time is also significantly reduced. As shown in the Fig 3.23, S-parameters of multiple modes on port 2 (the cavity sides) are recorded from the EM simulation. Subsequently, the modes are short-circuited to get reflection coefficient  $\Gamma$  from port 1. The dominant mode in the filter cavity is TE<sub>11</sub> mode, however there are higher-order modes exist, especially near discontinuities inside the cavity. Therefore, multiple modes should be considered in an EM simulation. The first few modes are listed in Table 3.3. In this section we plot responses of the first cavity with modes needed, to ensure good accuracy and at the same time reduce the difficulty in the data collection of ANN model development.

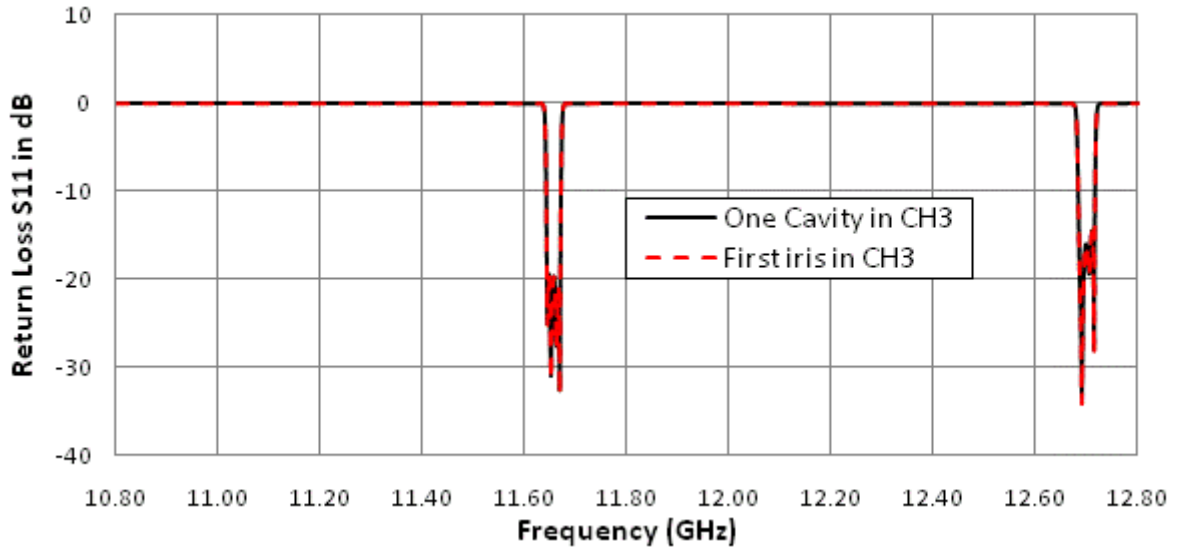


**Fig. 3.23 Compare CPRL in one cavity and first resonator of 3-channel multiplexer.**

The theoretical networks of a multiport equivalent circuit are shown in Fig. 3.24. In an EM simulator, the input port is defined with one mode, and the output port is defined with one mode, three modes and five modes, respectively. The process can be understood as an analysis of multiport networks [01]. The mode in input is considered as an external port; the modes on the output side are all recognized as the internal ports in the following calculation.

**Table 3.3 Values of  $p'_{nm}$  in different mode of a circular waveguide**

$f_0 = 11037.42 \text{ MHz}$		
Mode 1	TE11	$p'_{11} = 1.841$
Mode 2	TE11	$p'_{11} = 1.841$
Mode 3	TM11	$p'_{11} = 2.405$
Mode 4	TE21	$p'_{21} = 3.054$
Mode 5	TE21	$p'_{21} = 3.054$

\*  $p'_{nm}$  is the  $m$ th root of  $J'_n(k_c a) = 0$ , where  $\beta = \sqrt{k^2 - k_c^2}$ ,  $k$  is the

wavenumber and  $a$  is the radius of the circular waveguide.

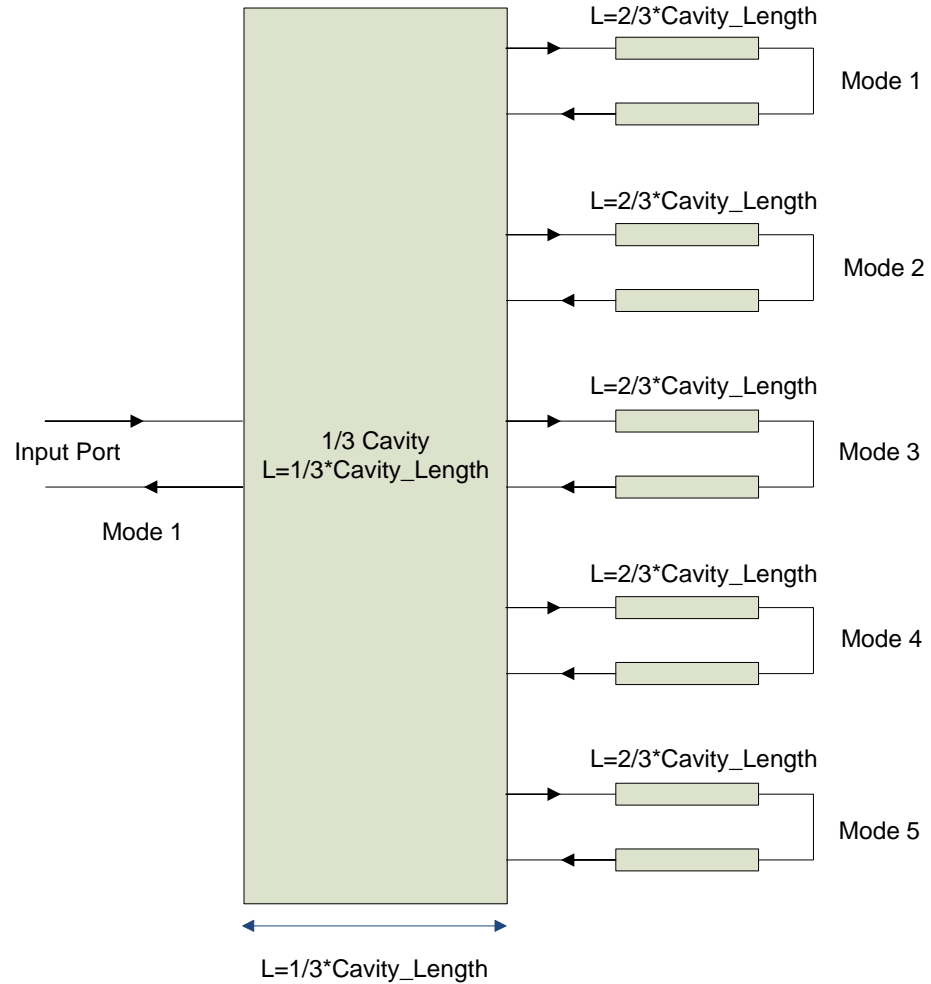


**Fig. 3.24 An arbitrary microwave network consisting of six-port networks connected together**

This section takes a full EM simulation with five modes in the output port as an example to explain the calculation process. The main steps are presented as follow:

Step 1) Export a data file from a full EM simulation with five modes in output. The frequency range covers 10.8 GHz to 12.8 GHz. The S-parameter matrix from EM simulation is a  $[6 \times 6]$  matrix, and the matrix is reciprocal, i.e.  $S_{ij} = S_{ji}$ . The matrix can be expressed as follows:

$$[S] = \begin{bmatrix} S1(1)1(1) & S1(1)2(1) & S1(1)2(2) & S1(1)2(3) & S1(1)2(4) & S1(1)2(5) \\ S2(1)1(1) & S2(1)2(1) & S2(1)2(2) & S2(1)2(3) & S2(1)2(4) & S2(1)2(5) \\ S2(2)1(1) & S2(2)2(1) & S2(2)2(2) & S2(2)2(3) & S2(2)2(4) & S2(2)2(5) \\ S2(3)1(1) & S2(3)2(1) & S2(3)2(2) & S2(3)2(3) & S2(3)2(4) & S2(3)2(5) \\ S2(4)1(1) & S2(4)2(1) & S2(4)2(2) & S2(4)2(3) & S2(4)2(4) & S2(4)2(5) \\ S2(5)1(1) & S2(5)2(1) & S2(5)2(2) & S2(5)2(3) & S2(5)2(4) & S2(5)2(5) \end{bmatrix} \quad (3.16)$$

The value inside the bracket means a mode-number, while the value outside the bracket represents a port-number.

Step 2) Rewrite the scattering matrix of network with external ports represented by ‘C’, and internal ports represented by ‘P’. Thus the overall matrix is divided into four sub-matrixes with five output ports short-circuited:  $S_{PP}$  of size  $[1 \times 1]$ ,  $S_{PC}$  of size  $[1 \times 6]$ ,  $S_{CP}$  of size  $[6 \times 1]$  and  $S_{CC}$  of size  $[5 \times 5]$  :

$$\begin{bmatrix} V_P^- \\ V_C^- \end{bmatrix} = \begin{bmatrix} S_{PP} & S_{PC} \\ S_{CP} & S_{CC} \end{bmatrix} \begin{bmatrix} V_P^+ \\ V_C^+ \end{bmatrix}$$

where

$$S_{PP} = [S1(1)1(1)] \quad S_{PC} = [S1(1)2(1) \quad S1(1)2(2) \quad S1(1)2(3) \quad S1(1)2(4) \quad S1(1)2(5)]$$

$$S_{CP} = \begin{bmatrix} S2(1)1(1) \\ S2(2)1(1) \\ S2(3)1(1) \\ S2(4)1(1) \\ S2(5)1(1) \end{bmatrix} \quad S_{CC} = \begin{bmatrix} S2(1)2(1) & S2(1)2(2) & S2(1)2(3) & S2(1)2(4) & S2(1)2(5) \\ S2(2)2(1) & S2(2)2(2) & S2(2)2(3) & S2(2)2(4) & S2(2)2(5) \\ S2(3)2(1) & S2(3)2(2) & S2(3)2(3) & S2(3)2(4) & S2(3)2(5) \\ S2(4)2(1) & S2(4)2(2) & S2(4)2(3) & S2(4)2(4) & S2(4)2(5) \\ S2(5)2(1) & S2(5)2(2) & S2(5)2(3) & S2(5)2(4) & S2(5)2(4) \end{bmatrix} \quad (3.17)$$

Step 3) Find a connection matrix  $\Gamma$ . This matrix is related to the internal ports and external ports. The equation can be expressed as:

$$V_C^- = \Gamma V_C^+ \quad (3.18)$$

where

$$\Gamma = \begin{bmatrix} \frac{1}{\Gamma_2} & \cdots & 0 \\ \vdots & \ddots & \vdots \\ 0 & \cdots & \frac{1}{\Gamma_6} \end{bmatrix} \quad (3.19)$$

Since the waveguide length of each mode is the same,

$$\Gamma_i (i = 2, 3 \dots 6) = -e^{-j2\beta l} \quad (3.20)$$

The constant propagation of the circular waveguide  $\beta$  is computed by the following equations

$$k = \frac{2\pi f_0 \sqrt{\epsilon_r}}{c}, \quad \beta = \sqrt{k^2 - \left(\frac{p}{a}\right)^2} \quad (3.21)$$

The dielectric constant  $\epsilon_r = 1$ , 'a' in (3.21) is a radius of the circular waveguide. In (3.20), 'l' represents the residual length of cavity. In EM simulation, length of port 2 is one third of the cavity length. Therefore l is two thirds of the cavity length.

Step 4) Find the resultant matrix  $[S^P]$ . Because there is only one external port in the network,  $[S^P]$  will be  $[1 \times 1]$  matrix, i.e. single value. The computation uses the following equation:

$$\Gamma = [S^P] = \frac{V_P^-}{V_P^+} = [S_{PP} + S_{PC}[\Gamma - S_{CC}]^{-1}S_{CP}] \quad (3.22)$$

With (3.22), the reflection coefficient  $\Gamma$  can be calculated in different frequencies. Other mode numbers are calculated with the same steps. A Matlab program is applied in Step 2 to Step 4.

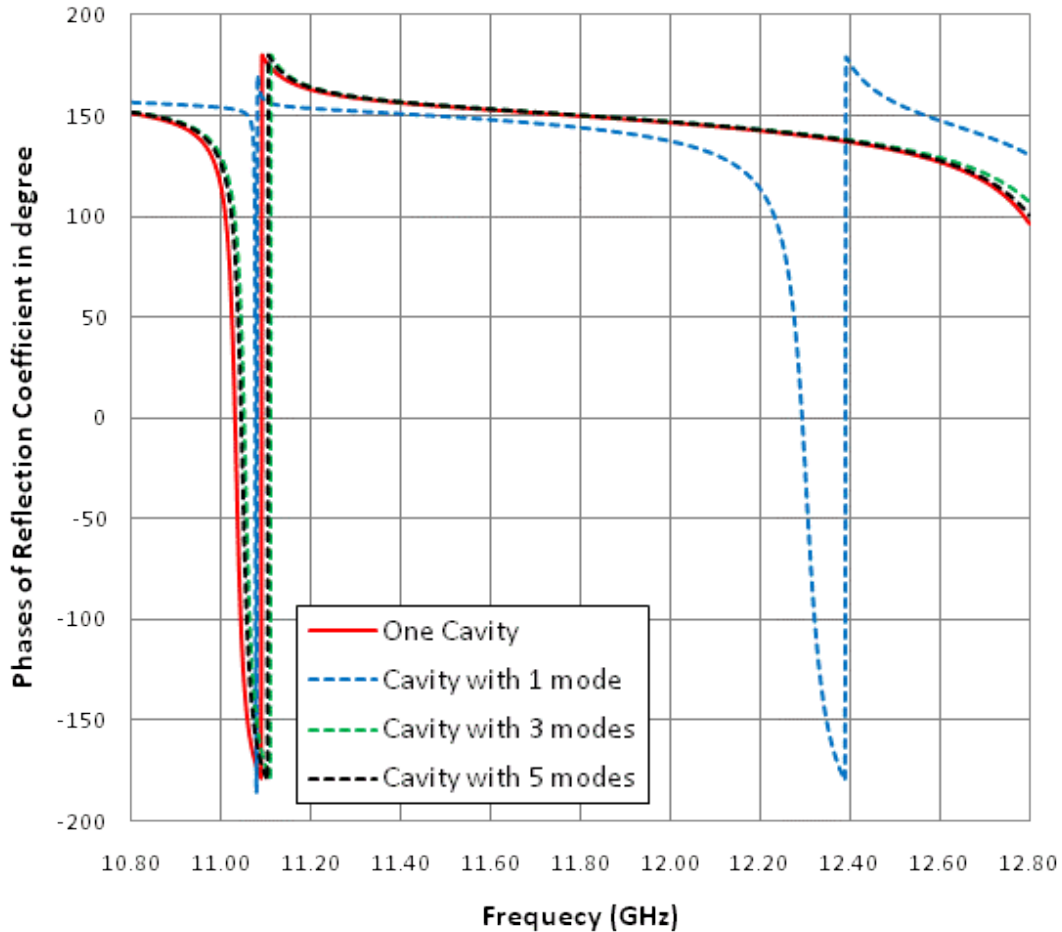
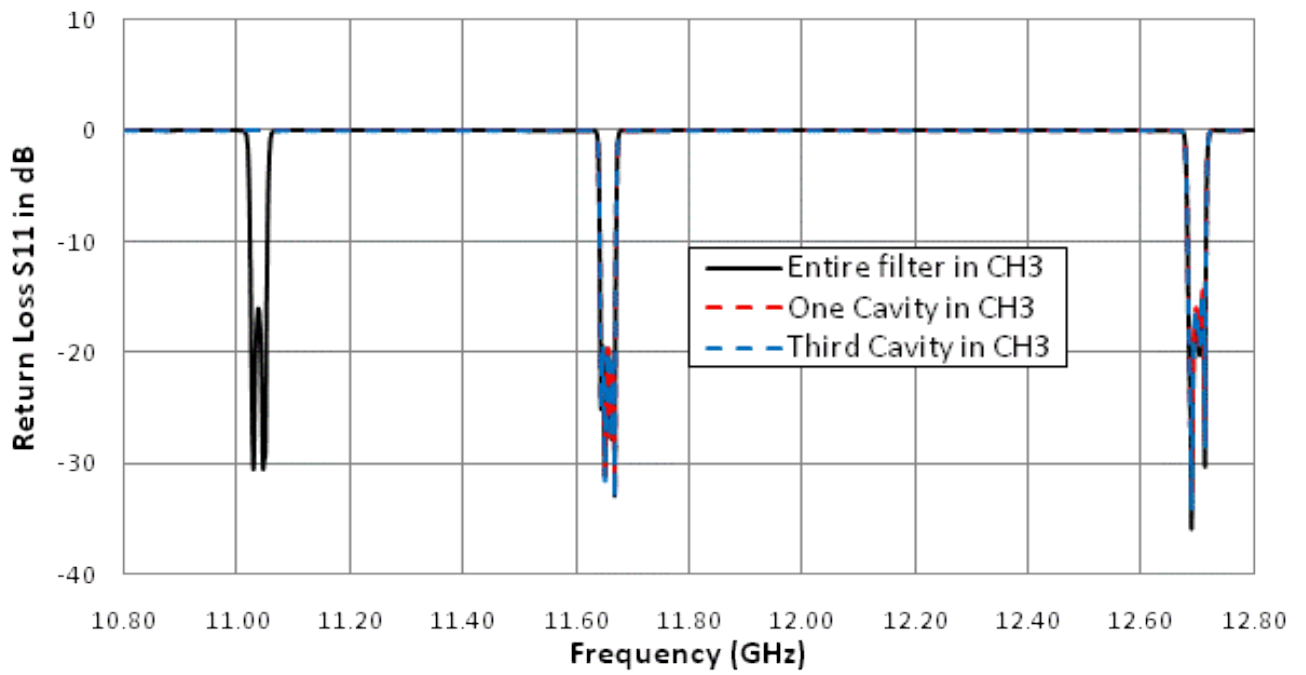
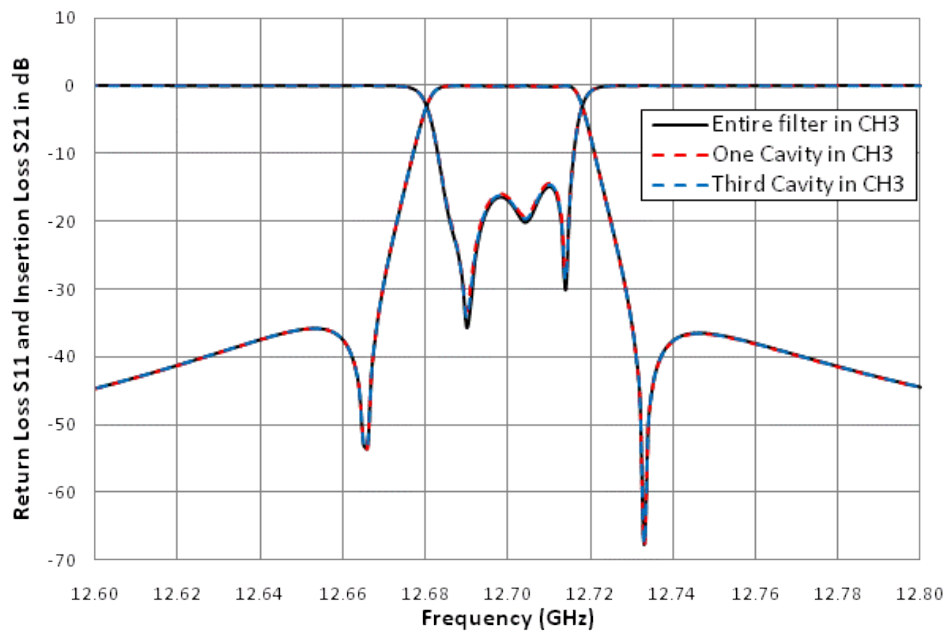


**Fig. 3.25 Phase comparison in different Modes**

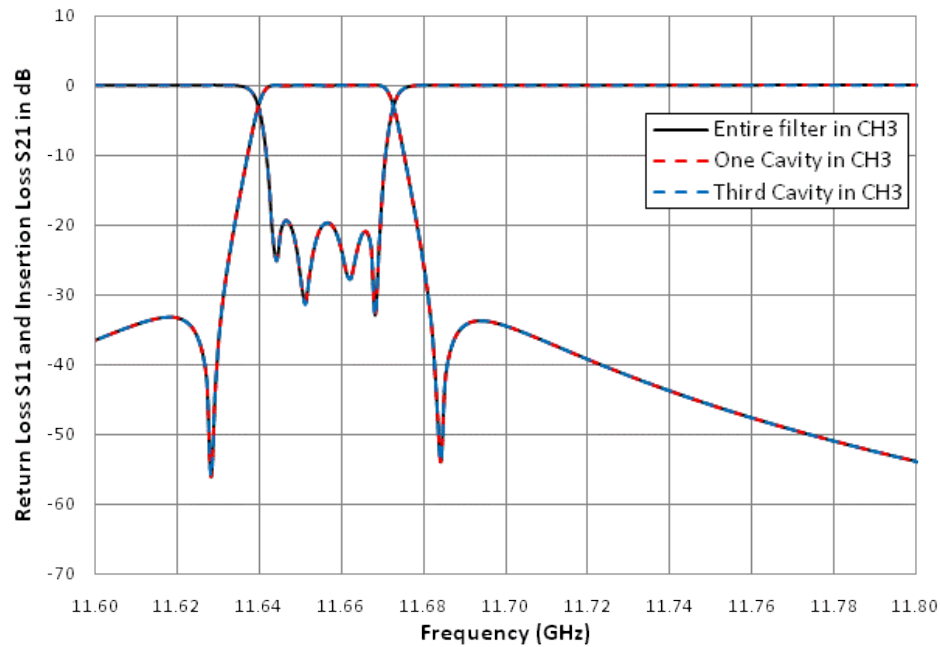
Fig. 3.25 shows the plots of a reflection coefficient phase with different modes using the steps described earlier. To evaluate the accuracy, an EM simulation of the entire first cavity is also simulated. Obviously, the response of one mode in the output has lost much information, and shows unreasonable glitch around 12.4 GHz. The plots with three modes and five modes are closer to the plot of the reflection coefficient of the one cavity. To ensure the accuracy, the following analysis will choose five modes.



(a)



(b)



(c)

**Fig. 3.26 Comparison between the Common Port Return Losses and Insertion Losses from a conventional 3-channel multiplexer, and from simplified 3-channel multiplexers. (a) Compare CPRL in different types of 3-channel multiplexer. (b) Compare CPRL and IL in Channel 1. (c) Compare CPRL and IL in Channel 2.**

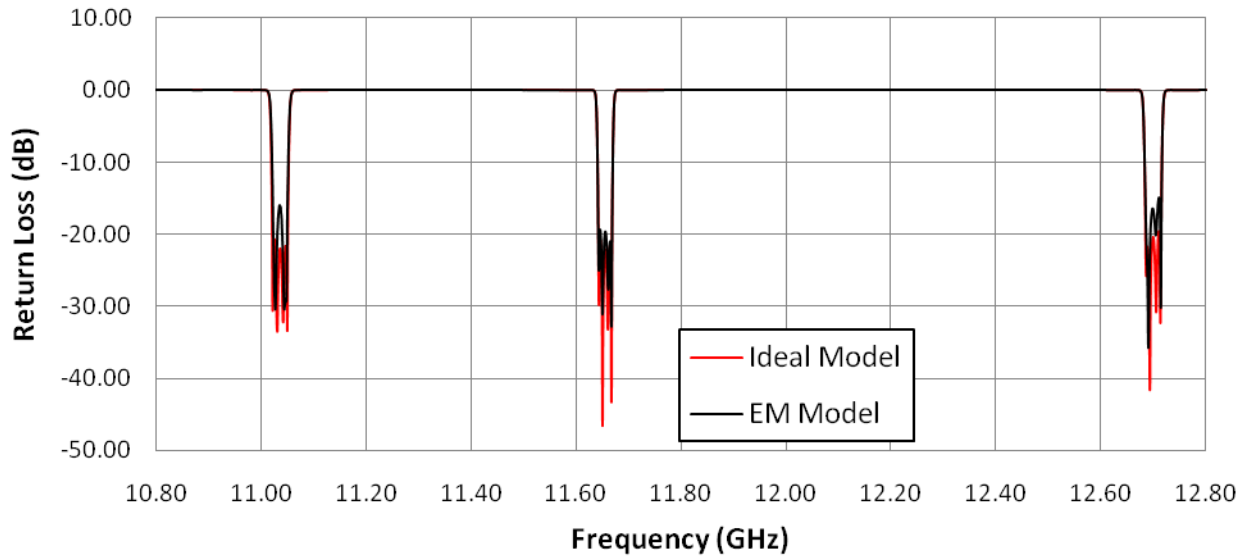
The s-parameters in five modes and in one cavity are applied into the three channel multiplexer circuit model in Agilent ADS to verify the results in section 3.2.1. The multiplexer model is the same one as shown in Fig. 3.11. For channel 3, we compare three sets of data: EM data file for the entire filter, which should be the most accurate, EM data for the entire first cavity, and processed data using EM data for the first iris. In this structure, Port 4 is short-circuited when single cavity data is attached. Fig. 3.26 shows the simulation results. The simplified multiplexer does not have any response around 11037.42 MHz, because channel 3 filter has been short-circuited. The responses of channel 1 and channel 2 agree very well for all three cases. The responses of the first slot in a filter can fully replace the entire filter for spurious mode analysis. This result can

save considerable time for ANN data collection. In the following, a combination of an EM simulator and a Matlab program is applied in the calculation.

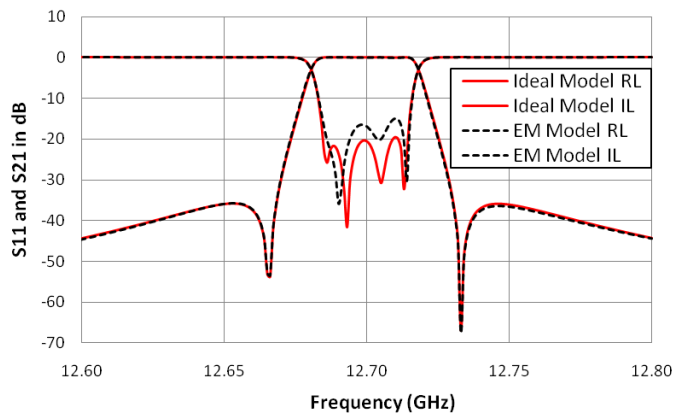
### 3.3 Artificial Neural Network Model

When we substitute an EM file to the ideal model of channel 3 in a circuit-based model, the response of return loss at common port and insertion loss of each channel (except channel 3) shows difference from the ideal model, as shown in Fig. 3.27, this fully illuminate the damage of the spurious mode. Before this multiplexer is manufactured, the effective of lower channel filter must be predicted and taken into account. Even though the simplified EM model has reduces the variables during the EM simulation, any edit on the first iris still require a full wave EM simulation. The full EM simulations take long time and are not practical for optimization. Implementing artificial neural network can speed up the simulation process with accurate results.

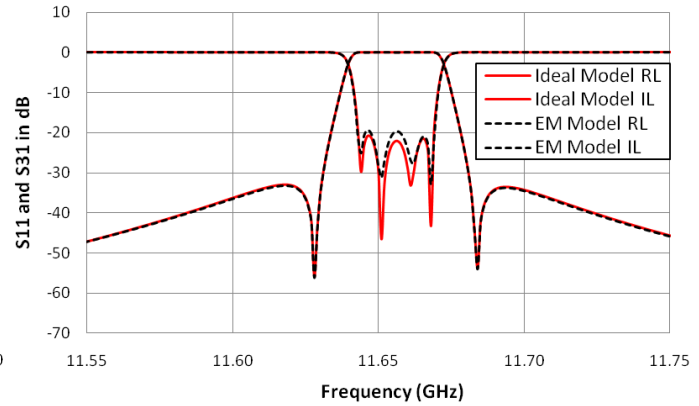
Artificial Neural Network (ANN) has been briefly discussed in Chapter 1. This section concentrates on the process of building a neural network model. The first step is to collect the training data and test data; the second step is to train and test a neural network model. NeuroModeler is used for NN model training and testing[36]. Three different methods of pre-processing data have been presented to reduce the training error. The third step is to apply the neural network model of a simplified filter into a circuit-based simulator, to verify the model.



(a)



(b)



(c)

**Fig. 3.27 Comparison of the multiplexer with EM model, and with Ideal Model.**  
**(a) Common Port Return Loss S11. (b) Insertions Loss and Return Loss in Channel 1. (c) Insertion Loss and Return Loss in Channel 2.**

### 3.3.1 Data Collection

Before data collection, both the input parameters and output parameters should be defined. The output parameters are S-parameters and the input parameters are resonance frequencies and the lengths of the first iris.

Section 3.2 has proved that the simulation of the first iris of a filter with five modes on port 2, can represent the effect of the entire filter in out-of-band frequency. With different iris lengths and frequencies, S-parameters have different magnitudes and phases. The length of the input slot in the filter, which has 36MHz bandwidth at 11037.42 MHz center frequency, is 0.30559 inch in section 3.1 after tuning. It changes from 0.25059 inch to 0.35059 inch as a variable to cover the input parameters' range. The EM simulation frequency starts from 10.8 GHz to 12.8 GHz to cover the three-channel multiplexer transmission bands. The cavity length, which dominates the resonance frequencies, is changed from 1.58656 inch to 2.01259 inch; and it is used in Matlab for calculating the reflection coefficients or simplifying S-parameter matrix. The length of the cavity in EM simulation is fixed. It is one third of the filter length when its center frequency is 11037.42 MHz. The calculated results of different resonance frequencies are list in Table 3.4.

In this table, the guided wavelength is calculated with (3.20) at different center frequencies. The cavity length is three times of the half guided wavelength. The residual cavity length is used in the calculation of the reflection coefficient.

**Table 3.4 Cavity lengths at Different Resonance Frequencies**

$f_0/\text{MHz}$	$k_0$	$\beta$	$\lambda_g/\text{inch}$	Cavity_length/inch $=3\lambda_g/2$	Simulated length in EM	Residual cavity length
10800.00	5.7454	4.6829	1.34173	2.01259inch	0.644137inch	1.368453inch
11037.42	5.8714	4.8360	1.29925	1.94887inch	0.644137inch	1.304733inch
12800.00	6.8093	5.9404	1.05771	1.58656inch	0.644137inch	0.942423inch

In a full EM simulation, the circular wavguide is defined with five propagating modes in the output port, and 20 samples in the length of the input slot. This EM data generation usually takes more than 90 minutes. More samples may take longer EM simulation time. After the simulation, each sample of the slot has a  $[6 \times 6]$  S-parameter matrix, which will be expressed in magnitude and phase, in different frequencies. These data will be used as training data to feed a Neural Network model. The simulation with another 10 samples of the slot length, which are still between 0.25059 inch and 0.35059 inch, will be repeated to gain the test data. With plenty of EM data, we can start the training of a neural network model.

### 3.3.2 Data Organization

Different strategies for data training critically affect the error during the training of neural network model process. This section focuses on the organization approaches. The EM data are  $[6 \times 6]$  S-parameter matrixes with different slot lengths in frequencies. Three approaches presented to reduce the error during the training of a neural network model.

#### A. Training $[6 \times 6]$ S-parameter Matrix

This is a very simple approach, as the organization is just sorting the original EM data without any calculation before training. If the training can be completed, a reflection coefficient can be calculated in Matlab with residual cavity lengths, before exporting a data file for Agilent ADS simulation. Considering the efficiency of ANN, each data file only contains two input parameters, which are frequencies and slot lengths; and two output parameters, which are magnitudes and phases of each S-parameter. There are

overall 21 files of training data, as the  $[6 \times 6]$  S-parameter matrix is reciprocal. The frequency step is chosen as 20 MHz. The unit of each S-parameter phase is expressed in degree.

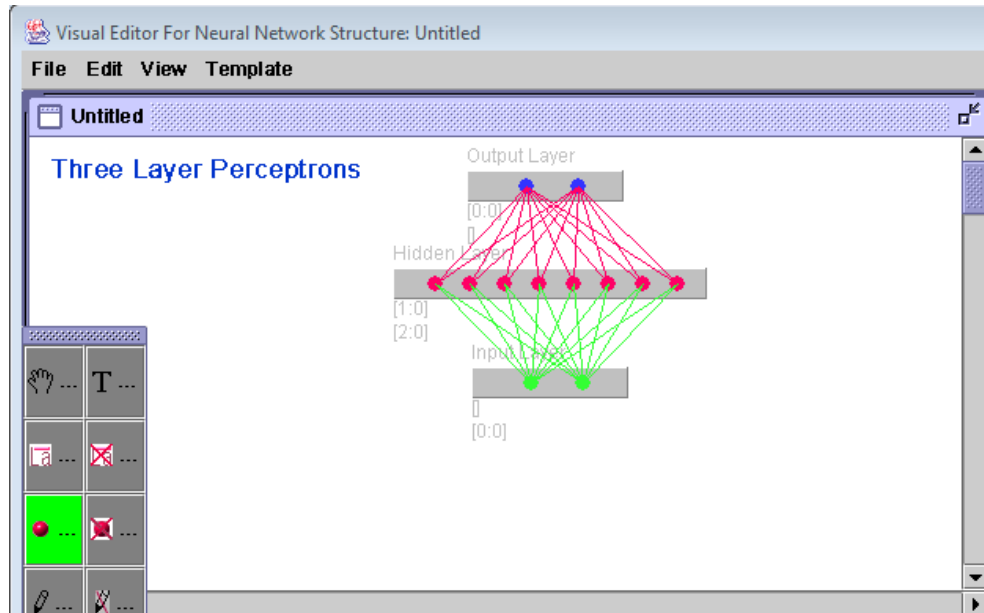
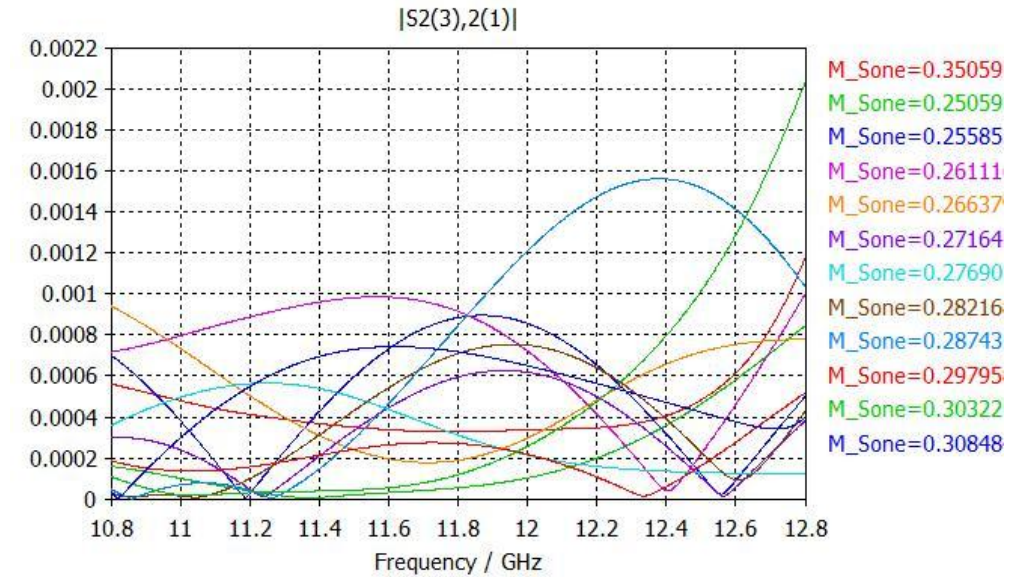


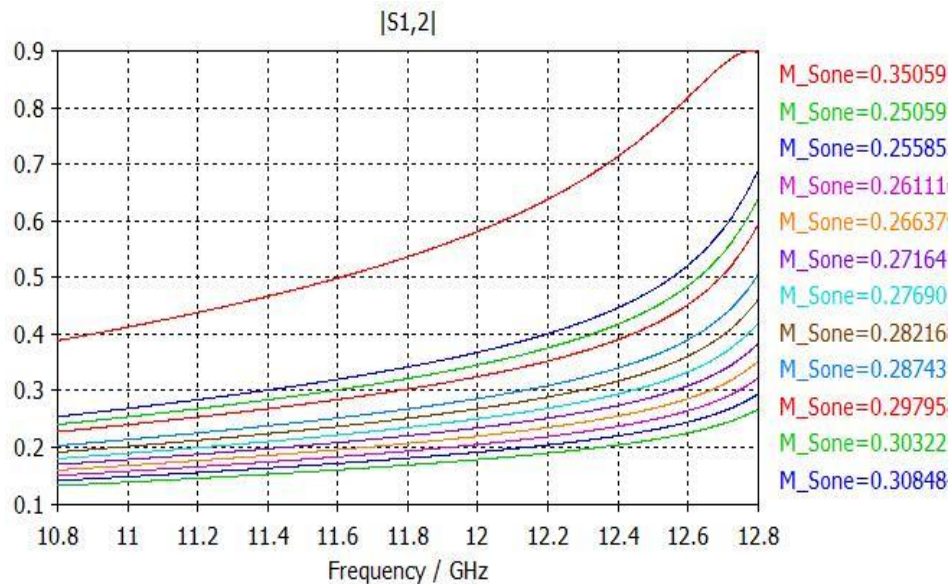
**Fig. 3.28 A three layer structure of Artificial Neural Network with two input parameters and two output parameters.**

After the organization, these training data are applied into ANN for building a neural network model. Fig. 3.28 shows a three-layer structure used in this approach. The structure has two input parameters and two output parameters, with eight hidden neurons, which can be changed. Increasing the number of hidden neurons will lower down the training error at first, but the training time will exponentially increase. Therefore, changing the approach of data training is necessary when there is no improvement on training error with increasing hidden neurons. In this approach, the worst training error is more than 20%, because of some data files with non-linear characteristics, and hard to train. This can also be found in an EM simulation result shown in Fig. 3.29. Magnitudes in Fig. 3.29(a) are not well-behaved as the slot length changes, when the magnitudes in

Fig 3.29(b) show good linearity. Thus the original data from EM simulator cannot be directly used into the Neural Network as training data.



(a)



(b)

**Fig. 3.29 EM simulation of one third cavity with five propagating modes in different slot lengths. (a) The magnitudes of S2(3)2(1) (low linearity). (b) The magnitudes of S1(1)2(1) (high linearity).**

## B. Training Reflection Coefficient

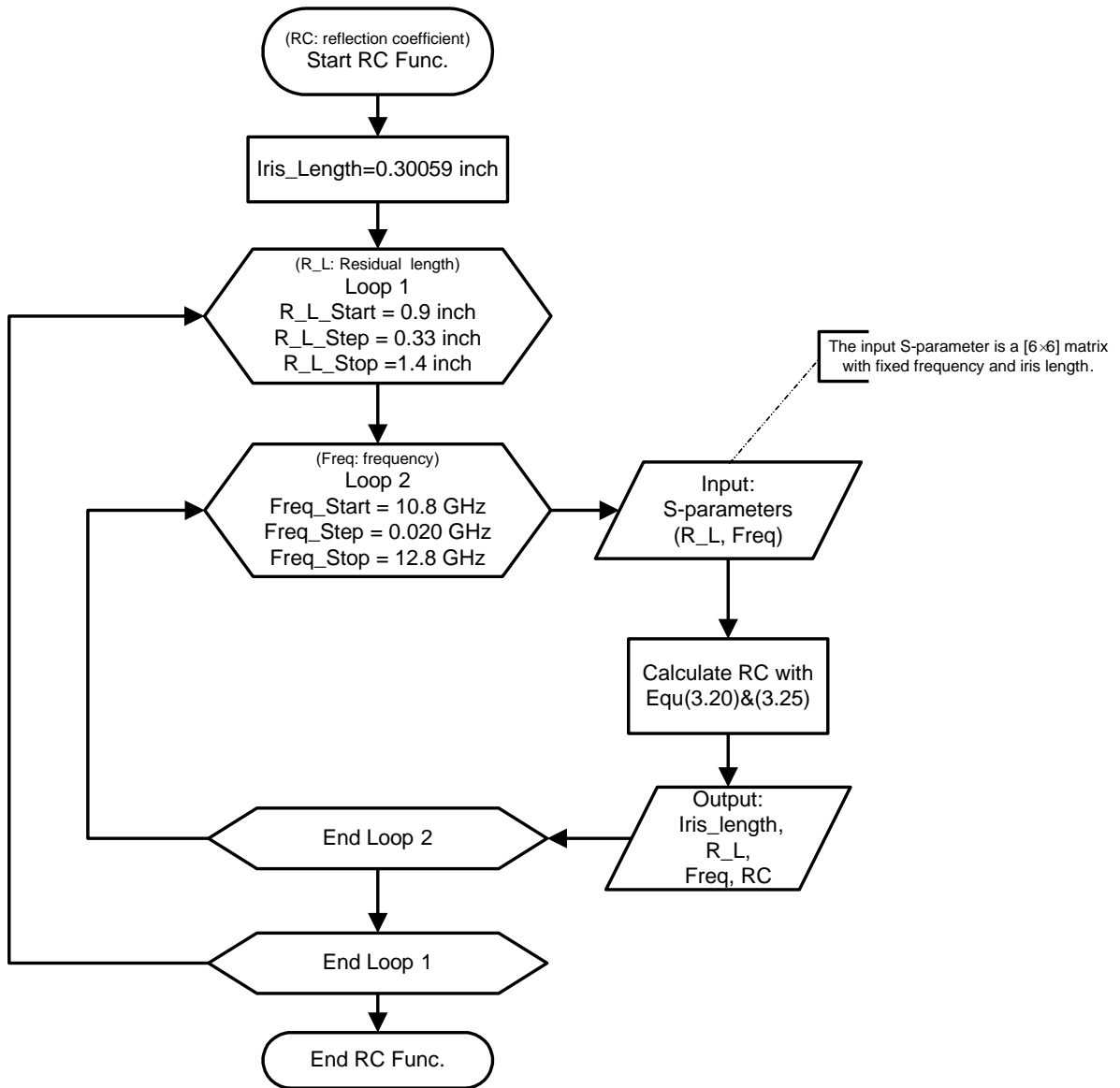


**Fig. 3.30 Simplified Matlab Flowchart**

The second approach is trying to calculate EM data before training a neural network model, in order to lower down the error in training process. In this method, the reflection coefficient will be pre-calculated after the EM data is generated with different lengths of the input slot. The residual length of the first cavity is also changing during the computation of reflection coefficients. An example will be present to illustrate this

approach. In Fig. 3.30, a fixed iris-length is used, i.e.  $l_{iris} = 0.30059 \text{ inch}$ , in calculation. The calculated data from the Matlab flowchart, include slot lengths, residual cavity lengths, frequencies and calculated reflection coefficients. A reflection coefficient is expressed in magnitude and phase format. Through the experiments on neural network model training process, the result shows lower error when the training data has better linearity.

In the approach, there are five variables in only one data file, they are iris length, cavity length, frequency, phase and magnitude of reflection coefficients. The structure of a neural network model shows in Fig. 3.31, there are three neurons in the input layer, two neurons in the output layers and twelve neutrons (by default) in the hidden layer. The first training error is 17% with 12 hidden neutrons, and the training error keeps going down to 13% when the number of neutrons is more than 50 in hidden layer.

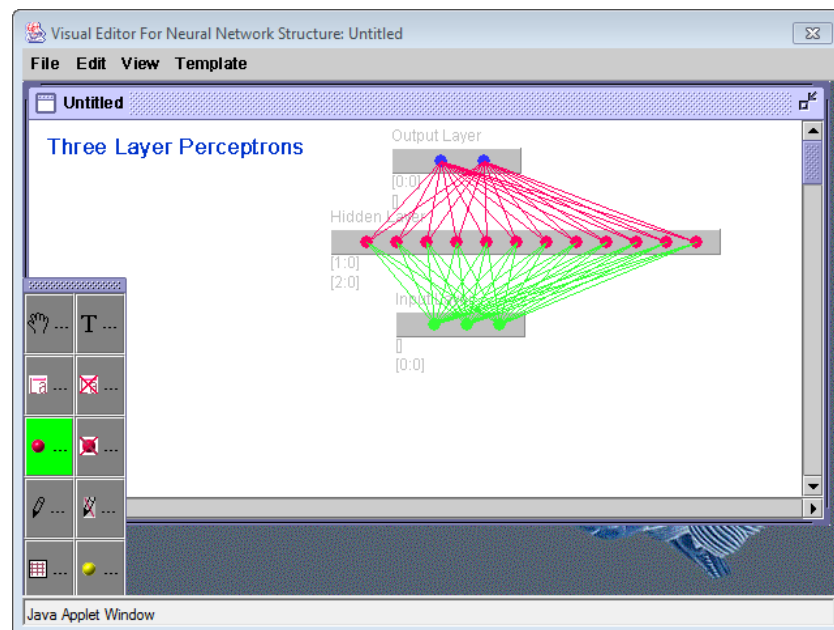


**Fig. 3.31** A three layer structure of Artificial Neural Network with three input parameters and two output parameters.

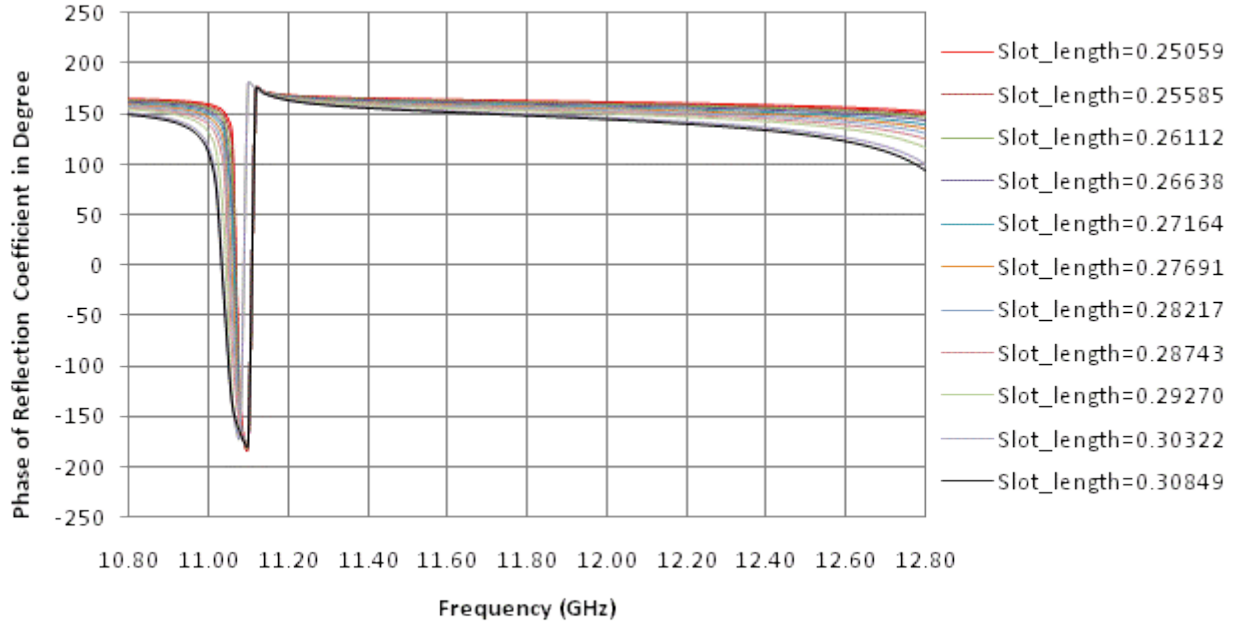


**Fig. 3.32** The phases of reflection coefficient with different slot lengths.

However the result is still not accurate enough to substitute the original EM data file; and training time is longer than a full EM simulation. The problem is the resonances occur at different frequencies, the results are shown in Fig. 3.32. Increasing hidden neurons is the only method to enhance the accuracy of a NN model. But with exponentially increasing training time, the process becomes impossible. Therefore, the second method is not successful either.

### C. Training $[2 \times 2]$ S-parameter Matrix

With two failed experiments, another approach is proposed. This method degrades a  $[6 \times 6]$  matrix in the **section A**, to a  $[2 \times 2]$  matrix. The S-parameter in a  $[2 \times 2]$  matrix is more linear than in a  $[6 \times 6]$  matrix, and each S-parameter data file is much smaller than the reflection coefficient data file in **section B**. This method combines the previous methods to overcome their disadvantages.

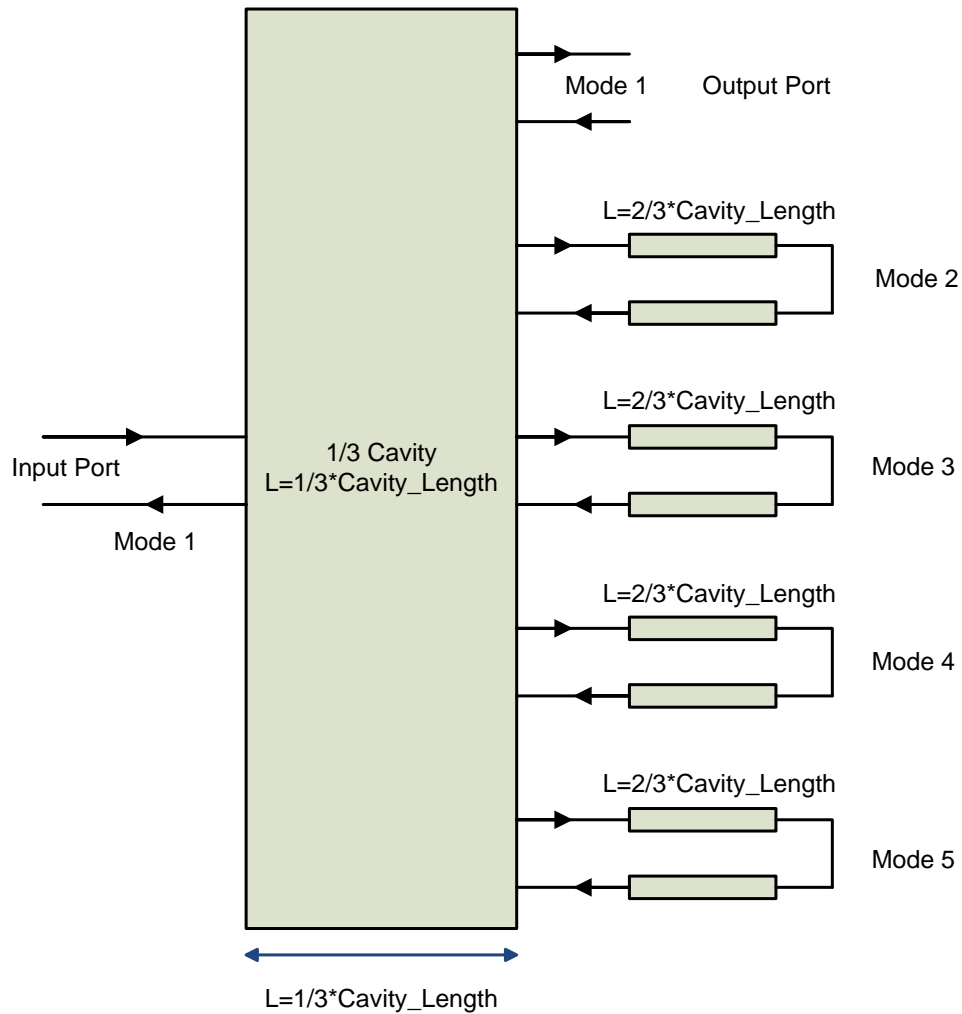


**Fig. 3.33 An arbitrary microwave network consisting of multiport networks connected together.**

The degraded equivalent circuit is presented in Fig. 3.33; the dominant mode TE<sub>11</sub> port is selected as an external port; and other modes in the output are all shorted.

(3.16) of six ports network is then rewritten as:

$$\begin{aligned}
S_{PP} &= \begin{bmatrix} S1(1)1(1) & S1(1)2(1) \\ S2(1)1(1) & S2(1)2(1) \end{bmatrix} & S_{PC} &= \begin{bmatrix} S1(1)2(2) & S1(1)2(3) & S1(1)2(4) & S1(1)2(5) \\ S2(1)2(2) & S2(1)2(3) & S2(1)2(4) & S2(1)2(5) \end{bmatrix} \\
S_{CP} &= \begin{bmatrix} S2(2)1(1) & S2(2)2(1) \\ S2(3)1(1) & S2(3)2(1) \\ S2(4)1(1) & S2(4)2(1) \\ S2(5)1(1) & S2(5)2(1) \end{bmatrix} & S_{CC} &= \begin{bmatrix} S2(2)2(2) & S2(2)2(3) & S2(2)2(4) & S2(2)2(5) \\ S2(3)2(2) & S2(3)2(3) & S2(3)2(4) & S2(3)2(5) \\ S2(4)2(2) & S2(4)2(3) & S2(4)2(4) & S2(4)2(5) \\ S2(5)2(2) & S2(5)2(3) & S2(5)2(4) & S2(5)2(4) \end{bmatrix}
\end{aligned}
\tag{3.23}$$

Re-calculating with (3.22), the matrix  $[S^P]$  is not a reflection coefficient anymore, but a reciprocal  $[2 \times 2]$  S-parameter matrix. The data in this  $[2 \times 2]$  S-parameter matrix has high linearity, as shown in Fig. 3.34. When this matrix is applied into ADS, the residual length of cavity is added using a circuit-based model in Agilent ADS. A Matlab flowchart in Fig.3.30 is still used in this situation with (3.23) but not (3.16). Similar to the second approach, the input parameters in each data file are slot length, cavity length and frequency; the output parameters are magnitudes and phases of each S-parameter. The structure of the neural network model also use the three layer structure as shown in Fig. 3.31. Each model training process takes more than 40 minutes with 40~50 hidden neurons. The result is significantly improved with this method with the training error lower than 2% in the worst case. The model after training process can be used to substitute the EM model.

When a resonance frequency or cavity length, and a slot length are fixed, the S-parameters are generated by the Neural Network model and exported as the .S2P file which will be used in Agilent ADS co-simulation process. This result is as precise as the EM data. It can be generated much faster than full EM simulation.

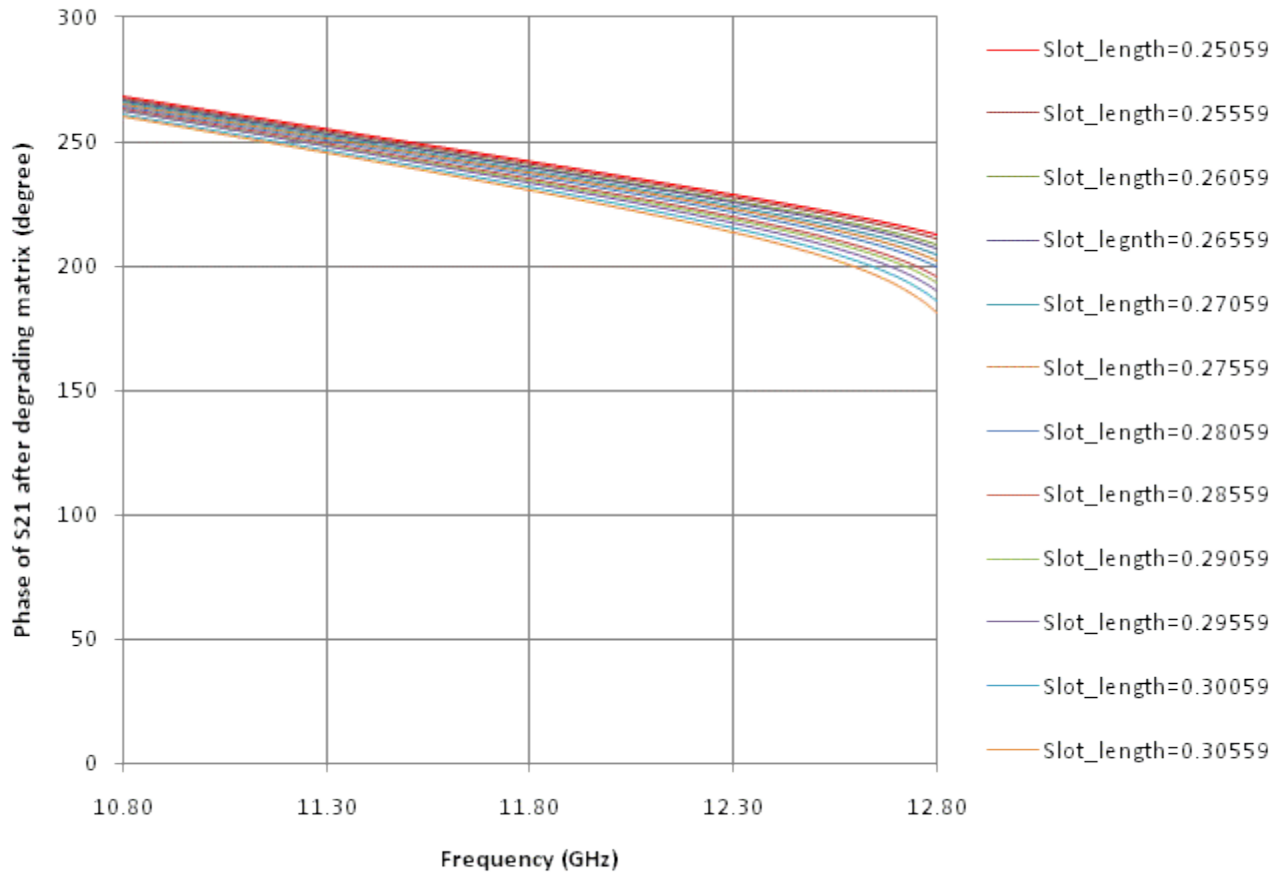
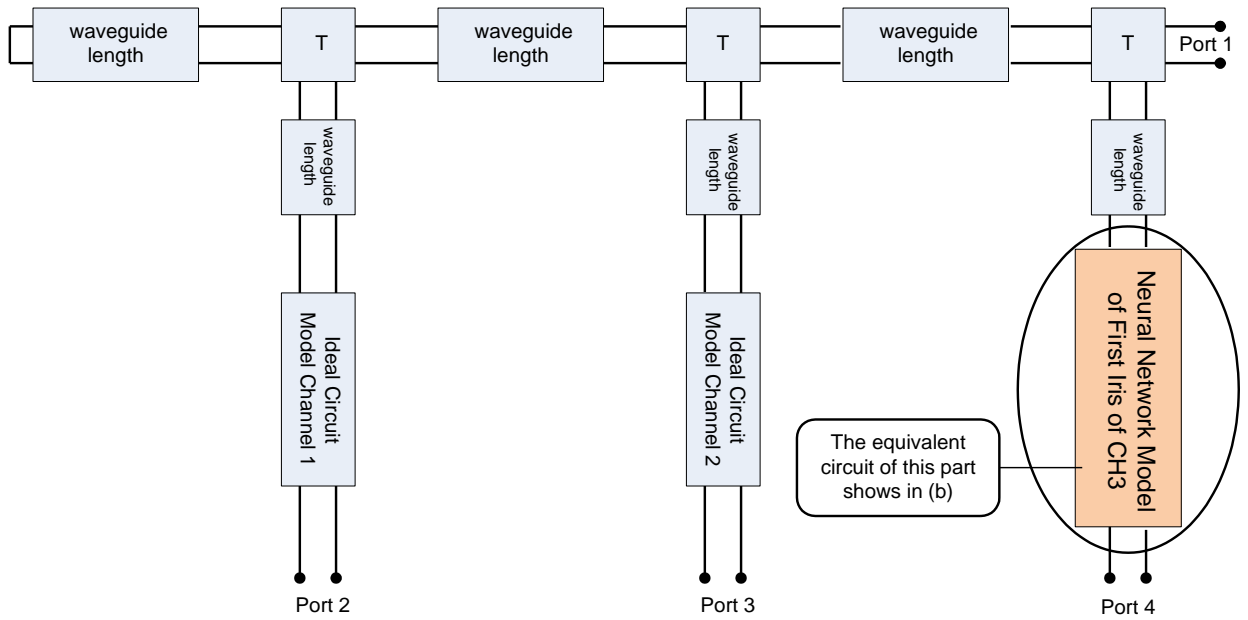


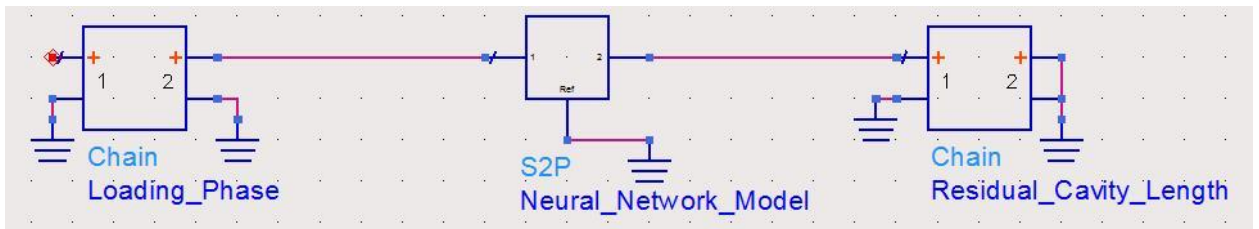
**Fig. 3.34 Phases of S21 after de-grading matrix**

### 3.3.3 Application of NN model in ADS

With a trained Neural Network (NN) model, the next step is to substitute channel 3 with the NN model to verify the effect in out-of-band frequencies. Since the NN model is a  $[2 \times 2]$  S-parameter matrix without residual cavity, the simulation in the ADS is added with the residual cavity length.



(a)

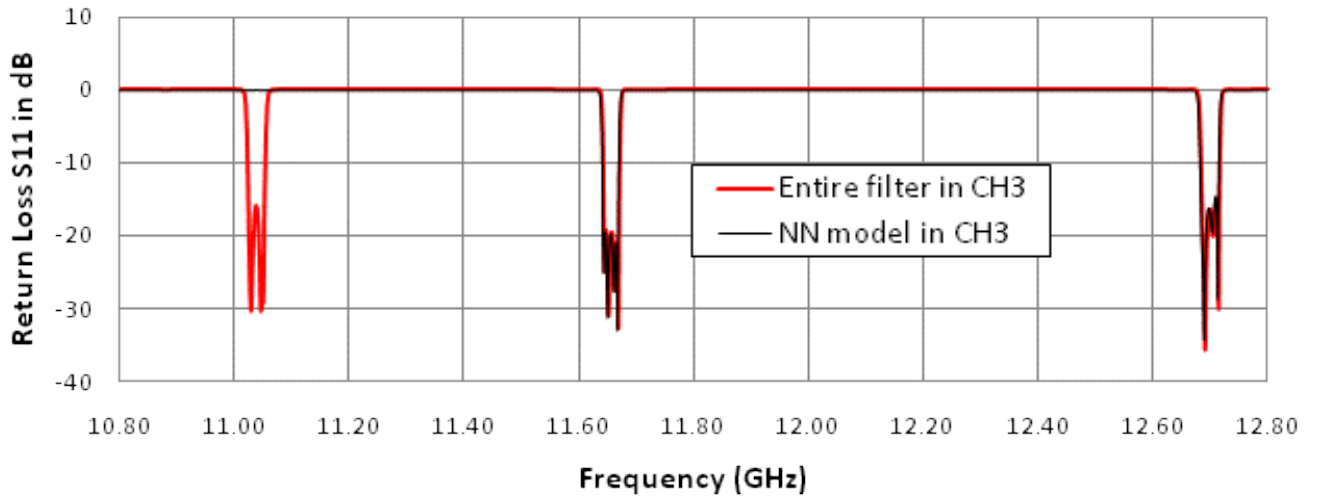


(b)

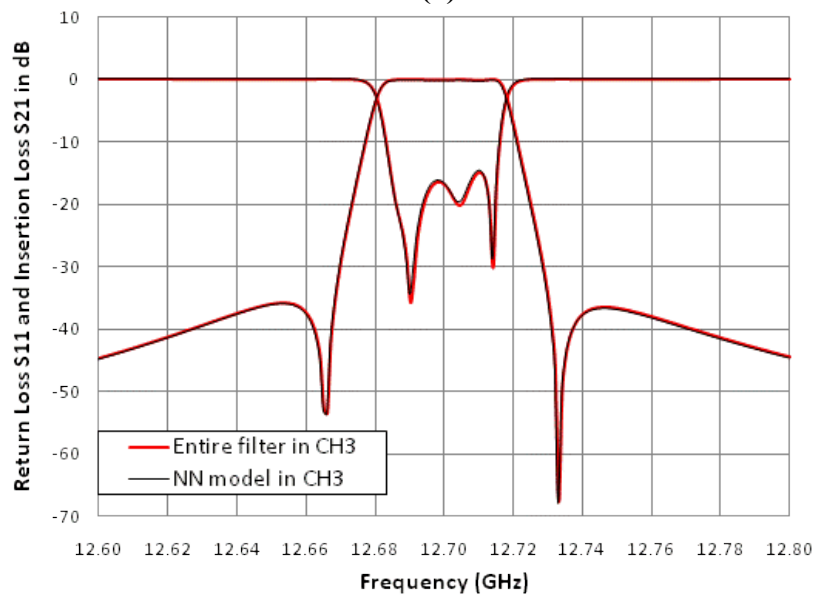
**Fig. 3.35 Three channel output multiplexer with Neural Network Model (a) Simplified equivalent circuit model with NN model at port 4. (b) Equivalent circuit model of NN model in ADS.**

A simplified equivalent circuit model with a NN model connected to port 4 is shown in Fig.3.35, which is similar to Fig.3.11 with a full EM model in channel 3. The detailed circuit at port 4, with loading phase and residual cavity length, are all shown in Fig. 3.35 (b). Because the Neural Network model only simulates the input slot of the filter at channel 3, the loading phase at input is considered in simulation process. The

residual cavity length in the figure depends on resonance frequency. In comparison with the original full EM model, 1.288903 inch is used as the residual cavity length in the simulation. Fig. 3.36 shows the simulation results of three-channel multiplexer with full EM model and a Neural Network (NN) model. Obviously, the proposed method has no return loss and insertion loss in pass-band of channel 3, since the neural network model only simulates the first cavity of the filter. In out-of-band frequency, the responses of the proposed method agree very well with the responses of conventional method. This illustrates that the NN model can simulate the responses of an EM model precisely.



(a)



(b)

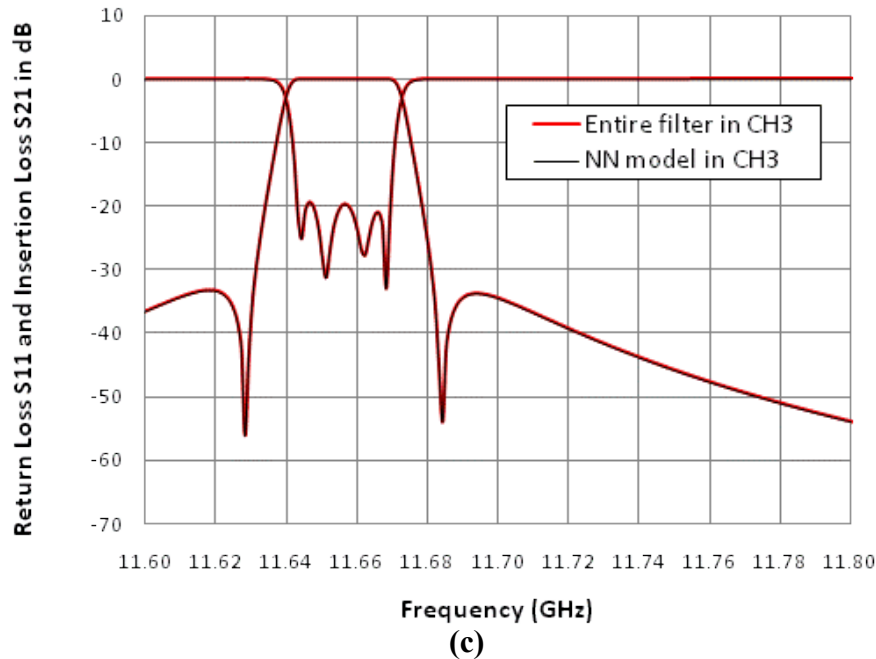


**Fig. 3.36 Comparison of the multiplexer with EM model, and with NN Model. (a) Common Port Return Loss S11. (b) Insertions Loss and Return Loss in Channel 1. (c) Insertion Loss and Return Loss in Channel 2.**

With statistical comparison in Table 3.5 and Table 3.6, the greatest benefit of artificial neural network can be illustrated much clearer. In Table 3.5, the training error and testing error are both very low. The relatively higher worst case error is due to the differences of phases in some specific frequencies. The difference might be higher than 2%, which is still considered a low phase error. Therefore, the neural network can be trusted with its accuracy. Table 3.6 has compared the simulation time in EM model and NN model. An EM simulator takes more than 3 minutes to simulate the I/O iris of the filter, and more than 10 minutes to simulate one cavity of the channel filter. An entire channel filter will require more than 50 minutes EM simulation time. While the NN model takes less than 1 second to simulate even the entire channel filter. The advantage makes ANN a powerful tool in multiplexer designs.

**Table 3.5 Error comparison between the ANN model and EM simulations for S-parameters**

	$S_{11}$	$S_{12}$	$S_{21}$	$S_{22}$
Training Error	0.00054	0.00065	0.00069	0.00061
Testing Error	0.00076	0.00076	0.00058	0.00077
Worst Case	0.0144	0.0156	0.0160	0.0137

**Table 3.6 Comparison of Time to obtain S-parameters by NN models and EM models**

t	I/O Iris	One Cavity	Entire Filter (in Narrow Band*)	Entire Filter (in Wide Band**)
EM Model	t>3 mins	t>10 mins	t>50 mins	t>70 mins
NN Model	t<1 s	t<1 s	t<1 s	t<1 s

\*Narrow Band: the EM simulation frequency range is less than 200 MHz including the pass-band of the filter.

\*\*Wide Band: the EM simulation frequency range is around 2 GHz including the pass-band of the filter.

### 3.4 Summary

For multiplexers in the satellite application, a spurious mode can destroy the responses in some frequency ranges. The responses of a channel filter in out-of-band frequency are not as ideal as a circuit-based model shows. Simulating the responses of a single channel filter in far-band frequency can help to avoid the damage result from a spurious mode. This chapter provides the methodology to solve this problem by using neural network technique and a simplified circuit model.

With a tuned filter of channel 3, which has the center frequency at 11037.42MHz with a 36 MHz bandwidth, the results of a three-channel multiplexer show obviously different responses at high frequency from an ideal circuit-based model. A spurious mode from channel 3 is damaging the responses of the multiplexer. Optimizing all variables can certainly help to improve the responses, when the simulation of the spurious mode is accurate. The most accurate data should be generated from a full EM simulation. Unfortunately it takes a long time to run a full EM simulation on an entire channel filter. Since the input side of each channel filter can fully reflect the responses in out-of-band frequency, a simplified model only using the EM data of input slot can be applied. However, the EM simulation of a simplified model still takes time, especially for iterative design and optimization. Artificial neural network as a fast and accurate tool is thus introduced to solve the problem. With a successfully trained neural network model, S-parameters of any input slot length at a specific resonance frequency can rapidly be generated. The accuracy has been proven in previous examples.

This methodology with a simplified EM model and artificial neural network improves the design process in the multiplexer.

## Chapter 4

### Conclusion

In conclusion, the thesis's objective of enhancing designs of both channel filter and multiplexer, has been achieved through the optimization of T-junction manifold and the improvement of simulating the effect of a channel filter in out-of-band frequencies.

Extra resonators in a multiplexer no doubt enhance the pass-band gain flatness and stop-band rejection, but also increase weight and size of the multiplexer. The proposed design using existing manifold provides an additional pole into the pass-band of the channel filters of a multiplexer. The group delay in a multiplexer T-junction, which is usually flat in conventional method [01], is purposely designed with a peak at resonance frequency to generate the extra pole. The result illustrates that a large group delay or small coupling value, can increase the performance of rejection but scarify the return loss; and large group is not suitable in multi-channel multiplexer design. In contrast to a

conventional method, the response of the proposed design shows better out-band rejection and wider in-band bandwidth. The method only alters the lengths of manifold but retains the overall size and weight, which is very important for satellite applications. Besides waveguide manifold, this method can also be applied in other transmission line configurations.

With the increase of the number of multiplexer channels, the accurate simulation of each channel filter in whole transmission band becomes necessary, since the out-of-band responses of a low channel filter can easily damage the responses of other channel filters. Unlike using LC elements to simulate a spurious mode, the proposed method using Artificial Neural Network (ANN) can provide fast and accurate responses to predict the effect in out-of-band frequency range. Mathematical deductions are presented to prove model simplification. Different approaches are tested to ensure the accuracy of the trained ANN model. S-parameters with required slot lengths at resonance frequency can be rapidly generated from the well-trained ANN model. The results are compared to EM simulated data of a tuned channel filter. This proposed method provides a fast and precise model to simulate of the spurious mode before re-optimizing a multiplexer to meet requirement specifications.

In the future research, the enhanced multiplexing network can be tested in other multiplexer configurations to verify its applications. ANN technology will be used for the modeling of whole channel filter or multiplexer to improve the simulation efficiency. Application of ANN can be considered for other types of filters and structures.

# Bibliography

- [01] R. J. Cameron, C. M. Kudsia, and R. R. Mansour, *Microwave Filters for Communication Systems: Fundamentals, Design and Applications*, John Wiley & Sons. 2007.
- [02] S. Shin, and S.Kanamaluru, "Diplexer Design Using EM and Circuit Simulation Techniques," *IEEE Microwave Magazine* , pp. 77-82, Apr. 2007.
- [03] Qi-Jun Zhang, K. C. Gupta, and V. K. Devabhaktuni, "Artificial Neural Network for RF and Microwave Design - From Theory to Practice." *IEEE Trans. Microwave Theory Tech.* , vol. 51, no.43, pp. 1339-1350, Apr. 2003.
- [04] H. Kabir, Y. Wang, M. Yu, and Q. J. Zhang, "Neural Network Inverse Modeling and Applications to Microwave Filter Design," *IEEE Trans. Microwave Theory Tech.* , vol. 56, no. 4, pp. 867-879, Apr. 2008.
- [05] Y. Wang, M. Yu, H. Kabir, and Q. J. Zhang, "Effective Design of Cross-Coupled Filter Using Neural Networks and Coupling Matrix," *IEEE MTT-S International Microwave Symposium Digest*, pp. 1431-1434, 2006.
- [06] M. Yu, and Y. Wang, "Enhanced Microwave Multiplexing Network," *IEEE Trans. Microwave Theory & Tech.* , vol. 59, no. 2, pp. 270-277, Feb. 2011.

- [07] Y. Wang, and M. Yu, "Performance Analysis of the Enhanced Microwave Multiplexing Networks for Applications in Communications Satellites," *IEEE MTT-S International Microwave Symposium Digest*. Baltimore, MD., Jun. 2011.
- [08] I. Wolff, "Design and Technology of Microwave and Millimeterwave LTCC Circuits and Systems," *International Symposium on, Signals, Systems and Electronics*, pp. 505-512, 2007, Issue'07.
- [09] V. Piatnitsa, E. Jakku, and S. Leppaevuori, "Design of a 2-Pole LTCC Filter for Wireless Communications," *IEEE Trans. on Wireless Communications*, vol. 3, no. 2, pp. 379-381, Mar. 2004.
- [10] C. Kudsia, R. Cameron, and W.-C. Tang, "Innovations in Microwave Filters and Multiplexing Networks for Communications Satellite Systems," *IEEE Trans. Microwave Theory Tech.*, vol. 40, no. 6, pp. 1133-1149, Jun. 1992.
- [11] N. Marcuvitz, *Waveguide Handbook*, Piscataway, NJ: The Institute of Electrical Engineers, 1986.
- [12] D. Bariant, S. Bila, D. Baillargeat, S. Verdeyme, P. Guillon, D. Pacaud, and J.-J. Herren, "Method of Spurious Mode Compensation Applied to Manifold Multiplexer Design," *2002 IEEE MTT-S International*, pp. 1461-1464, 2002.
- [13] M. A. Ismail, D. Smith, A. Panariello, Y. Wang and M. Yu, "EM-Based Design of Large-Scale Dielectric-Resonator Filters and Multiplexers by Space Mapping," *IEEE Trans. Microwave Theory & Tech.*, vol. 52, no. 1, pp. 386-392, Jan. 2004.

- [14] J. W. Bandler, Q. S. Cheng, D. M. Hailu, and N. K. Nikolova, "A Space-Mapping Design Framework," *IEEE Trans. Microwave Theory & Tech.*, vol. 52, no. 11, pp. 2601-2610, Nov. 2004.
- [15] M. Meng and K.-L. Wu, "An Analytical Approach of Extracting Coupling Matrix and Unloaded Q of A Bandpass Filter," *IEEE MTT-S International Microwave Symposium Digest*, pp. 1345-1348, 2009.
- [16] V. Miraftab and M. Yu, "Advanced Coupling Matrix and Admittance Function Synthesis Techniques for Dissipative Microwave Filters," *IEEE Trans. Microwave Theory & Tech.*, vol. 57, no. 10, pp. 2429-2438, 2009.
- [17] C. Kudsia, R. Cameron, and W.-C. Tang, "Innovations in microwave filters and multiplexing networks for communications satellite systems," *IEEE Trans. Microwave Theory & Tech.*, vol. 40, no. 6, pp. 1133-1149, Jun. 1992.
- [18] S. Cogollos, M. Brumos, V. E. Boria, B. Vicente, B. Gimeno and M. Gglielmi, "New Distributed Model for Synthesis of Classical Dual Mode Filters," *IEEE MTT-S International Microwave Symposium Digest*, pp. 437-440, May 2010.
- [19] CST STUDIO SUITE, ver.2011, Sonnet Software, (2011).
- [20] J. W. Bandler, M. Biernacki, S. H. Chen, P. A. Grobelny and R. H. Hemmers, "Space Mapping Technique for Electromagnetic Optimization," *IEEE Trans. Microwave Theory & Tech.*, vol. 42, no. 12, pp. 2536-2544, Dec. 1994.

- [21] F. Ling, W. Harris, X. Wang and E. A. Dengi, "An Incremental Fullwave EM Simulator for RF and Microwave Design," *Microwave Symposium, IEEE/MTT-S International*, pp. 289-292, Jun. 2007.
- [22] J. Bandler, S. Daijavad and Q.-J. Zhang, "Exact simulation and sensitivity analysis of multiplexing networks," *IEEE Tran. Microwave Theory Tech. MTT-34*, pp. 111-102, Jan. 1986.
- [23] R. J. Carmeron and M. Yu, "Design of Manifold-Coupled Multiplexers," *IEEE Tran. Microwave Theory Tech. MTT*, pp. 46-59, Oct. 2007.
- [24] G. Matthaei, L. Young, and M. T. Jones, "Microwave Filters, Impedance Matching Networks and Coupling Structures," *Norwood, MA: Artech House*, 1985.
- [25] M. H. Chen, "Singly-terminated pseudo-elliptic function filter," *Comsat Technical Rev.*, vol. 7, pp. 527-541, Fall 1977.
- [26] R.F. Baum, "Design of unsymmetrical band-pass filters," *IRE Trans. Circuit Theory CT-4*, pp. 33-40, Jun. 1957.
- [27] R. J. Cameron, "General prototype network synthesis methods for microwave filters," *ESA J.6*, pp. 193-206, 1982.
- [28] M. Guglielmi, "Simple CAD procedure for microwave filters and multiplexers," *IEEE Transactions on Microwave Theory and Techniques*, vol. 42, no. 7, pp. 1347-1352, Jul. 1994.

- [29] L. Q. Bui, D. Ball and T. Itoh, "Broad-band millimeter-wave E-plane bandpass filters," *IEEE Transactions on Microwave Theory and Techniques* , vol. 32, no. 12, pp. 1655-1658, Dec. 1984.
- [30] J. D. Rhodes, and R. Levy, "A Generalized Multiplexer Theory," *IEEE Trans. Microwave Theory and Tech. MTT*, pp. 111-123, Feb. 1979.
- [31] J. D. Rhodes, "Design of General Manifold Multiplexers," *IEEE Trans. Microwave Theory and Tech.* , vol. MTT-27, pp. 111-123, Feb. 1979.
- [32] G. Tanne, S. Toutain, J. F. Favennec, P. Jarry, and C. Boschet, "Optimal design of Contiguous-Band output Multiplexers (COMUX)," *Electronics Letters* , vol. 29, no. 19, pp. 1674-1675, Sep. 1993.
- [33] A. E. Atia, "Computer-Aided Design of Waveguide Multiplexers," *IEEE Trans. Microwave Theory and Tech.*, pp. 332-336, Mar. 1974.
- [34] Agilent ADS, ver. 2009, Agilent Technol. (2011), Santa Rose, CA.
- [35] Q. J. Zhang, NeuroModelerPlus. Dept. Electron. Carleton Univ., Ottawa, ON, Canada. 2011.